

# **Controls of hydrothermal quartz vein mineralisation and wall rock alteration between Ameralik and Sermilik, southern West Greenland**

Jochen Kolb, Bo Møller Stensgaard,  
Denis Martin Schlatter  
& Annika Dziggel

(1 CD-Rom included)



# **Controls of hydrothermal quartz vein mineralisation and wall rock alteration between Ameralik and Sermilik, southern West Greenland**

Jochen Kolb<sup>1</sup>, Bo Møller Stensgaard<sup>1</sup>,  
Denis Martin Schlatter<sup>1</sup>  
& Annika Dziggel<sup>2</sup>

<sup>1</sup> Geological Survey of Denmark and Greenland, GEUS

<sup>2</sup> Institute for Mineralogy and Economic Geology, RWTH Aachen University, Germany

(1 CD-Rom included)

# Content

<b>Content</b>	<b>3</b>
<b>Abstract</b>	<b>4</b>
<b>Introduction</b>	<b>5</b>
<b>Geological setting</b>	<b>6</b>
Færingehavn terrane.....	6
Tre Brødre terrane .....	8
Tasiusarsuaq terrane .....	9
<b>Regional geology of the Buksefjorden and Kangiata Nuna map sheets (63 V. 1/2 N)</b>	<b>10</b>
The Tasiusarsuaq terrane .....	10
Structural geology .....	12
The Tre Brødre Terrane .....	20
Structural geology .....	22
Færingehavn terrane.....	24
Structural geology .....	27
Færingehavn straight belt and Qarliit Nunaat fault.....	30
Færingehavn – Kangerdluarssoruseq profile .....	31
<b>Hydrothermal mineralisation and alteration (Kangiata Nuna)</b>	<b>34</b>
Camp 1 area: south of Kangerdluarssungup taserssua .....	34
Camp 2 area: north of Isortuarssup tasia .....	38
Camp 3 area: northeast of camp 2.....	39
<b>Hydrothermal mineralisation and alteration (Buksefjorden)</b>	<b>45</b>
Camp 1 area: Qarajat kuat, north of Buksefjorden .....	45
Camp 2 area: south of Qaaqatsiaq, central Tasiusarsuaq terrane.....	47
Camp 3 area: north of central Alangordlia, southern Tasiusarsuaq terrane .....	52
Camp 4 area: south of the outlet of Buksefjorden, central Tre Brodre terrane .....	54
Reco stop: south of Ameralik .....	56
Reco stop: south of central Alangordlia.....	57
Narsaq .....	60
Qilangaarsuit.....	63
Simiutat.....	68
<b>Summary and discussion</b>	<b>71</b>
<b>Conclusions and future work</b>	<b>73</b>
<b>References</b>	<b>74</b>

## Abstract

This field report describes localities studied in 2008 in the Buksefjorden and Kangiata Nuna map sheet areas. The localities studied in the field were chosen with the aim to locate and interpret hydrothermal mineralisation and alteration in the area. Two hydrothermal alteration and mineralisation types were identified in the field: (1) Quartz veins with associated Bt-Qtz-Po-Ccp±Grt±Hbl±Di±Py alteration and (2) massive sulphide lenses comprising mainly Po and minor amounts of Py, Ccp, Mo and Sp. These lenses are surrounded by rocks containing orthorhombic amphiboles and Grt, which is interpreted as a metamorphosed hydrothermal alteration zone.

The quartz veins are widespread, normally 5–20 cm wide and can be followed over 200–1500 m along strike. They are generally only weakly enriched in Au with values up to 20 ppb. Only on the island of Qilanngaarsuit, the quartz veins and the alteration zones record Au grades of up to 800 ppb. The quartz veins are structurally controlled by the F<sub>3</sub> folds that are obvious from the map pattern. The veins are most abundant in the steep limbs of the folds and in limbs sheared off by D<sub>3</sub> strike-slip deformation. This deformation stage is possibly related to deformation along the Ivinnguit fault. Therefore a genetic relationship between the hydrothermal quartz veins in the study area and known gold occurrences along the Ivinnguit fault, namely Storø, Qussuk, Bjørnøen and SW Isua, is likely.

The massive sulphide lenses are 2–7 m in diameter and 5–30 m long. Although several lenses may occur along strike, the total size of the mineral occurrences is regarded as being too limited to be of economic significance. These massive sulphides are interpreted as a syngenetic hydrothermal mineralisation, possibly related to hydrothermal activity on a palaeo-seafloor. The rocks were later metamorphosed and deformed into boudins, representing the massive sulphide lenses.

The study area was investigated to a great detail but no significant hydrothermal mineralisation has been found. It is, therefore, likely that the area is largely barren with respect to this type of mineralisation. Only the elevated Au grades on Qilanngaarsuit are worth mentioning and the mineralisation style will be studied further, possibly in a Ph.D. project.

# Introduction

This is a field report covering localities studied in June–July 2008 south of Ameralik on the Buksefjorden and Kangiata Nuna 1:100 000 geological map sheets in SW-Greenland. The field expedition and the follow-up research work is co-financed by GEUS and the Bureau of Minerals and Petroleum (BMP, Nuuk, Greenland) under the project entitled “Strukturelt kontrolleret hydrotermal omdannelse og mineralisering i regional skala og detaljestudium af udvalgte grønstensbælter i Sydvestgrønland 61°30’ – 64°00’”. The aim of this report is to document the field investigations and the data collected during field work, and combining and discussing this new data together with previous investigations and published accounts. A special focus is drawn on the potential for hydrothermal mineralization and the documentation of the studied occurrences.

In the first three weeks of field work, two teams worked in selected areas from north to south supported by helicopter: (1) A. Dziggel (RWTH) and B. Møller Stensgaard (GEUS) worked on the western corridor in the Buksefjorden map sheet area and (2) J.Kolb (GEUS, project leader) and D.M. Schlatter (GEUS, expedition leader) covered the eastern corridor on the Kangiata Nuna map sheet. As a basis not only the 1:100 000 geological map sheets were used but also the detailed field maps and field reports of the geologists that worked in the area previously were taken into account and were found to be very useful. The field maps turned out to be very detailed and no major discrepancy between the maps and our investigations were found. However, there are several different interpretations between the field maps and the published 1:100 000 geological map sheets, which should be taken into account while reprocessing the maps. This will be addressed in discussions with the colleagues from the mapping department in GEUS in their own project with the BMP.

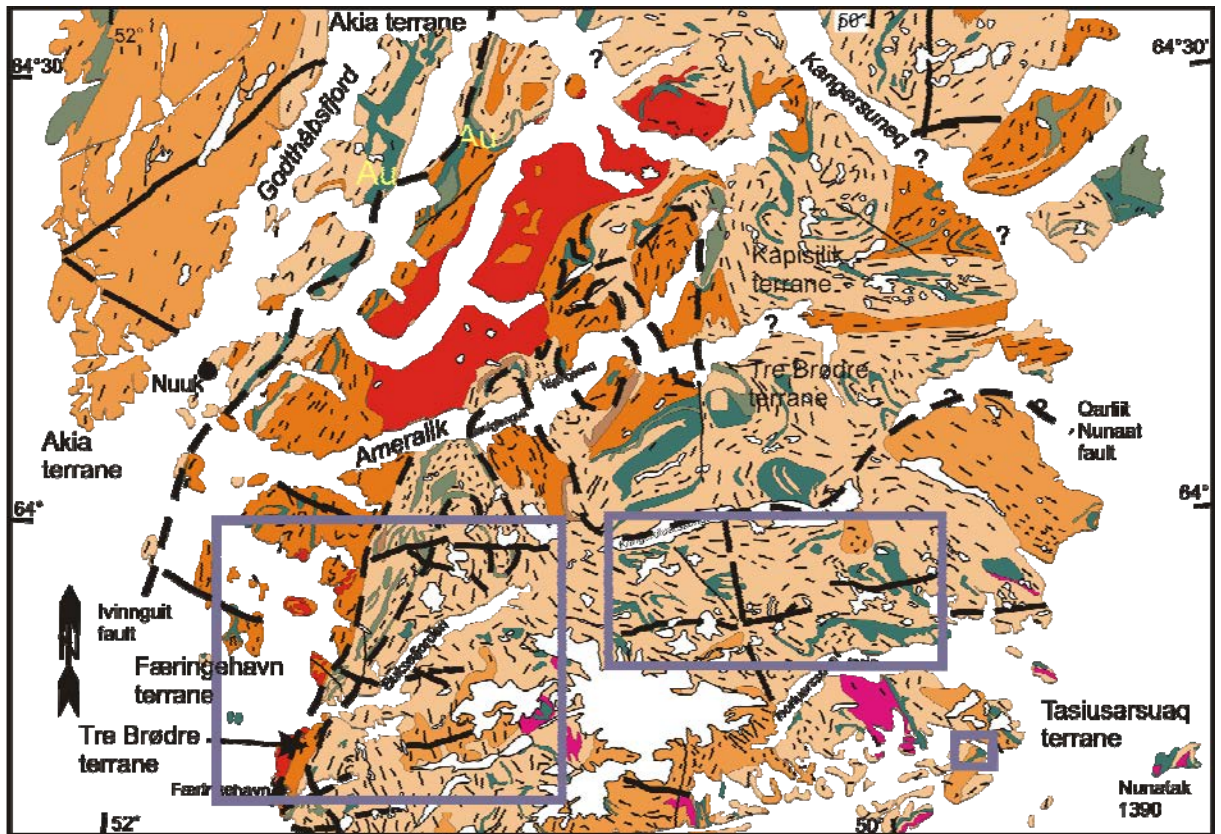
The last two weeks of the field season, the two teams had a joint camp in order to accomplish detailed geological mapping, sampling and profiles on the island of Qilanngaarsuit to the west of Buksefjorden, where the field map by Brian Chadwick was used as a basis. A. Dziggel left on the 21<sup>st</sup> July. B. Møller Stensgaard, J.Kolb and D.M. Schlatter continued work for 1 week based on a ship (M/C Rink). The field work concentrated on coastal outcrops of the island Simiutat and the northern shores of Kangerdluassoruseq and Sermilik.

## Geological setting

The study area is situated in the Archaean craton of southern West Greenland in the Nuuk area (Fig. 1). This area has a long tradition of Archaean geology research since the first comprehensive regional geological mapping by (McGregor 1973). The area has been subdivided into various different terranes mainly based on U–Pb zircon ages of protolith formation and metamorphism arguing for a different tectono-metamorphic evolution (see, Nutman & Friend 2007, for a recent comprehensive review). From north to south, the Akia, the Isukasia, the Færingehavn, the Kapisilik, the Tre Brødre and the Tasiusarsuaq terranes are distinguished (Friend & Nutman 2005; Friend *et al.* 1987, 1988; Friend *et al.* 1996). Extensive high grade metamorphism between ca. 2720–2700 Ma and a clockwise P–T path in the Neoarchaean are interpreted as a response of crustal thickening and stacking of the terranes (Friend *et al.* 1996; Nutman *et al.* 1989). A late-tectonic pegmatite was dated at  $2725 \pm 2$  Ma by U–Pb zircon dating, which was interpreted that shearing along the Qarliit Nunaat fault, the terrane boundary between the Tasiusarsuaq and the Tre Brødre terranes, occurred after ca. 2725 Ma (Crowley 2002). High pressure metamorphism recorded in supracrustal rocks of the Færingehavn terrane at its southern boundary was dated at metamorphic zircons by U–Pb dating at about 2715 Ma, which was interpreted to support terrane accretion between ca. 2720–2700 Ma (Nutman & Friend 2007). This terrane juxtaposition was followed by folding in the amphibolite facies at about 5 kbar and 550°C–700°C (Bridgwater *et al.* 1974; Chadwick & Nutman 1979; Nutman *et al.* 1989) and ca. 2565 Ma shearing in the Færingehavn straight belt (Friend *et al.* 1987; Nutman & Friend 2007; Nutman *et al.* 1989). The Qôrqt granite intruded rocks of the Færingehavn and the Tre Brødre terranes late-to post-tectonically as sheet-like intrusions at  $2530 \pm 30$  Ma (U–Pb zircon multi grain and Rb–Sr whole rock, Baadsgaard 1976; Moorbath *et al.* 1981).

### Færingehavn terrane

The Færingehavn terrane forms a ca. 30 km wide, mainly N–S trending belt that is situated between the Akia terrane in the W and the Tre Brødre terrane in the E. To the N and E, it is bordered by the Kapisilik terrane (Fig. 1). The Færingehavn terrane is dominated by ca. 3850–3600 Ma quartzo-feldspatic gneiss (e.g., Nutman & Friend 2007, and references therein; Nutman *et al.* 2004) that were intruded by a swarm of mafic dykes (the Ameralik dykes) in the Palaeoarchaean. The gneiss is overlain by, and in tectonic contact with, a variety of supracrustal rocks of the Malene supracrustal sequence (Chadwick & Nutman 1979). The Malene supracrustal sequence includes meta-ultramafic rocks, amphibolite derived from basaltic protoliths, and aluminous, mostly sillimanite-bearing paragneiss derived from a ca. 2840 Ma volcanic source (e.g., Friend *et al.* 1996). The Færingehavn terrane and overlying supracrustal rocks were metamorphosed to amphibolite, and, locally, granulite facies conditions, and record a complex and polyphase metamorphic history. An early low- to medium-pressure granulite facies metamorphic event was proposed based on relict occurrences of orthopyroxene-bearing mafic and intermediate granulites and the presence of metamorphic zircons that were dated at ca. 3400–3650 Ma (Nutman & Friend 2007).



-  fault: minor, major
-  foliation trend
-  dolerite dyke
-  Qorqut granite
-  Ilivertalik granite/charnockite
-  enderbitic gneiss
-  TTG gneiss (c. 2.8 - 3.0 Ga)
-  meta-sedimentary rock
-  amphibolite/mafic granulite
-  meta-anorthosite/-leucogabbro
-  TTG gneiss (> 3.7Ga)

**Figure 1.** Geological map of the Nuuk region and location of the study area covered by field work in 2008 (modified after, Escher & Pulvertaft 1995). The small Færingehavn, Tre Brødre and Kapisilik terranes are tectonically imbricate between the Tasiusarsuaq terrane in the south and the Akia terrane in the north in a 25–50 km wide, SW–NE trending zone.

This was followed by high-pressure metamorphism at ca. 2715 Ma, as evidenced by the presence of Grt-Cpx-Hbl-Pl-Qtz assemblages in mafic granulite on southern Qilangaarsuit. The exhumation of the Færingehavn terrane was associated with widespread low-pressure amphibolite facies metamorphism, and immediately followed the high-pressure metamorphic event. Decompression is indicated by Hbl-Pl symplectites rimming Grt in mafic granulite, and the development of cordierite replacing garnet-kyanite assemblages in the aluminous paragneiss (Nutman & Friend 2007).

Four deformation events can be distinguished (Chadwick & Nutman 1979). D<sub>1</sub> took place before the intrusion of the Ameralik dykes, and was associated with the development of a migmatitic foliation and gneissic banding. The D<sub>2</sub> deformation was proposed to be related to thrusting along the contact between lithological units, but, to date, the vergence of these thrusts is unknown. D<sub>3</sub> resulted in the formation of nappes and recumbent isoclinal folds, and may represent a continuation of D<sub>2</sub> (Fig. 1). D<sub>4</sub> occurred during continued high-grade metamorphism, was superimposed on D<sub>3</sub> nappes and was related to the formation of N–S trending dome structures (Fig. 1).

## Tre Brødre terrane

The Tre Brødre terrane is an about 5 km wide sheet between the Færingehavn terrane in the north and the Tasiusarsuaq terrane in the south (Fig. 1). It mainly comprises amphibolite facies tonalitic-granodioritic gneiss, the Ikkattoq gneiss, mainly comprising Qtz, Pl and Hbl. U–Pb zircon ages of several Ikkattoq gneiss samples indicate that the intrusion age has a narrow span around 2825 Ma (Crowley 2002; Friend *et al.* 1987; McGregor *et al.* 1991). These gneisses include abundant sequences of metamorphosed gabbro-anorthosite complexes and amphibolite (Fig. 1, Chadwick & Coe 1983; Frei & Konnerup-Madsen 2007). The metamorphosed gabbro-anorthosite complexes occur as sheets or larger enclaves within the gneiss (Fig. 1). The contacts between both lithologies are generally tectonic (Chadwick & Coe 1983). Locally, graded banding in the less deformed meta-gabbro and meta-anorthosite units and a transition from coarse-grained, cumulate-like to finer-grained, banded, sheared rocks is observed. The mineralogy is dominated by plagioclase, which locally forms megacrysts up to 10 cm in diameter, and hornblende up to 5 mm in diameter, with minor Czo, Bt, Qtz, opaques and accessory Zrn, Spn, Ap, Crn, Rt and Grt (Chadwick & Coe 1983). The amphibolite is a medium-grained rock mainly composed of Hbl, Cpx, Pl and Grt (Chadwick & Coe 1983). Several hundred meter wide bands of St-Grt-Sil-Bt schist are spatially associated with the amphibolite and are interpreted as meta-sediments (Chadwick & Coe 1983; Crowley 2002).

Two fold stages are obvious from the interference pattern on the maps (Fig. 1). The first stage forms outcrop-scale folds with E–W to ESE–WNW shallow easterly plunging fold axes. The second stage forms the dominant, map-scale, upright folds with fold axes plunging S to SW (Chadwick & Coe 1983; Crowley 2002). This second deformation stage is interpreted to slightly predate the intrusion of a pegmatite that was dated at 2710 ± 2 Ma (U–Pb zircon age), which is contemporaneous to amphibolite facies metamorphism dated at 2708 ± 4 Ma on monazite in St-Grt-Sil-Bt schist (U–Pb, Crowley 2002). A late thermal event was dated by U–Pb titanite dating at 2510 ± 5 Ma in the Ikkattoq gneiss, but its significance is, so far, unclear (Crowley 2002).

## Tasiusarsuaq terrane

The Tasiusarsuaq terrane extends from approximately Ameralik in the north to Grædefjord in the south (Fig. 1). It consists mainly of TTG gneiss that yielded zircon U–Pb ages between 2920–2810 Ma with a maximum between 2860–2840 Ma, which are interpreted as intrusion ages (Crowley 2002; Friend & Nutman 2001; Nutman & Friend 2007; Næraa & Scherstén 2008; Schiøtte *et al.* 1989). Supracrustal rocks occur as small lenses and belts in the TTG gneiss and are dominated by amphibolite and mafic granulite with minor meta-sediments and meta-ultramafic rocks (Chadwick & Coe 1983; Friend *et al.* 1996). The amphibolite and the meta-ultramafic rock, locally, show pillow structures testifying to their volcanic origin (Scherstén *et al.* 2008). Their trace element pattern is similar pointing to a MORB-like signature for both rock types. The meta-ultramafic rock has a komatiitic composition (Scherstén *et al.* 2008). However, it must be noted that most of the data stems from Nunatak 1390 far east in the terrane and, although geochemical signatures are similar, a correlation of rocks from the nunatak and from the main land is, to date, not straight forward. The same is true for an age estimation of the supracrustal suite by U–Pb zircon dating of a meta-rhyolite from Nunatak 1390 that yielded an age of  $2876 \pm 5$  Ma (Næraa & Scherstén 2008).

In the south, mostly conformable layers of porphyritic granitoids, the Ilivertalik granite, occur in a zone that extends about 50 km in E–W direction and 20 km in N–S direction (Fig. 1). The syn- to late-tectonic granitoid locally contains hyperstene owing to its intrusion into the deeper crust at  $2835 \pm 10$  Ma (Pidgeon & Kalsbeek 1978). Granulite-facies metamorphism was dated on a metamorphic zircon at  $2795 +11/-7$  Ma (Pidgeon & Kalsbeek 1978).

Granulite-facies metamorphism is the characteristic metamorphic facies of the Tasiusarsuaq terrane (Chadwick & Coe 1983). The granulite-facies was followed by amphibolite-facies retrogression, which was nearly complete in a several km wide band at the northern terrane boundary to the Tre Brødre terrane (Friend *et al.* 1987, 1988; Nutman *et al.* 1989). The granulite-facies metamorphic stage was dated at the northern terrane boundary by U–Pb zircon dating of an Opx-bearing pegmatite at  $2805 \pm 2$  Ma, which is within error of the age estimation of granulite-facies metamorphism in the south (Crowley 2002). Amphibolite-facies retrogression was dated using metamorphic Zrn, Tnt and Mnz suggesting that this lasted from ca. 2740–2700 Ma (Crowley 2002).

Two fold stages are obvious from the interference pattern on the maps (Fig. 1). The first stage forms outcrop-scale folds with E–W to ESE–WNW shallow easterly plunging fold axes. The second stage forms the dominant, map-scale, upright folds with fold axes plunging S to SW (Chadwick & Coe 1983; Crowley 2002).

# Regional geology of the Buksefjorden and Kangiata Nuna map sheets (63 V. 1/2 N)

## The Tasiusarsuaq terrane

The Buksefjorden and Kangiata Nuna map sheets are dominated by 3 different Archaean lithological units of the Tasiusarsuaq terrane (cf., Fig. 1): (1) TTG-gneiss, (2) supracrustal, mainly mafic meta-volcanic rocks, and (3) the Ilivertalik and Taserssuatsiait granitoids (Fig. 1). These rocks are intruded by a conjugate set of un-metamorphosed dolerite dykes of possible Proterozoic age. They are near vertical and trend either E–W or NE–SW.

The TTG-gneisses comprise numerous variations of gneissic to migmatitic rocks with streaky, nebulitic and agmatitic fabrics (Fig. 2a). The fabrics and the foliation pattern of the gneiss may vary on an outcrop scale from strongly to even weakly foliated with porphyritic textures. The contacts between rocks of different fabrics are always gradational. Mineralogically, the gneiss is generally medium-grained with abundant Qtz, Pl and mafic minerals, which are either Bt or Hbl or Opx commonly surrounded by Hbl. Locally, Mag and Ms are observed. This suggests that at least some of the gneissic rocks were metamorphosed in the granulite-facies and then retrogressed under amphibolite-facies conditions. Opx appears to be more abundant in the southern parts of the Kangiata Nuna map sheet. The intrusion age of tonalitic gneiss was estimated at  $2868 \pm 4$  Ma by zircon dating (Næraa & Scherstén 2008). A metamorphic age was estimated based on zircon dating at  $2719 \pm 5$  Ma (Næraa & Scherstén 2008).

The supracrustal rocks form a few larger belts and numerous smaller lenses and stringers within a gneiss matrix (Fig. 1). Locally, pillow fabrics were observed by previous mappers owing to the volcanic nature of the rocks. No primary contact relationships were observed; all contacts between supracrustal rocks and gneiss are tectonic. The larger supracrustal belts represent km-scale upright synforms with moderately SE plunging fold axis (Fig. 3b). In the N of the Buksefjorden and Kangiata Nuna map sheets, the supracrustal rocks comprise generally medium-grained, locally layered, granoblastic amphibolites with (i) a Hbl, Pl, Qtz, Bt assemblage or (ii) a Hbl, Grt, Pl, Qtz  $\pm$  Cpx assemblage. About 5 cm wide pegmatitic to aplitic dykes and about 20 cm thick pockets occur in the amphibolite, comprising Qtz, Pl  $\pm$  Hbl (Fig. 2b). Dykes and pockets have a 1–2 cm wide Hbl halo. To the S, the supracrustal rocks are characterised by medium-grained, locally layered, granoblastic mafic granulite, consisting of Hbl, Pl, Opx, Grt  $\pm$  Cpx. Supracrustal belts in the Buksefjorden area, additionally, contain large proportions of “leucogabbro”, a coarse-grained mafic granulite consisting of Opx, Cpx, Pl, Hbl, and, locally, Grt (Fig. 2c). In contrast, the Kangiata Nuna map sheet is characterized by the local presence of up to 100 m wide lenses of ultramafic granulite (Fig. 2d), which comprise (i) a massive, medium-grained greenish to brownish weathering rock with an Ol, Grt, Bt, Mag, Opx assemblage, (ii) a layered, medium-grained grey rock with a Cpx  $\pm$  Pl, Mag assemblage, and (iii) a massive, medium-grained, black rock with a Cpx, Opx, Po, Mag assemblage.

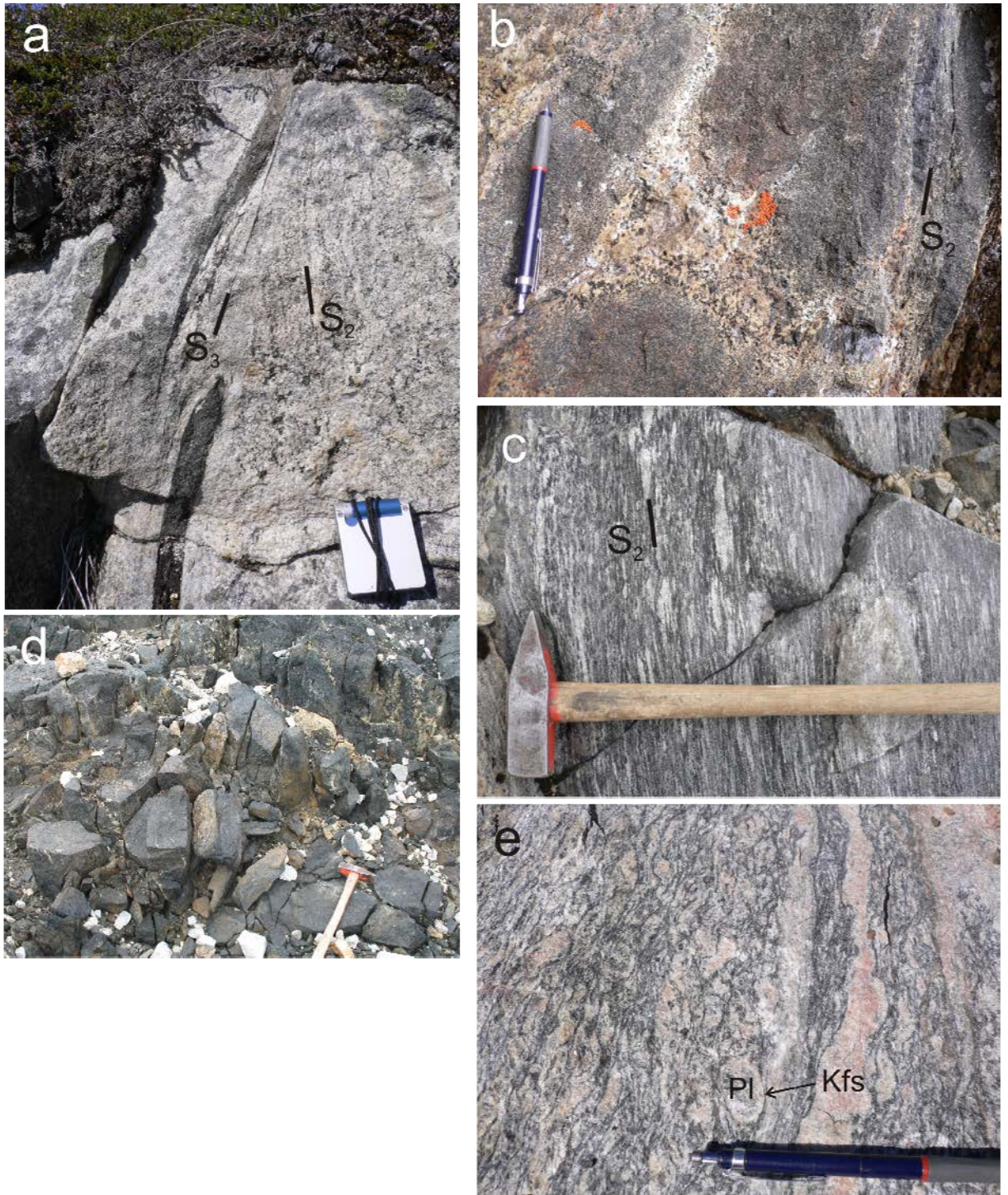


**Figure 2.** (a) Characteristic TTG gneiss with a nebulitic fabric and weak foliation. Note the amphibolite boudins (08dms3). (b) Mafic granulite with a typical pocket of felsic material comprising Qtz, Pl  $\pm$  Hbl, interpreted as a melt pocket indicating in situ partial melting. Note the gradual increase of felsic material towards the melt pocket (08dms10). (c) A coarse-grained mafic granulite consisting of Opx, Cpx, Pl, Hbl mapped as “leucogabbro” (08bms73). (d) A massive, fine-grained meta-ultramafic rock that is only weakly foliated and, locally shows the typical brownish weathering colour (08dms64). (e) Augen gneiss of the Ilivertalik granitoid from inner Sermilik, showing the characteristic rapakivi-fabric (08bms128).

These ultramafic rocks are relatively rare in the Buksefjorden area, where they are generally less than ca. 5–10 m thick. In the supracrustal belt 1, located about 20 km northeast of Isortuarssuup tasia, about 500 m thick, medium-grained, granoblastic pyroxenite with a Cpx, Ilm, Mag assemblage occurs overlying the mafic granulite. A thin layer (1–10 m thick) of pyroxenite forms the uppermost unit and shows abundant pillow fabrics. Feeder dikes to this unit, about 1–30 m thick, crosscut mafic granulites and pyroxenites. Locally observed Grt-Bt schist is interpreted to represent a metasedimentary rock. It comprises Bt, Grt, Qtz, fibrous Sil, Pl, Crd and minor Ap and Zrn.

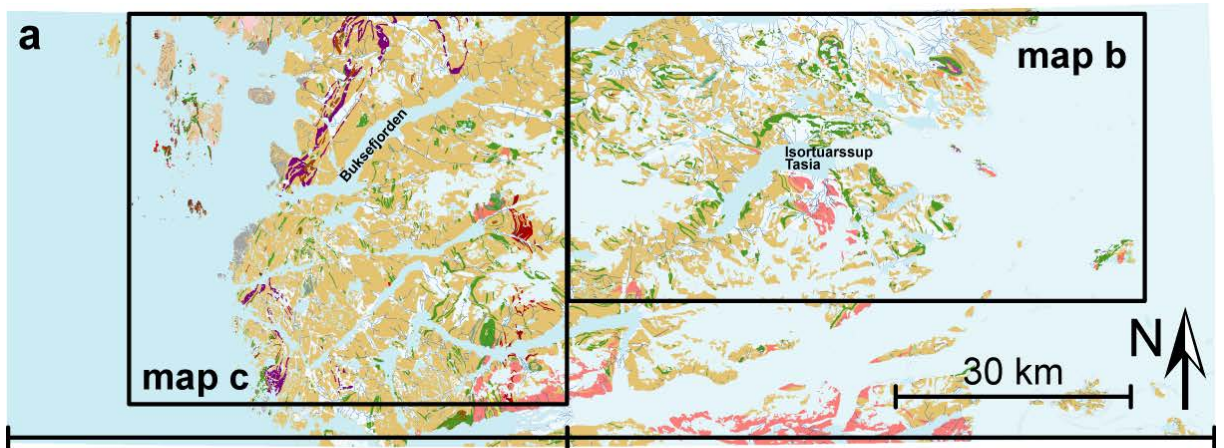
The rocks of the Ilivertalik and the Taserussuatsiait granitoids intruded TTG-gneiss and supracrustal rocks. In the study area, various rocks are correlated with the Ilivertalik granitoid (Fig. 2e) based on their intrusive relationship to the country rocks. Dioritic to granodioritic, mainly homogeneous medium-grained gneiss range in composition from Bt, Hbl, Pl, Qtz ± Opx to more felsic Pl, Kfs, Bt, Qtz ± Hbl, Ap assemblages. The feldspar is recrystallized and forms myrmekitic textures and, locally, antiperthitic exsolution fabrics. Quartz shows a chess-board pattern indicating deformation in the high-quartz field. Possibly related to this are variably deformed, up to 10 m wide granitic gneiss layers and abundant pegmatites. The Taserussuatsiait granite is best exposed in the central parts of the Buksefjord map sheet, where it mainly consists of Kfs, Qtz, Pl, Opx, and Cpx. The intrusive relationships and granulite-facies mineral assemblage suggest that it intruded before the peak of granulite facies metamorphism.

## Structural geology

The general map pattern of the Tasiusarsuaq terrane is characterised by the outline of the supracrustal, mainly mafic meta-volcanic rocks, which display an open to close fold pattern with SE trending axial traces, and the massive intrusion of the Ilivertalik and the Taserussuatsiait granitoids in the S (Figs. 1 & 3). The fold pattern represents the latest deformation stage before the mainly brittle faults developed. In detail, the rock fabrics indicate 4 different deformation stages ( $D_1$ – $D_4$ ).

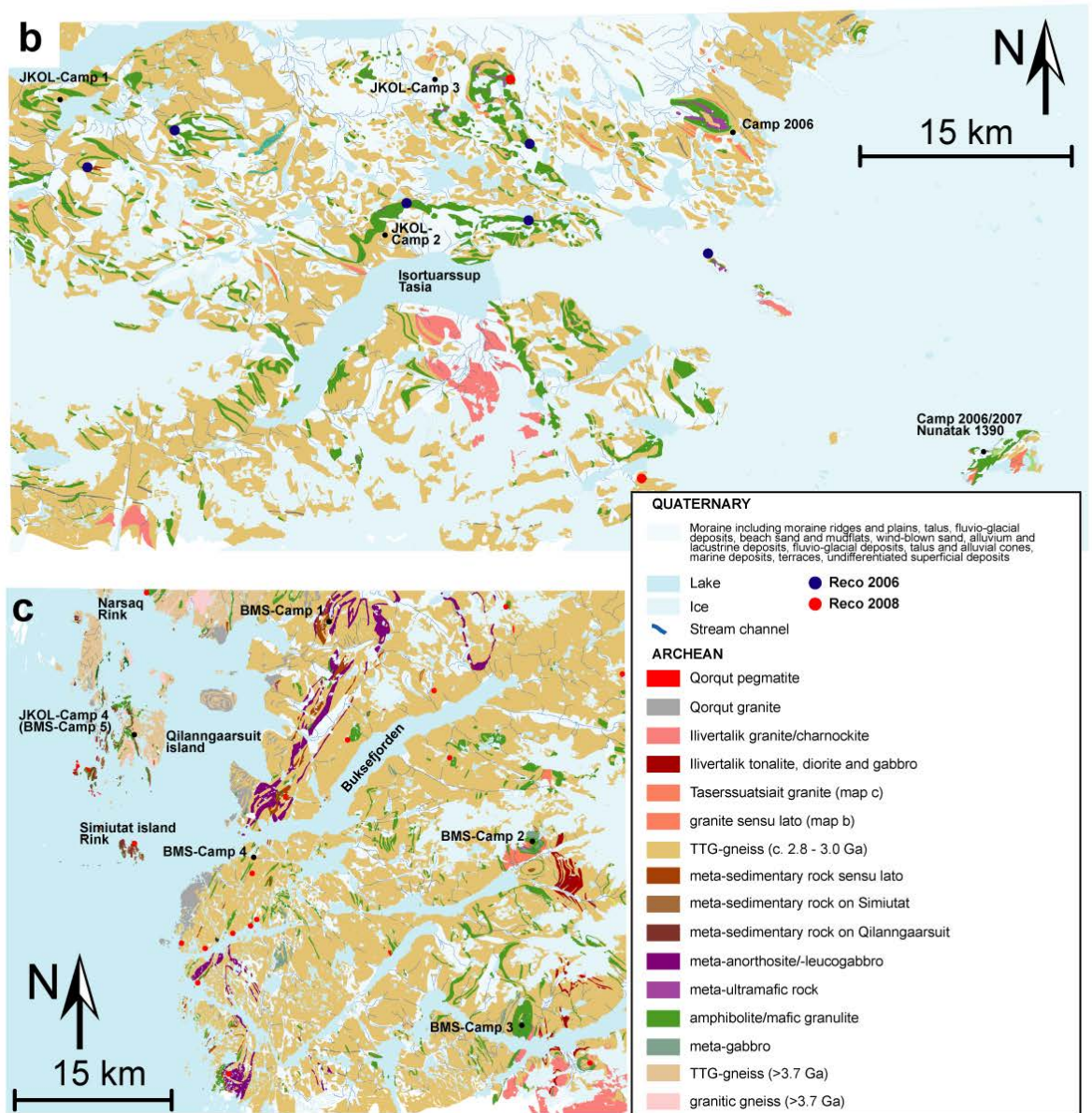
$D_1$  fabrics are preserved in low strain enclaves, where a  $S_1$  foliation and/or  $S_1$ -parallel aplitic dykes are preserved in later isoclinal folds (Fig. 4a). This is mainly observed in the TTG gneiss. In the S, the  $S_1$  foliation is defined by Cpx and Opx and the  $S_1$ -parallel dykes contain Opx that is often surrounded by a Hbl halo, which suggests that the  $D_1$  deformation stage occurred under granulite-facies conditions (Fig. 4b).

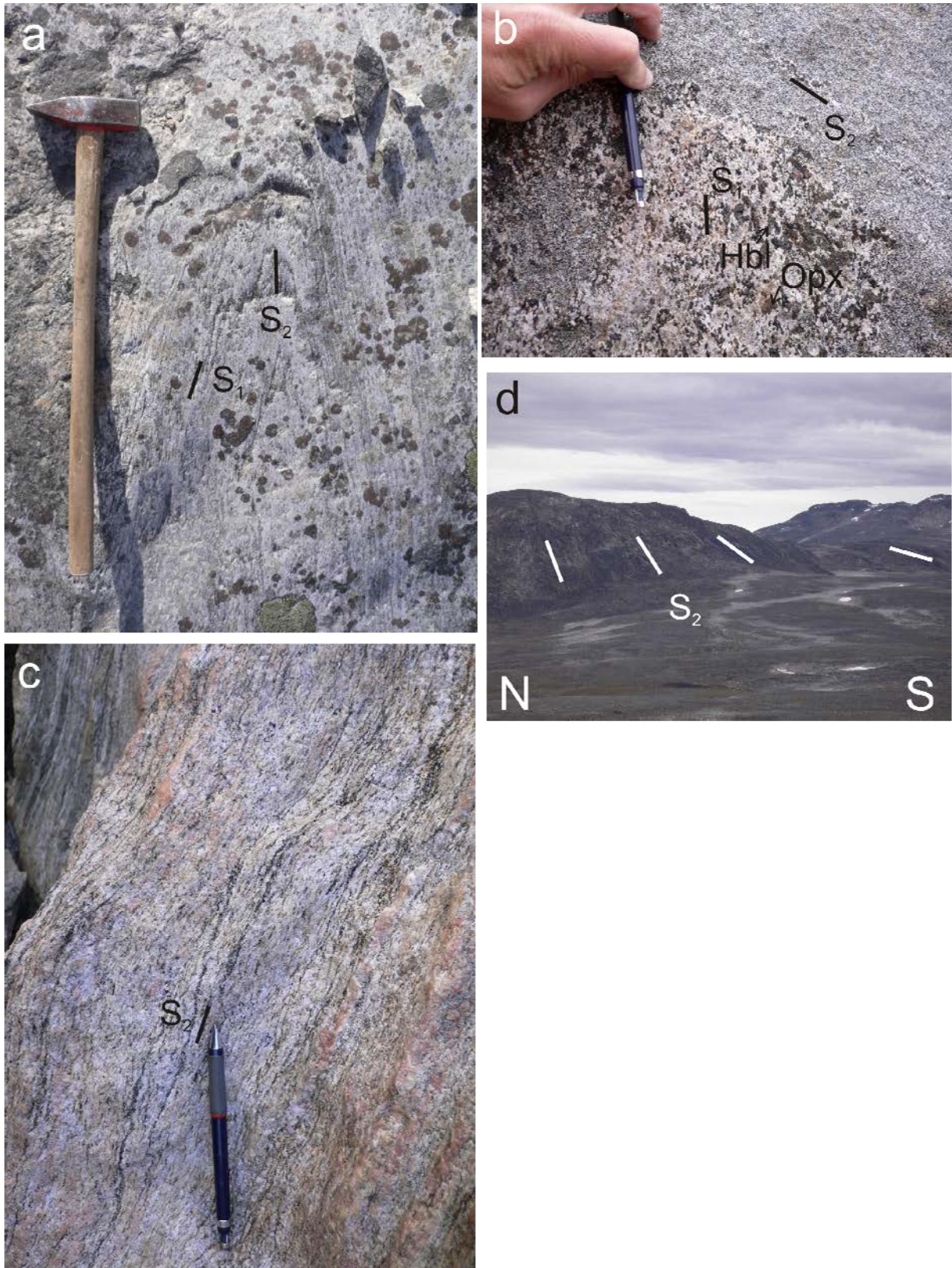
**Figure 3.** (a) Geological overview over the study area south of Nuuk (cf.; Fig. 1). (b) Enlarged geological map of the Kangiata Nuna area showing the sites that were studied during field work. Note the mushroom-like fold interference pattern around camp 3. Most of the mafic granulite-amphibolite sheets form synforms with fold axes plunging SE. The synforms are sheared off along NW–SE trending shear zones. (c) Enlarged geological map of the Buksefjord area showing the sites that were studied during field work. The map pattern is dominated by synform-antiform pairs that have N-S trending axial traces.



from 1:100 000 map-sheet 64 V. 1 SYD

from 1:100 000 map-sheet 64 V. 2 SYD

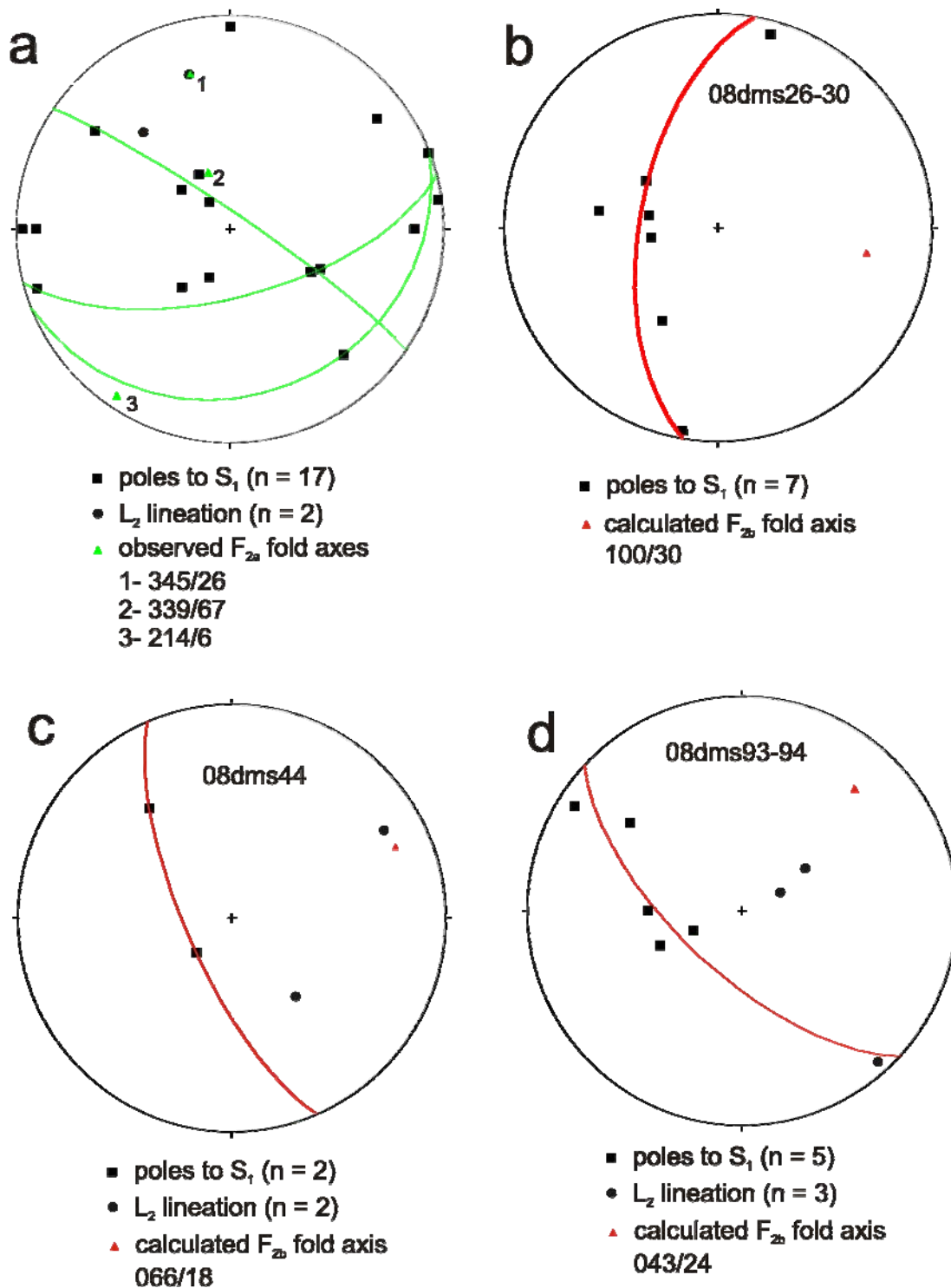




**Figure 4.** *D<sub>2</sub> fabrics. (a) TTG gneiss showing a typical F<sub>2a</sub> fold of the S<sub>1</sub> foliation. The S<sub>2</sub> foliation forms an axial planar foliation (08dms9). (b) Coarse-grained pocket in gneiss with Opx and retrograde Hbl parallel to S<sub>1</sub>. The finer-grained gneiss is characterised by Hbl parallel to S<sub>2</sub> (08dms95). (c) Typical appearance of the mylonitic gneiss with a closely-*

*spaced S<sub>2</sub> foliation (08dms46). (d) Regional variation of S<sub>2</sub>-orientation in a N–S section due to F<sub>2b</sub> folding with slightly ENE plunging fold axis.*

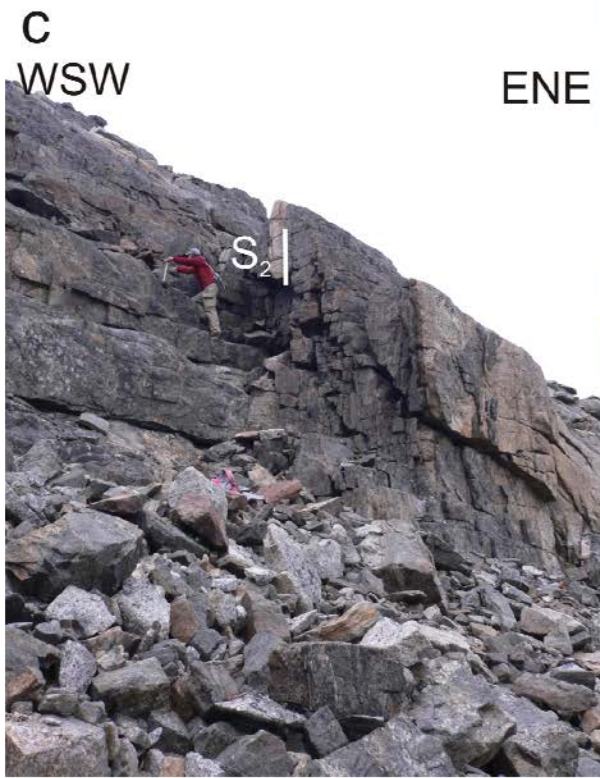
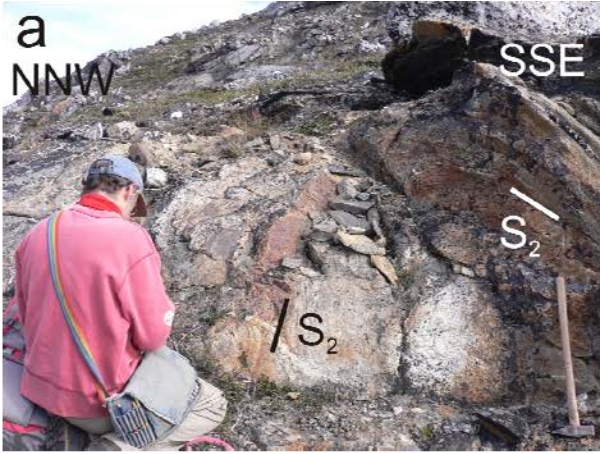
During D<sub>2</sub>, the S<sub>1</sub> foliation was isoclinally folded (F<sub>2a</sub>) and an axial planar S<sub>2</sub> foliation developed. The isoclinal F<sub>2a</sub> folds form rootless, intrafolial folds in S<sub>2</sub> or, in low strain enclaves, form up to 50 cm wide (half wavelength) rootless folds (Fig. 4a). The axial plane is always parallel to S<sub>2</sub>, however, the F<sub>2a</sub> fold axes are variable and show no distinct orientation maximum (Fig. 5a). The S<sub>2</sub> foliation is the penetrative foliation in the map sheet area and is mainly closely spaced and defined by Bt, Hbl, Cpx, and Pl (Fig. 4c). Several 10's of meters wide mylonitic zones with S<sub>2</sub> as the mylonitic foliation are observed, but were not mapped out in this field project. The F<sub>2a</sub> fold axes are parallel to the mineral stretching lineation in these zones (Fig. 5a). The mineral stretching lineation (L<sub>2</sub>) defined by Hbl, Cpx, and Pl plunges at moderate angles (15°–50°) to the SE (Fig. 5a). Shear sense indicators such as  $\sigma$ -,  $\delta$ -clasts and S-C fabrics point to a reverse sense of movement broadly to the NW. Boudins of amphibolite, about 1 m wide and up to 3 m long, are parallel to S<sub>2</sub> and L<sub>2</sub>, and display necking perpendicular to L<sub>2</sub>. Away from these shear zones, the S<sub>2</sub> foliation is locally folded into upright, open to close F<sub>2b</sub> folds with a wavelength of up to 3 km (Fig. 4d). The F<sub>2b</sub> fold axis is oriented approximately perpendicular to the mineral stretching lineation and plunges at shallow angle to the ENE (Figs. 5b–d).

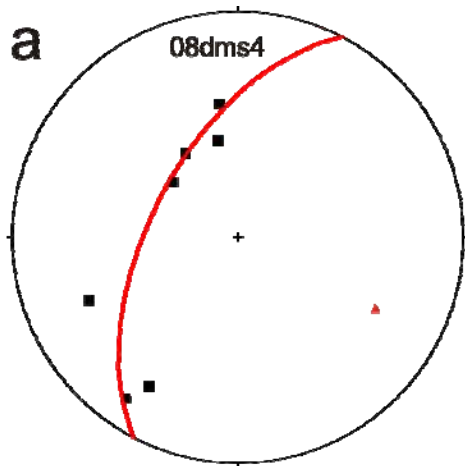


**Figure 5.** Pole figures for  $D_1$  and  $D_2$  fabrics (equal area, lower hemisphere projection). (a) Poles to  $S_1$  foliation plotted together with observed  $F_{2a}$  fold data as great circles. Note that  $b_{2a}$  are variable and locally overlap with measured  $L_2$ , suggesting that they represent an intersection lineation between  $S_1$  and  $S_2$ . (b), (c), (d) Poles to  $S_1$  and  $L_2$  lineation data from different outcrops, indicating that  $S_1$  transposed into  $S_2$  is folded into  $F_{2b}$  folds with variable, shallow E–NE plunging fold axes. Some of the  $L_2$  lineation measurements overlap with the calculated fold axes and, thus, represent intersection lineations. Some  $L_2$  lineation data shows SE plunge interpreted as the orientation of a  $L_2$  mineral stretching lineation.

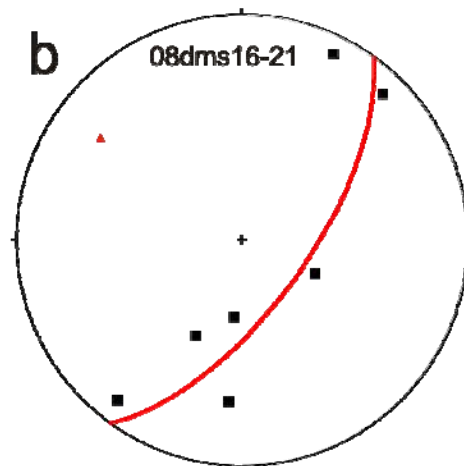
The  $D_3$  stage represents the regional-scale fold stage that is obvious from the map pattern. The  $S_2$  foliation is folded into upright, open to tight folds with NW–SE trending axial traces on a km-scale (Figs. 1 & 3). Higher order folds down to cm-scale are abundant (Figs. 6a & b). The  $F_3$  fold axes mainly plunge at shallow to moderate angles ( $5^\circ$ – $25^\circ$ ) SE (Fig. 7a–e), but non-cylindrical folds were also observed with  $b_3$  plunging both SE and at around  $20^\circ$  NW (Fig. 7b). Locally, type 2 fold interference patterns incorporating  $F_{2b}$  and  $F_3$  folds form weak mushroom-like patterns on the map (Fig. 3b), because the relief of the area is too high to show the ideal pattern (Ramsay & Huber 1987). The  $F_3$  folds show a repeated, progressive decrease in wavelength from gentle to isoclinal, which is connected to an increase in amplitude at various scales. Near vertical limbs trending NW–SE often show chocolate-tablet boudinage of competent mafic lithologies, where the single boudins are about 20 cm wide and 50 cm long (Fig. 6c). The limbs of the tight to isoclinal  $F_3$  folds are sheared off. This is also observed at all scales: higher order folds are sheared off by up to 2 m wide shear zones, whereas map-scale folds are sheared off by 20–100 m and, locally, up to 1 km wide shear zones (Fig. 3b). The most abundant shear zones are characterised by a closely spaced, near vertical, NW–SE trending  $S_3$  foliation (Fig. 7f). The  $L_3$  mineral stretching lineation, defined by Hbl, Bt, and Pl, plunges predominantly at  $5^\circ$ – $20^\circ$  to the SE (Fig. 7f). Shear sense indicators such as  $\sigma$ -,  $\delta$ -clasts, S-C and S-C' fabrics are often ambiguous and both sinistral (Fig. 2a) and dextral sense of shear may be indicated in the same zone. If both sinistral and dextral sense are observed the indicators of sinistral sense of shearing dominate by approximately 80:20, but often are dextral shear sense indicators conspicuous by their absence. However, locally shear zones with predominant dextral shear sense indicators are observed. No systematic difference in the orientation of the shear zones,  $S_3$  foliation or  $L_3$  lineation is related to the different shear sense indicators. Recumbent, WSW-verging  $F_3$  folds are locally observed (mainly in the NW around camp 1), where the foot wall limb of anticlines is activated as up to 1 m wide, near horizontal reverse shear zones. The reverse deformation is directed to the WSW (Fig. 6d). The  $D_4$  stage is characterised by several sets of faults that were not studied in detail and are therefore grouped here. The main orientations of faults are NW–SE, N–S, and E–W (Figs. 1 & 3). They show a lateral displacement of marker horizons on the map by up to 1 km. Dolerite dykes are often parallel to the E–W-trending faults (Figs. 1 & 3).

**Figure 6.**  $D_3$  fabrics. (a) TTG gneiss showing a typical  $F_3$  fold of the  $S_2$  foliation. The fold has a flat southern limb and a steeper northern limb. The fold axis plunges to the SE. Note the rusty appearance of the gneiss surface, resulting from weathering of disseminated sulphide minerals (08dms12). (b) Higher-order  $F_3$  folds in gneiss (08dms57). (c) Chocolate-tablet boudinage of a mafic granulite on the steep limb of a  $F_3$  fold. The single boudins are about 20 cm wide and 50 cm long (08dms96). (d) Near horizontal  $D_3$  reverse shear zone in well-foliated, retrogressed mafic granulite (08dms2).

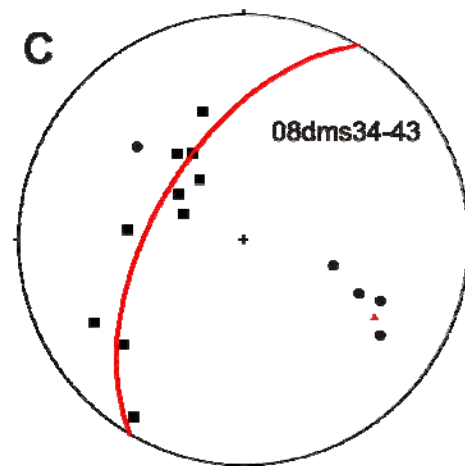




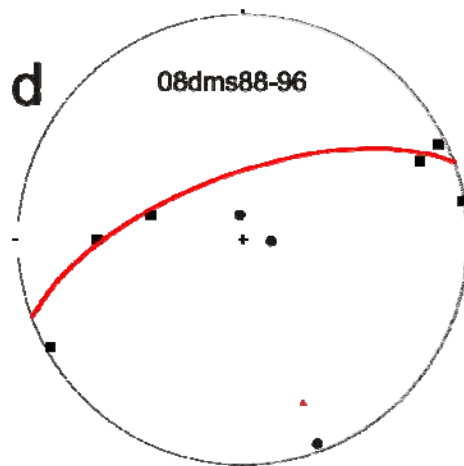
- poles to  $S_2$  ( $n = 7$ )
- ▲ calculated  $F_3$  fold axis 118/32



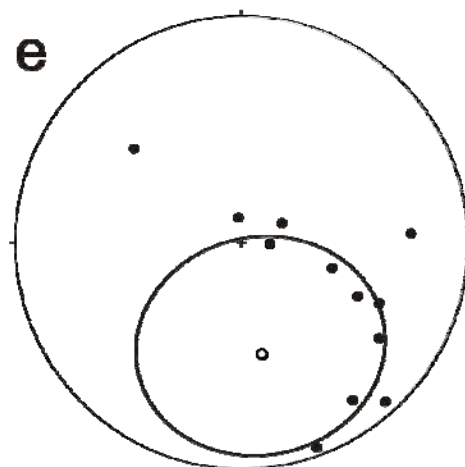
- poles to  $S_2$  ( $n = 8$ )
- ▲ calculated  $F_3$  fold axis 306/24



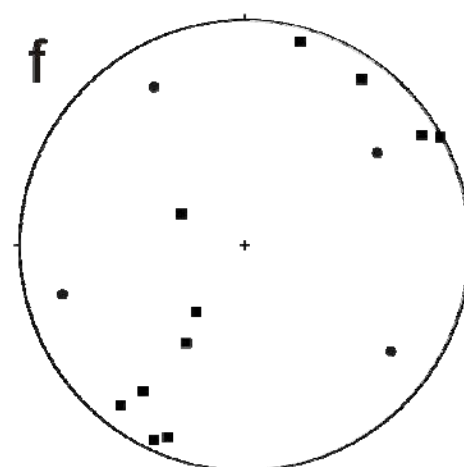
- poles to  $S_2$  ( $n = 10$ )
- $L_2$  lineation ( $n = 5$ )
- ▲ calculated  $F_3$  fold axis 120/33



- poles to  $S_2$  ( $n = 6$ )
- $L_2$  lineation ( $n = 3$ )
- ▲ calculated  $F_3$  fold axis 160/24



- $L_2$  lineation ( $n = 12$ )
- calculated small circle axis 170/48 (halfangle 43°)



- poles to  $S_3$  ( $n = 13$ )
- $L_3$  lineation ( $n = 4$ )

**Figure 7.** Pole figures for  $D_3$  fabrics (equal area, lower hemisphere projection). (a)–(d) Poles to  $S_2$  and  $L_2$  data from different outcrops. The data were used to calculate  $F_3$  fold axes.  $L_2$  lineation data cluster around the calculated fold axes, but also show marked deviation from the  $b_3$  orientation. (e)  $L_2$  lineation data summarised from outcrops from the entire Kangiata Nuna map sheet. The  $L_2$  lineation data have a small circle symmetry indicating that the  $L_2$  lineation was deformed by folding. The calculated small circle has an opening angle of  $43^\circ$  and an axis plunging  $170/48$  consistent with the regional  $F_3$  fold geometry. The interpretation of this  $L_2$  lineation symmetry is, that the lineation originated as mineral stretching lineation during  $D_2$  deformation and was later folded together with the  $S_2$  foliation during  $D_3$ .

## The Tre Brødre Terrane

The Tre Brødre terrane forms a prominent north–south trending belt along the coastline on the Buksefjorden map sheet (Figs. 1 & 3). The terrane consist of TTG gneiss (the 2825 Ma Ikkattoq gneiss; Crowley, 2002), abundant, up to several km thick and dismembered meta-anorthosite complexes, minor mafic metavolcanic rocks as well as a variety of clastic metasedimentary rocks. The rocks are metamorphosed to amphibolite facies conditions. Locally, the sequence has been intruded by pegmatite dyke swarms that crosscut all lithological units.

The TTG gneiss was not studied in detail, and will only briefly be discussed. The Ikkattoq gneiss is generally granodioritic in composition, and contains a well-developed foliation. The contact between the gneiss and supracrustal rocks is tectonic, primary intrusive relationships were not observed. In the camp 1 area on the Buksefjorden map sheet, the gneiss consists of Qtz, Pl, Kfs and Bt and/or Hbl, with Pl commonly forming up to 1 cm large porphyroclasts.

The clastic metasedimentary rocks are exposed as an up to several hundred m thick and dismembered sequence of fine- to medium-grained aluminous paragneiss. The paragneiss is pervasively foliated and strongly migmatitic, and is made up of variable proportions of Grt, Bt, Crd, Oam, Sil, Qtz, Op, Pl, Kfs, and, locally, St, Chl and And. The leucosomes are made up of Qtz, Pl, and locally Grt (Fig. 8a). A characteristic feature of the paragneiss is the development of Crd coronas rimming the up to several cm large Grt porphyroblasts (Fig. 8b). This replacement texture is probably related to decompression at relatively high temperatures. The paragneiss locally preserves irregular-shaped pyroclasts that vary in size between a few mm to up to several cm (Fig. 8c). These textures are restricted to low-strain domains, i.e. mega-boudins that are aligned parallel to the foliation. Within the boudins, the rocks are unfoliated. The pyroclasts are embedded in a highly aluminous matrix that is dominated by up to several cm long Sil needles (Fig. 8c). The irregular-shaped pyroclasts consist of medium-grained Qtz-Fsp aggregates. Mafic metavolcanic rocks are relatively rare in the Tre Brødre terrane. Where exposed, they form thin layers and boudins of amphibolite, with a maximum thickness of ca. 10 m. The typical mineral assemblage is Hbl, Pl, and Qtz. In the study area, rare amphibolite boudins with a mineral assemblage of Grt, Hbl, Oam, Cpx, Pl, Qtz contain abundant leucosomes, pointing to in situ partial melting (Fig. 8d).

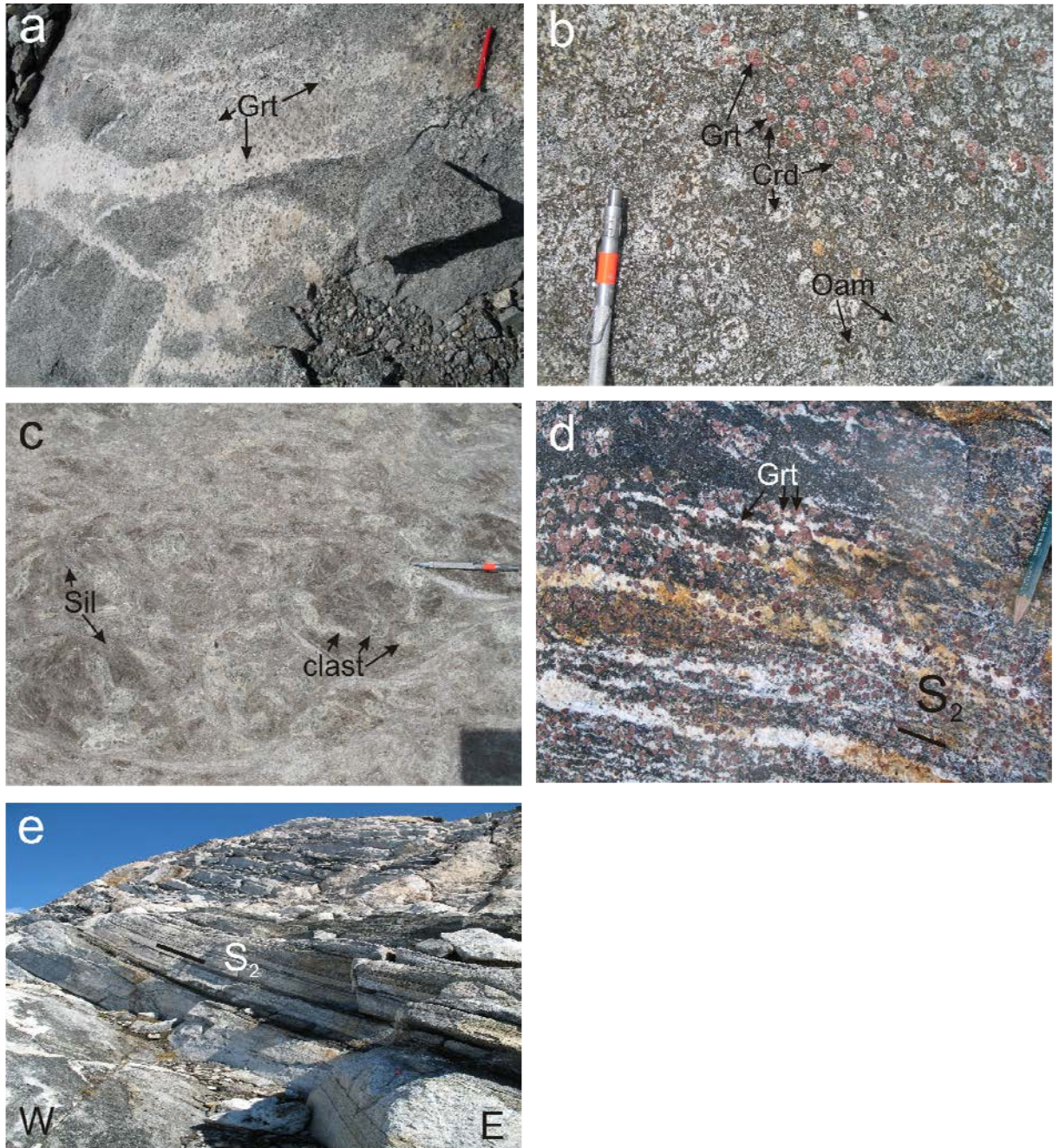


**Figure 8.** (a) Typical massive, medium-grained paragneiss with abundant leucosomes. The rock is mainly composed of Grt, Oam, Bt, Pl and Qtz, and Qtz, Pl and Grt in the leucosome. (b) Enlargement of (a) showing the characteristic corona textures with Crd rims surrounding Grt in the core. (c) Paragneiss with whitish angular clasts that are interpreted representing pyroclasts in a meta-pyroclastic rock comprising several cm long Sil needles in the matrix. (d) Garnet amphibolite with leucosomes parallel to the  $S_2$  foliation. Note that Grt overgrows the  $S_2$  foliation indicating late- to post-tectonic Grt-growth. (e) Characteristic outcrop of the finely banded, light grey anorthosite. The banding marks the closely-spaced  $S_2$  foliation.

The anorthosite forms up to 30 m thick sheets that are intercalated with the mafic volcanic rocks and paragneiss. The Pl-dominated anorthosite contains a well-developed foliation that is defined by up to one cm thick and several dm long schlieren, consisting of Cpx, Hbl and Mag (Fig. 8e).

## Structural geology

The general map pattern of the Tre Brødre terrane in the study area is characterized by two different structural domains. The southern part of the Tre Brødre terrane is exposed as a N–S trending high-strain belt that is dominated by schistose to mylonitic ortho- and paragneisses that are interlayered with amphibolite (Fig. 3c). In the north, the supracrustal rocks and anorthosites define an open to tight upright fold pattern with southerly trending axial traces. This fold pattern represents the regional  $D_3$  deformation that predates the intrusion of the pegmatite dykes. In detail, three deformation stages can be distinguished:  $D_1$  fabrics are only preserved in the fold hinges of rare, rootless, isoclinal, intrafolial folds in the Ikkattoq gneiss (Fig. 9a). A  $S_1$  foliation is developed as a cm-scale banding, and it is likely that this early deformation also occurred under amphibolite facies conditions. During  $D_2$ , the  $D_1$  fabrics were isoclinally folded ( $F_{2a}$ ), and an axial planar  $S_2$  foliation developed (Figs. 9a). The  $S_2$  foliation is best-developed in the amphibolite and paragneiss and is mainly closely spaced (Fig. 9b). It is defined by the peak metamorphic mineral assemblages, indicating that  $D_2$  occurred under amphibolite facies conditions. In the camp 1 area, the  $S_2$  foliation dips at ca.  $30^\circ$  to the S and SE. The rocks contain a well-developed mineral stretching lineation that plunges at ca.  $30^\circ$  to the SE. The lineation is defined by Sil, Crd, Oam, and Bt. Rare  $F_{2b}$  folds are oriented parallel to the mineral stretching lineation. Shear sense indicators such as  $\sigma$ -clasts and S-C fabrics point to a reverse sense of movement broadly to the N and NNW (Fig. 9b). Isoclinal  $F_{2a}$  folds have a near-vertical fold axis and are refolded into open to tight  $F_3$  folds with a half wavelength of about 50 cm and moderately southeast plunging fold axis (Figs. 9b and 10). The limbs of the  $F_3$  folds are parallel to the penetrative  $S_3$  foliation and commonly the  $F_3$  folds are sheared off at their limbs (Fig. 9c). The  $D_3$  deformation is characterized by regional-scale folding of the  $S_2$  foliation and subsequent intrusion of a prominent NE–SW trending pegmatite dyke swarm (Fig. 9d). The  $S_2$  foliation is folded into upright, N–S trending folds.

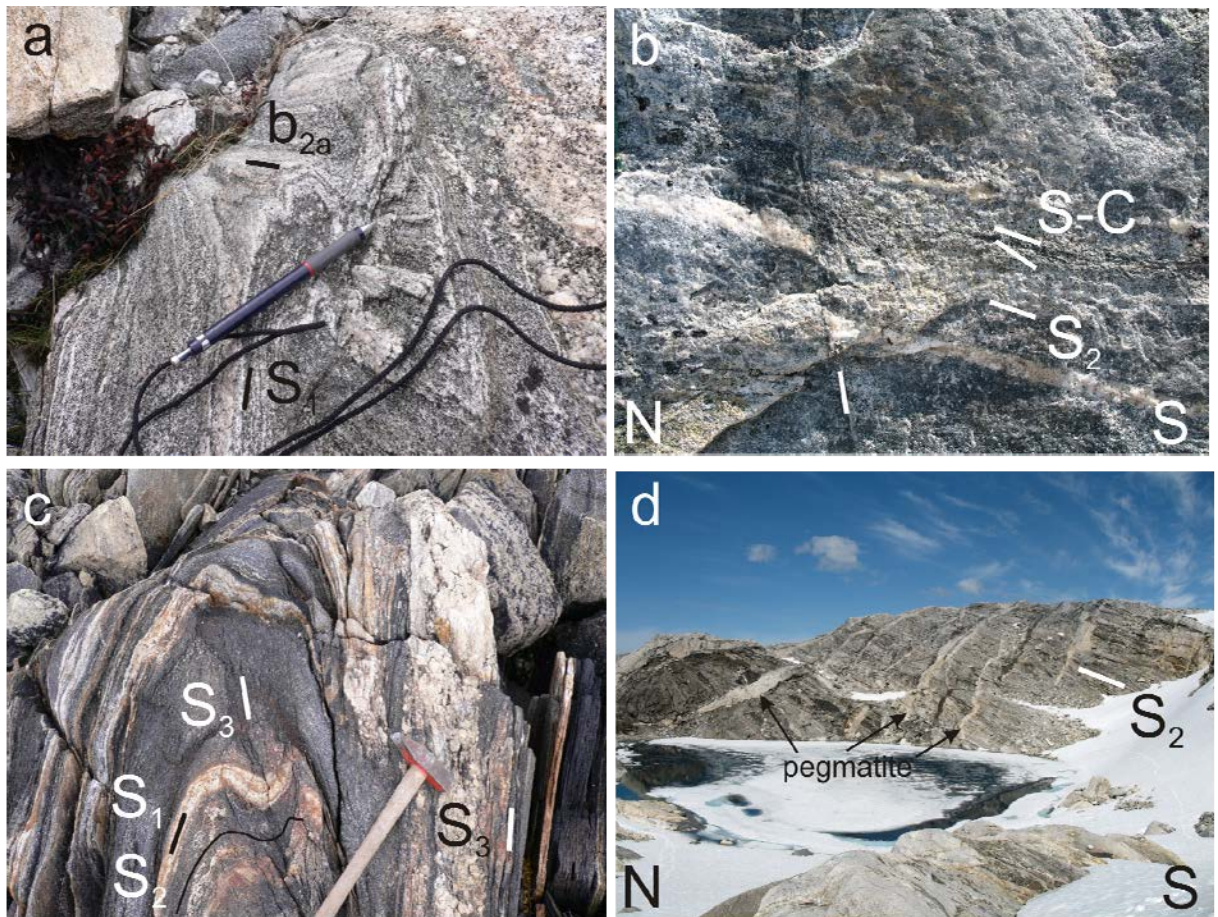


**Figure 9.** *Fabrics in rocks from the Tre Brødre terrane. (a) Gneiss showing typical  $F_{2a}$  folds of the  $S_1$  foliation. Plunge of the fold axis  $b_{2a}$  is near-vertical (08bms118). (b) Mylonitic paragneiss with a closely-spaced  $S_2$  foliation. The S-C fabrics point to a reverse sense of movement to the north. Note the late, near-vertical shear with the normal sense of movement in the centre of the photograph. This is interpreted to be related to late, possibly Palaeoproterozoic faulting. (c) Fold interference pattern in amphibolite with cm-scale felsic bands. The felsic bands mark the  $S_1$  foliation, which is folded into isoclinal  $F_{2a}$  folds. The  $F_{2a}$  folds are refolded by  $F_3$  resulting in a type 3 interference pattern in the outcrop (08bms118). (d) Pegmatite dyke swarm that intruded into the supracrustal rock assemblage.*

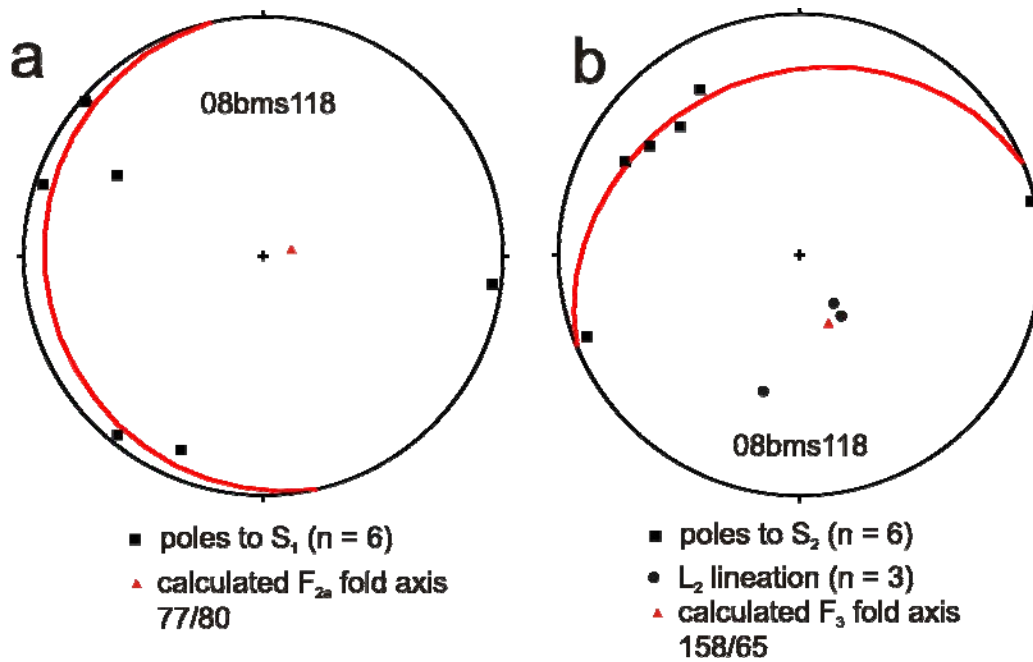


**Figure 10.** Pole figures for S<sub>1</sub>, S<sub>2</sub> foliations and L<sub>2</sub> lineation (equal area, lower hemisphere projection). (a) Poles to S<sub>1</sub> forming a F<sub>2a</sub> fold with a near-vertical F<sub>2a</sub> fold axis. (b) Poles to S<sub>2</sub> showing F<sub>3</sub> folding with a F<sub>3</sub> fold axis plunging at moderate angles to the SE. The L<sub>2</sub> lineation is parallel to the F<sub>3</sub> fold axis, probably representing an intersection lineation.

## Færingehavn terrane

The north-westernmost part of the Buksefjorden map sheet is dominated by Palaeo- to Mesoarchaeoan rocks of the Færingehavn terrane (Figs. 1 & 3c). The geology of the terrane was studied on the islands of Qilangaarsuit and Simiutat, which are situated about 15 km northwest of Buksefjorden and about 35 km south of Nuuk.

The ancient rocks on Qilangaarsuit are quartzo-feldspatic gneiss, metamorphosed mafic dykes, BIF and other metamorphic mafic to ultramafic rocks, formerly known as the Amitsoq gneiss, Ameralik dykes and Akilia association. These rocks were not studied in detail and, therefore, only a brief description is given. The gneiss is medium-grained with variable fabric ranging from banded, nebulitic to agmatitic (Fig. 11a). It comprises mainly Qtz, Pl, Bt and, locally, Hbl. Leucosomes are composed of Qtz, Fsp and Grt. Structural fabrics are variable ranging from weakly foliated gneiss characterised by cm-scale close to isoclinal folds in low-strain enclaves to finely banded mylonitic gneiss in high-strain zones. The metamorphosed Ameralik dykes are mainly homogeneous, black, medium-grained amphibolites comprising Pl, Hbl, Qtz and Di. They are a few m thick and can be followed 5–10 m along strike (Fig. 11a). Locally, they have apophyses into the wall rock. Discordant and concordant dykes are observed. The discordant dykes cross cut the S<sub>1</sub> foliation in the gneiss.

Amphibolites of the Akilia association are medium- to coarse-grained comprising Hbl, Pl, Qtz, Cpx and Grt and form lenses within the ancient gneiss. Locally, small lenses of BIF occur, comprising Qtz, Mag and Cpx in cm-scale layers (Fig. 11b).

The rocks of the ca. 2840 Ma Malene supracrustal sequence form up to 500 m thick tectonic sheets in the Palaeoarchaeon gneiss basement (Fig. 3c). The contact between the supracrustal rocks and the ancient gneiss is always tectonic. Two types of amphibolites are distinguished: (1) banded amphibolite shows a cm-scale lamination of dark Hbl-Pl-Qtz layers and pale Cpx-Hbl-Pl-Qtz layers together with abundant leucosomes (Fig. 11c); and (2) homogeneous, dark green amphibolite comprising Hbl, Pl, Qtz and Grt with local leucosomes (Fig. 11d). Meta-ultramafic rocks form up to 10 m thick lenses parallel to the main foliation (Fig. 3c). They comprise Ol, Opx, Hbl and Bt, and are locally retrogressed to Tr-Act schist. Meta-sedimentary rocks form brownish paragneiss, composed of Grt, Sil, Mag, Qtz, Pl, Bt and Oam (Fig. 11e). Locally, Grt has a Pl corona and bluish Ky is observed to be retrogressed to Sil. On northern Qilangaarsuit, small lenses of marble occur within the paragneiss. On Simiutat, the paragneiss has a distinct mineralogy and is made up of Crd, Oam and Qtz, and locally of Crd, Oam, St and Grt (Fig. 11f). These rocks are spatially associated with massive sulphide lenses mainly comprising Po.

Abundant thin horizons of Qtz – fuchsite Ms rocks are interpreted to represent quartz veins (Fig. 11g), because they occur structurally controlled at various tectono-stratigraphic levels. The rocks are intruded by various generations of pegmatite dykes and, later, by Palaeoproterozoic dolerite dykes.

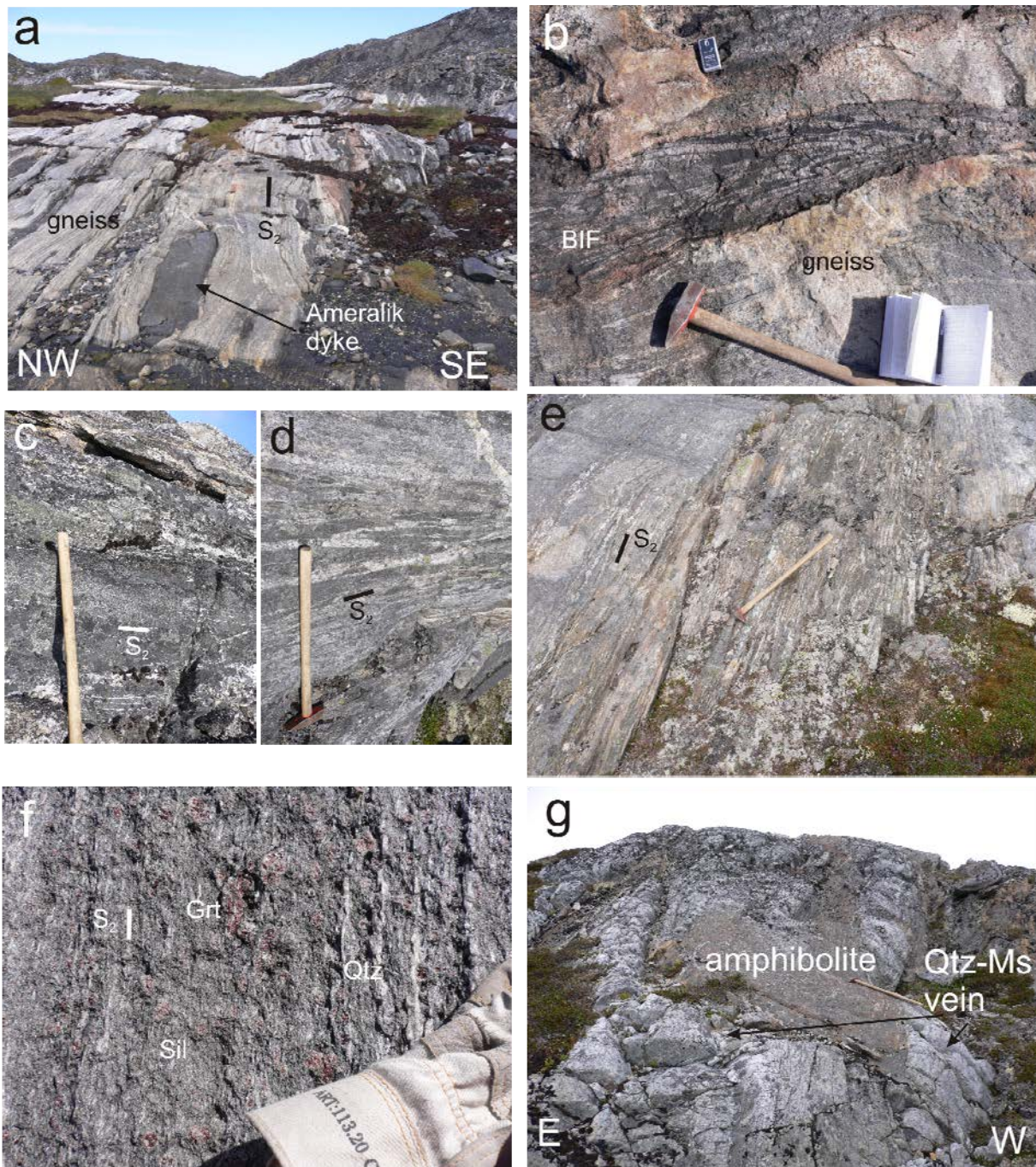


**Figure 11.** (a) Typical outcrop of the Palaeoarchaeon gneiss (Amitsoq gneiss) containing lenses of amphibolite representing Ameralik dyke parallel to a closely-spaced  $S_2$  foliation (08dms125). (b) Small, cm-scale BIF lens of the Akilia association in gneiss (08dms147). (c) Banded amphibolite showing lamination of black Hbl-Pl-Qtz layers and pale greenish Cpx-Hbl-Pl-Qtz layers together with abundant leucosomes parallel to the  $S_2$  foliation (08bms97). (d) Homogeneous amphibolite with abundant leucosomes parallel to the prominent  $S_2$  foliation. The leucosomes are, locally, folded into  $F_{2a}$  folds. Note the pegmatite dyke that cross cuts the main fabric in the upper right corner (08bms97). (e) Characteristic outcrop of paragneiss on Qilanngaarsuit, showing a prominent  $S_2$  foliation and parallel leucosomes (08bms97). (f) Paragneiss from Simiutat comprising Qtz, Grt, Sil and Oam. (g) Amphibolite lense cross cut by Qtz – fuchsitic Ms veins (08bms111).

## Structural geology

The structure is dominated by synform-antiform pairs marked by the 200–500 m wide layers of supracrustal rocks (Fig. 3c). The axial traces of these folds trend about N–S. In detail, four deformation stages ( $D_1$ – $D_4$ ) can be distinguished.

$D_1$  fabrics are only rarely preserved as  $S_1$  foliation in gneiss and amphibolite, that is folded into isoclinal, up to 30 cm wide (half wavelength), rootless  $F_{2a}$  folds during  $D_2$  (Figs. 12a & 13a). The axial plane of the  $F_{2a}$  folds is parallel to the  $S_2$  foliation. The  $F_{2a}$  fold axes are variable and show no distinct orientation maximum. One example of northern Qilangaarsuit shows a plunge of the  $F_{2a}$  fold axis to the SW (Fig. 13a). The pervasive foliation of the rocks is a closely spaced  $S_2$  foliation defined by amphiboles, Bt, Cpx, Pl, and Sil (Fig. 12b). The mineral stretching lineation ( $L_2$ ) is defined by amphiboles, Bt, Cpx, and Sil and plunges at moderate angles ( $15^\circ$ – $50^\circ$ ) to the S. Shear sense indicators such as  $\sigma$ -,  $\delta$ -clasts and S-C fabrics point to a reverse sense of movement broadly to the N (Fig. 13b). Especially at the hanging wall and foot wall contacts of supracrustal rocks and gneiss, the  $S_2$  foliation is closely spaced and represents a mylonitic foliation, indicating a sheared contact between gneiss and the supracrustal rocks. The  $S_2$  foliation is folded into upright, open to close  $F_{2b}$  folds with a wavelength of 500 m to 3 km (Fig. 12c). The  $F_{2b}$  fold axis is oriented approximately perpendicular to the mineral stretching lineation and plunges at shallow angle to the E (Fig. 13a).

The  $D_3$  stage represents the fold stage that is obvious from the map pattern (Fig. 3c). The  $S_2$  foliation is folded into upright, open to tight folds with N–S trending axial traces on a km-scale. Higher order folds down to cm-scale are abundant (Figs. 12d, e). The  $F_3$  fold axes mainly plunge at shallow to moderate angles ( $5^\circ$ – $25^\circ$ ) SE, locally forming non-cylindrical folds (Figs. 13c, d & 14).

The  $D_4$  stage is characterised by several sets of faults that were not studied in detail and are therefore grouped here. The main orientations of faults are NE–SW, N–S, and E–W. They show a lateral displacement of marker horizons on the map by up to 100 m. Dolerite dykes are often parallel to the E–W-trending faults.



**Figure 12.** (a) Low-strain area in gneiss showing cm-scale  $F_{2a}$  folds of a  $S_1$  foliation. The axial planes are parallel to the  $S_2$  foliation (08bms90). (b) Closely-spaced  $S_2$  foliation in amphibolite and paragneiss. Shear sense indicator point to transport towards east (cf.; Fig. 13b; 08bms97). (c) Homogeneous amphibolite showing a closely-spaced  $S_2$  foliation that is folded into an open  $F_{2b}$  fold, which has a shallow east-plunging fold axis (08bms104). (d) Fold interference pattern on a near-horizontal weathering surface of homogeneous amphibolite. Note the axial traces of the 3 different fold generations (08bms104). (e) Typical outcrop pattern of higher-order  $F_3$  folds in homogeneous amphibolite (08bms99).

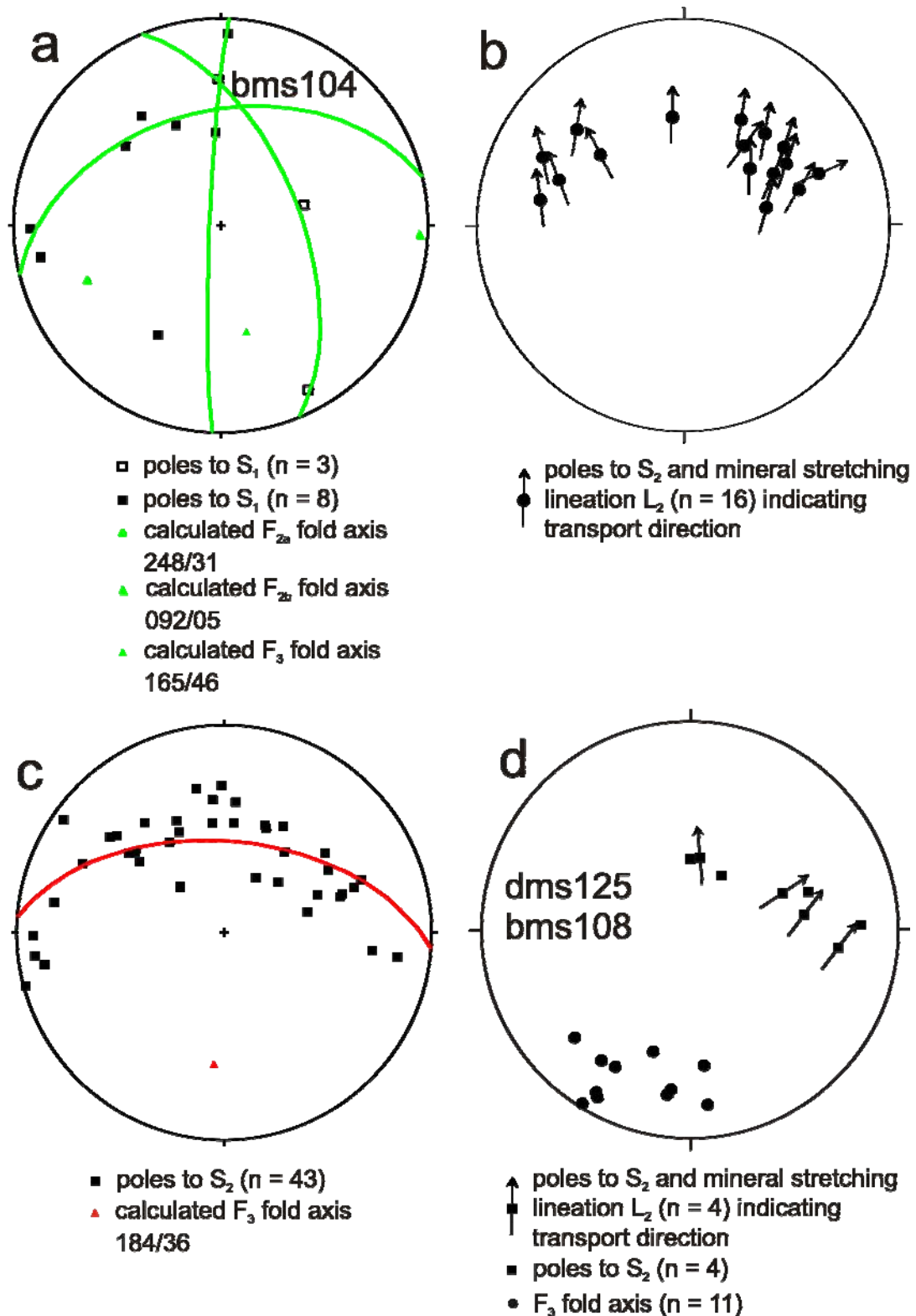


**Figure 13.** Pole figures for foliations and lineation collected from Qilangaarsuit (equal area, lower hemisphere projection). (a) Poles to  $S_1$  forming a  $F_{2a}$  fold with a  $F_{2a}$  fold axis plunging moderately to the SW. Poles to  $S_2$  forming a  $F_{2b}$  fold with a near-horizontal, E-plunging  $F_{2b}$  fold axis and a  $F_3$  fold with a moderately SSE-plunging  $F_3$  fold axis. In the outcrop, a complex triple fold interference pattern is developed. (b) Poles to  $S_2$  with arrow indicating orientation of mineral stretching lineation and sense of shearing (Hoeppener plot). (c) Poles to  $S_2$  with a distinct great circle geometry related to  $F_3$  folding. The

calculated  $F_3$  fold axis plunges moderately to the S. (d) Detailed outcrop data for one location showing  $S_2$ , mineral stretching lineation, sense of deformation and  $F_3$  fold axis data. The  $F_3$  folds in this outcrop are non-cylindrical indicated by the variability in  $F_3$  fold axes orientation.

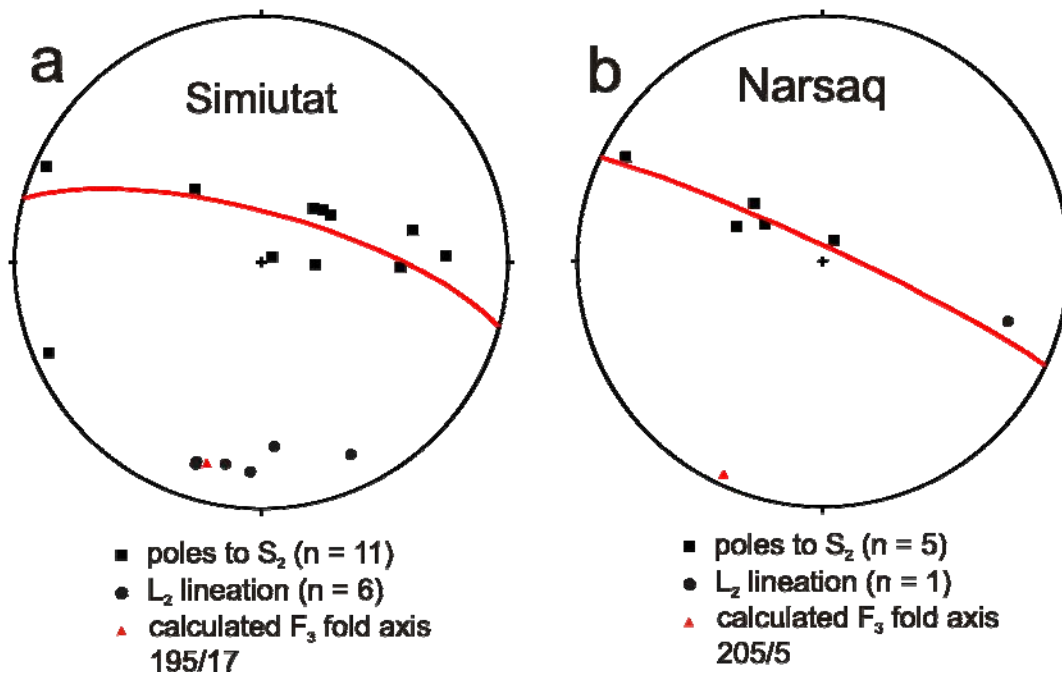


**Figure 14.** Pole figures for  $S_2$  foliations and  $L_2$  lineation from Simiutat and Narsaq (equal area, lower hemisphere projection). (a) Simiutat. Poles to  $S_2$  forming a  $F_3$  fold with a  $F_3$  fold axis plunging SSW. The  $L_2$  lineation clusters around the calculated fold axis, indicating that most of them represent intersection lineations. (b) Narsaq. Poles to  $S_2$  showing  $F_3$  folding with a  $F_3$  fold axis plunging at moderate angles to the SSW.

## Færingehavn straight belt and Qarliit Nunaat fault

In the Buksefjorden-Tre Brødre region, the Færingehavn straight belt and the Qarliit Nunaat fault form an about 5 km wide zone of well-foliated gneisses, which have mylonitic to ultramylonitic fabrics (Fig. 1, Crowley 2002; Friend *et al.* 1987, 1988; Nutman *et al.* 1989). The Tre Brødre terrane is only 200 m wide in this area (Fig. 1, Friend *et al.* 1987). The Qarliit Nunaat fault, the boundary between the Tasiusarsuaq and the Tre Brødre terranes, is represented by a zone of up to 50 m wide mylonites (Crowley 2002; Friend *et al.* 1987, 1988; Nutman *et al.* 1989). A late-tectonic pegmatite was dated at  $2725 \pm 2$  Ma by U–Pb zircon dating, which was interpreted that shearing along the Qarliit Nunaat fault occurred around 2725 Ma (Crowley 2002). Mineral lineations are reoriented by later deformation and shear sense indicators are either not present or ambiguous (Crowley 2002; Friend & Nutman 1991; Friend *et al.* 1987, 1988; Nutman *et al.* 1989). This later deformation formed the NNE–SSW trending Færingehavn straight belt at ca. 2565 Ma (Friend & Nutman 1991; Friend *et al.* 1987; McGregor *et al.* 1991; Nutman & Friend 2007; Nutman *et al.* 1989).

## Færingehavn – Kangerdluarssoruseq profile

This profile was studied in 2 days operated from Rink and a rubber dinghy. Detailed field studies were made around Færingehavn and several reconnaissance stops were made until about 8 km inland on the northern shore of Kangerdluarssoruseq.

The major lithology around the abandoned settlement of Færingehavn is tonalitic to granodioritic gneiss and amphibolite with a penetrative NNE–SSW trending foliation with moderate dips to the southeast. The gneiss comprises mainly PI, Qtz, Bt and Hbl. The amphibolite (Hbl, PI ± Qtz) forms 50 cm to several m wide lenses and rafts in the gneiss matrix parallel to the foliation. Numerous pegmatites intruded parallel to the foliation. They show variable width from 20 cm to up to several m and comprise mainly PI, Kfs, Bt and Qtz with a grain size to up to 1 cm (Fig. 15a). The pegmatites are variably deformed or undeformed: (1) The undeformed pegmatites can be followed over several 100 m parallel to the foliation; (2) Weakly deformed pegmatites show pinch and swell structures and (3) stronger deformed pegmatites have a foliation that is parallel to the penetrative foliation in the gneiss at the dyke walls. In the centre of the pegmatite dykes, the foliation changes from the general NNE–SSW trend to a more E–W oriented trend resulting in a sigmoidal fabric.

In low strain areas, fold interference pattern suggest two stages of deformation predating the development of the penetrative foliation in the Færingehavn area (see also, Crowley 2002; Friend & Nutman 1991). Isoclinal folds ( $F_{2a}$ ) of the  $S_1$  foliation have a near-vertical fold axis and are refolded into open to tight  $F_3$  folds with a half wavelength of about 50 cm and moderately southeast plunging fold axis (Figs. 9 & 10). The limbs of the  $F_3$  folds are parallel to the penetrative  $S_3$  foliation and commonly the  $F_3$  folds are sheared off at their limbs (Fig. 9c). In the western part of this profile, the  $S_3$  foliation is the dominant fabric representing a closely-spaced mylonitic foliation in an about 8 km wide belt, namely the Færingehavn straight belt (McGregor *et al.* 1986). The foliation shows moderate to steep dips to the SE with a prominent mineral stretching lineation plunging at moderate angles to the SSW (Figs. 15 & 16). The gneiss has a mylonitic to ultramylonitic fabric with only locally developed Fsp porphyroclasts (Fig. 15b). Shear sense indicators, such as  $\sigma$ - and  $\delta$ -clasts, S-C as well as S-C' fabrics, point to an oblique sinistral sense of shearing (Figs. 15b & 16). However, namely in the area around the abandoned settlement of Færingehavn and to the west, the foliation is steeper and, locally overturned, with down-dip lineation and a reverse sense of shear (Figs. 15c & 16). These reverse shear zones are discrete, up to 10 m wide zones that can be followed over several hundred m along strike (Fig. 15c). These structures were mapped as thrust (Chadwick & Coe 1983), but are probably better described as reverse shear zones because no large displacement along these relatively discrete structures is likely. Abundant pegmatites intruded parallel to this shear zone. Similarly in these reverse shear zones and the sinistral oblique-slip shear zones, the pegmatites show either no signs of internal deformation or weak pinch-and-swell fabrics as well as a weak foliation at their selvages. This suggests late- to post-tectonic intrusion of the pegmatites (Fig. 15c). The relative and absolute timing of the reverse and sinistral oblique shear zones must remain equivocal, because no age data is available and no cross cutting relationships were observed in the field; the structures are virtually parallel (Fig. 16).



**Figure 15.** (a) Gneiss showing a closely-spaced  $S_3$  foliation. It is intruded by a pegmatite, which has no internal fabric but is slightly boudinaged, suggesting late-tectonic intrusion (08dms100). (b) Close-up of Fig. 15a, showing S-C and S-C' fabrics in the mylonitic gneiss indicating sinistral strike-slip deformation (cf.; Fig. 16; 08dms100). (c) Pegmatite intruded into amphibolite and gneiss showing a weak  $S_3$  foliation. The pegmatite intruded late-tectonically. The  $S_3$  foliation has a down-dip lineation, which together with shear sense indicators points to a reverse sense of movement (cf.; Fig. 16; 08bms116).

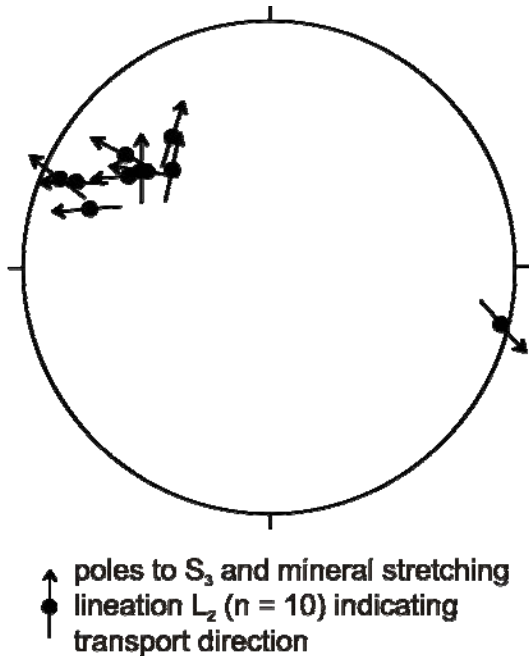


**Figure 16.** Poles to  $S_3$  with arrow indicating orientation of mineral stretching lineation and sense of shearing (Hoeppener plot). Note that some S–L pairs indicate sinistral strike-slip deformation and others indicate reverse deformation. The foliation is virtually parallel and no cross cut relationships are found. The two different geometries refer to shear zones shown in Figs. 15a, b and c.

## Hydrothermal mineralisation and alteration (Kangiata Nuna)

Numerous quartz veins were observed in the Kangiata Nuna map sheet area as traces of hydrothermal mineralisation. They are 1–20 cm wide and are continuous along strike and down dip over several m to up to 200 m. Besides Qtz they contain minor Po, Py and Ccp. In general, most of the veins are parallel to  $S_2$  on the limbs of  $F_3$  folds or they are parallel to  $S_3$  in the  $D_3$  shear zones. They often form at the gneiss-amphibolite contact. Some of the quartz veins formed in a-c orientation of  $F_3$  folds. Locally, a striation on the quartz vein surface of  $S_3$  parallel veins is observed to be parallel to the  $L_3$  mineral stretching lineation. The quartz veins are surrounded by a 5 cm to 1 m wide alteration halo of variable composition, depending on the wall rock type. Composite systems of several parallel quartz veins together with alteration zones can be 50–200 m wide and can be followed along strike and down dip to up to 250 m if the outcrop situation allows that.

In the TTG-gneiss, the hydrothermal alteration comprises Ms, Qtz, Ccp and Po. In the amphibolite a Bt, Qtz, Act, Po and Ccp alteration formed, locally with Ms and Ep. The mafic granulites in the central part of the map sheet have a slightly different alteration containing Bt, Di, Tm, Qtz, Po, Py and Ccp, whereas the alteration assemblage in nearby gneiss is the same to that described above.

In the following we describe some occurrences of hydrothermal quartz veins and the associated alteration in detail, in order to give a detailed overview of the mineralisation style.

### Camp 1 area: south of Kangerdluarssungup taserssua

Several locations with quartz veins and associated hydrothermal alteration were observed. The quartz veins are parallel to the foliation and preferably developed at the contact of amphibolite and gneiss (Fig. 17). The structural control of the quartz veins is, therefore, strongly related to the overall structure. An about 200–300 m wide amphibolite band represents a marker horizon (Fig. 18), showing the open to tight  $F_3$  folding with mainly shallow SE plunging fold axes. Locally developed NW plunging  $F_3$  fold axes are explained by interference with  $F_{2b}$  folds with about E–W trending fold axes. In a cross section of about 6 km, progressive tightening of the  $F_3$  folds is observed. Very tight folds are sheared off by near vertical, NW–SE trending shear zones with a closely spaced  $S_3$  foliation and a shallow SE plunging mineral stretching lineation ( $L_3$ ). They are dominated by sinistral oblique-slip deformation. In the area of tight folding and oblique-slip shearing, several parallel zones of hydrothermal alteration are developed. Up to 20 cm wide quartz veins are associated with up to 2 m wide alteration halos and are (1) parallel to  $S_3$  in the steep limbs of  $F_3$  folds (031/42) and  $D_3$  shear zones (022/81), (2) occupy m-scale dilational jogs in parasitic  $F_3$  z-folds (053/25), (3) parallel to  $S_2$  in recumbent folds with thicker veins in the steep limb (Fig. 6a) and (4) as extension veins linking stepping  $D_3$  deformation zones in dilational jogs, very similar to the structure described in (2) but cross cutting the  $S_2$  foliation (Fig. 19). All these structural controls are consistent with the interpretation that the quartz veins and the associated hydrothermal alteration formed synchronous with the  $D_3$  deformation. The quartz veins are either parallel to  $S_3$  or directly related to  $F_3$  folding. In the recumbent folds,

where the quartz veins appear to be parallel to  $S_2$  the relationship to  $D_3$  is explained by reactivation of  $S_2$  during  $F_3$  flexural slip. This is supported by the observation of thicker quartz veins in the steep limbs that are in a local extensional site in the  $D_3$  regime.

Two profiles were studied in detail. The profile at station 8 shows an about 5 cm wide quartz vein surrounded by a hydrothermal alteration halo mainly comprising Bt and sulphides (Figs. 17 & 20). Geochemical analysis of the alteration zone (508304) yields slightly elevated Fe, however Au is below detection limit ( $< 2$  ppb) and base metal contents are low. A quartz vein (508306, 08dms9) close to this profile records 3 ppb Au. Two other quartz veins from the area show 3 ppb and 6 ppb Au.

A second profile shows two about one meter wide quartz veins hosted in a package of amphibolite and leuco-amphibolite. The leuco-amphibolite is moderately silicified and, therefore, probably represents a hydrothermal alteration zone. Geochemical analysis of the altered rock (508316) and the quartz vein (508317) record Au below detection limit.

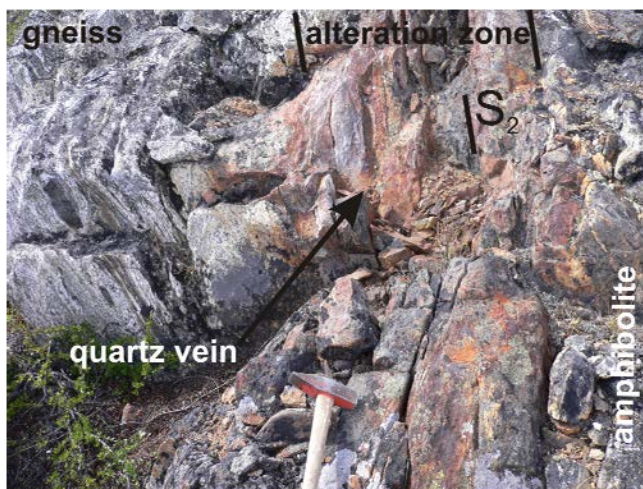
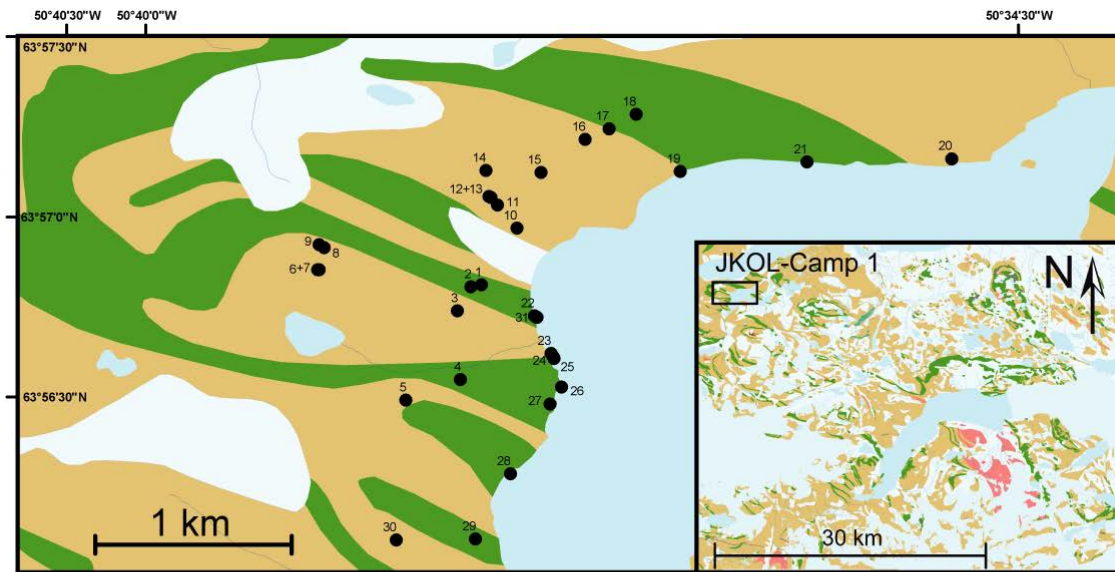


**Figure 17.** Photograph of a typical outcrop, showing an about 5 cm wide quartz vein surrounded by a rusty alteration halo. The quartz vein is developed parallel to the  $S_2$  foliation at a gneiss-amphibolite contact (08dms8).



- Quaternary (moraine and talus)
- Mafic granulite locally retrogressed to amphibolite
- Lake
- Gneiss
- Stream channel
- Stations  
(e.g. '5' refers to station 08DMS005)

**Figure 18.** Schematic geological map showing the studied locations in the camp 1 area. The camp was located close to station 10.

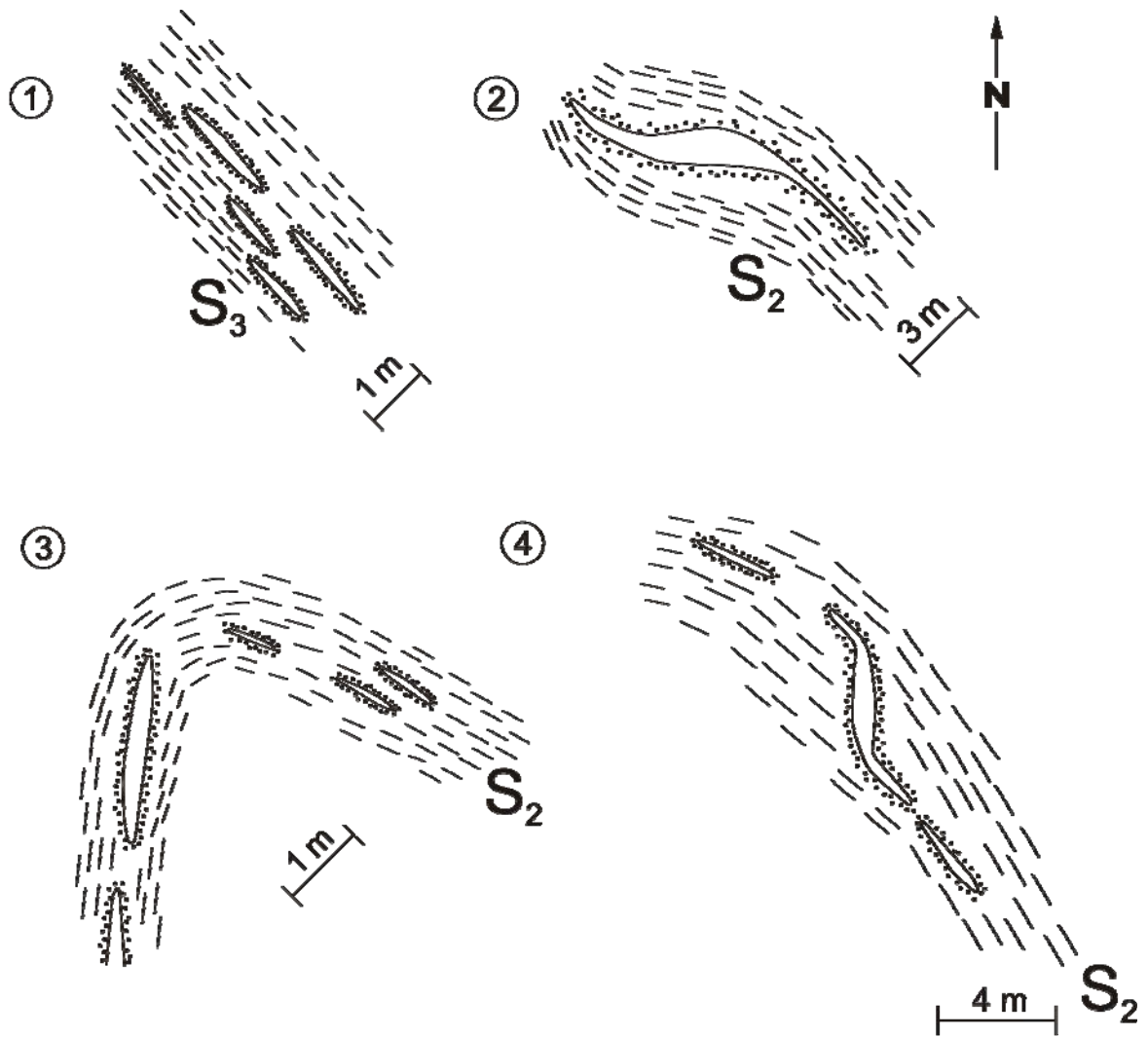


**Figure 19.** Sketches illustrating the structural control of quartz veins and alteration halos: (1) parallel to  $S_3$  in the steep limbs of  $F_3$  folds (031/42) and  $D_3$  shear zones (022/81), (2) occupying m-scale dilational jogs in parasitic  $F_3$  z-folds (053/25), (3) parallel to  $S_2$  in recumbent folds with thicker veins in the steep limb and (4) extension veins linking stepping  $D_3$  deformation zones in dilational jogs, very similar to the structure described in (2) but cross cutting the  $S_2$  foliation.



to that described for camp 1. Especially the type (4) dilational jogs were observed with tips parallel to  $S_2$  (032/82) and the jog trending N–S (095/43). The gold content in the altered rocks is generally below detection limit.

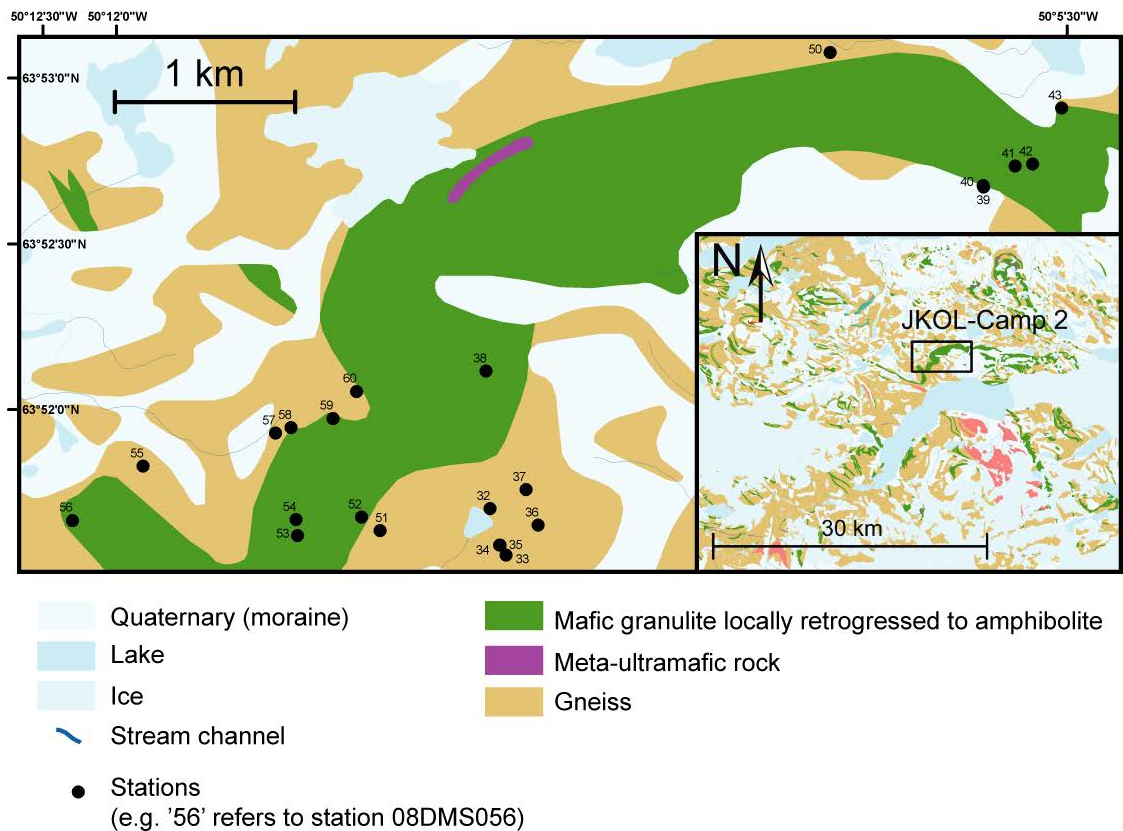
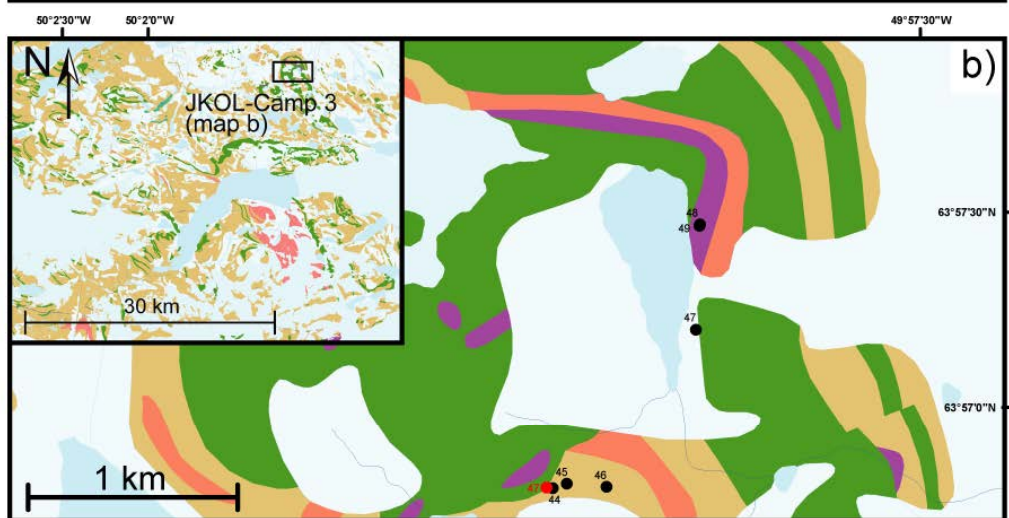
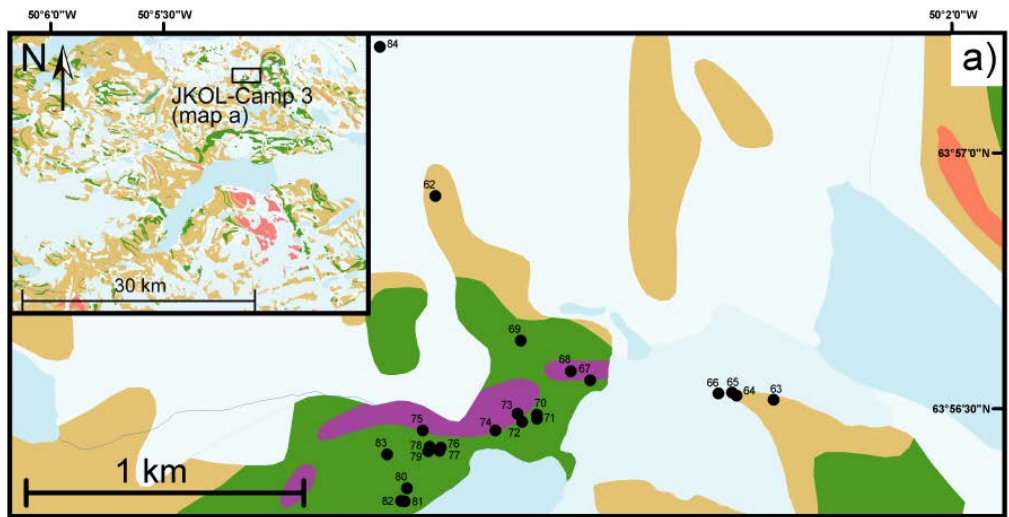


**Figure 22.** Schematic geological map showing the studied locations in the camp 2 area. The prominent  $F_3$  fold appears well from the folded mafic granulite. Station 32 shows the location of camp 2.

### Camp 3 area: northeast of camp 2

Two locations with quartz veins and hydrothermal alteration were observed, one in gneissic wall rocks north of camp 3 and one in the mafic granulites south of camp 3 (Fig. 23). The mafic granulites form a map-scale syncline and the quartz veins are hosted in parasitic higher-order  $F_3$  folds mainly on the south-western limbs. The hydrothermal alteration forms up to 1 m wide halos surrounding the up to 20 cm wide quartz veins (Fig. 24) comprising Bt, Di, Tm, Qtz, Po, Py and Ccp. Locally, malachite and bornite are weathering products together with a rust-staining of the altered rocks. In areas of closely-spaced quartz veins, the alteration zones overlap and, hence, form a pervasive hydrothermal alteration assemblage replacing the peak metamorphic Hbl, Pl, Opx  $\pm$  Cpx, Grt assemblage. This quartz vein hosted hydrothermal mineralisation was observed in an area of 500 m by 300 m in outcrop. However, geochemical analyses reveal that neither the sample from the quartz veins nor the sample from the immediate alteration envelopes contain gold (508353 and 508354).



- |   |   |   |                      |
|---|---|---|----------------------|
|  | Quaternary (moraine and minor talus)  |  | Granite              |
|  | Lake  |  | Mafic granulite      |
|  | Ice   |  | Meta-ultramafic rock |
|  | Stream channel  |  | Gneiss               |
|  | Stations<br>(e.g. '69' [map a] refers to station 08DMS069<br>note that station '47' in red [map b] equals to a station of the team „BMS„) |   |                      |

**Figure 23.** Schematic geological map showing the studied locations in the camp 3 area. (a) the map shows the central southern part of the camp 3 area. Profiles were studied at stations 73 and 75. Meta-ultramafic rocks at the stations 67, 68, 69, 71 and 73 reveal elevated to highly elevated Cr and Ni contents. (b) the map shows the eastern part of the camp 3 area. This area was visited by a reconnaissance stop for several hours. (c) the map shows the western part of the camp 3 area. One alteration zone sample has an elevated gold content of 106 ppb Au . Station 61 represents the location of the camp.

Three structural settings of quartz veins are distinguished (Figs. 24–26): (1)  $S_2$ -foliation parallel veins (Figs. 24a, d & e), (2) veins in a-c orientation to the hosting fold structure (Figs. 24a & b) and (3) en-echelon sigmoidal veins (Fig. 24c). The similar hydrothermal alteration assemblage and mutual cross cutting relationships suggest that the veins formed contemporaneously (Fig. 24a). The  $S_2$  parallel veins most probably formed during transposition of  $S_2$  by  $D_3$  flexural slip folding as shear veins. The veins in a-c orientation are extension veins during  $F_3$ . This is supported by the observation that they are parallel to the tips of the sigmoidal veins (Fig. 25). The sigmoidal veins display a dextral sense of rotation on the south-western limb of the syncline, which is explained by dextral shear deformation on the limb during  $F_3$  flexural slip (Figs. 24c & 26).

On a larger scale, the mafic granulite syncline is bounded to the west by a NW–SE trending, about 1 km wide  $D_3$  high strain zone (Fig. 3b). The south-western limb of the syncline is sheared off in a most probably sinistral oblique-slip deformation during progressive fold amplification during  $D_3$ . This large-scale structure may have acted as fluid conduit for the hydrothermal alteration and mineralisation in the adjacent  $F_3$  structures and, therefore, may represent the lower-order structural control of the mineralising system.

To the north of camp 3 (Fig. 23c; station 88-89), several parallel, 2–5 cm wide quartz veins occur in the gneiss. The hydrothermal alteration forms about 1 m wide halos of Qtz, Ms and Bt replacing the Qtz, Pl and Hbl assemblage of the tonalitic wall rock gneiss. In an about 200 m wide corridor, three parallel hydrothermal alteration zones can be followed along strike over about 500 m. The quartz veins are parallel to the  $S_2$  foliation and dip moderately to the SE. Geochemical analyses of the quartz veins and the hydrothermally altered gneiss at the immediate contact show that these rocks are barren of gold and base metals show only background values (e.g.; sample 508365).

West of camp 3 (Fig. 23c) a 10 cm wide quartz vein with thin alteration envelopes occurs (station 96). This narrow, rusty alteration zone is mica-rich and the gold content is 106 ppb (sample 508373). Interestingly, analysis of a stream sediment sample yields elevated gold (station 98, sample 508375, 43 ppb). This sample is located about 2.5 km east of the alteration zone with slightly elevated gold content and suggests that this area may contain gold mineralisation.

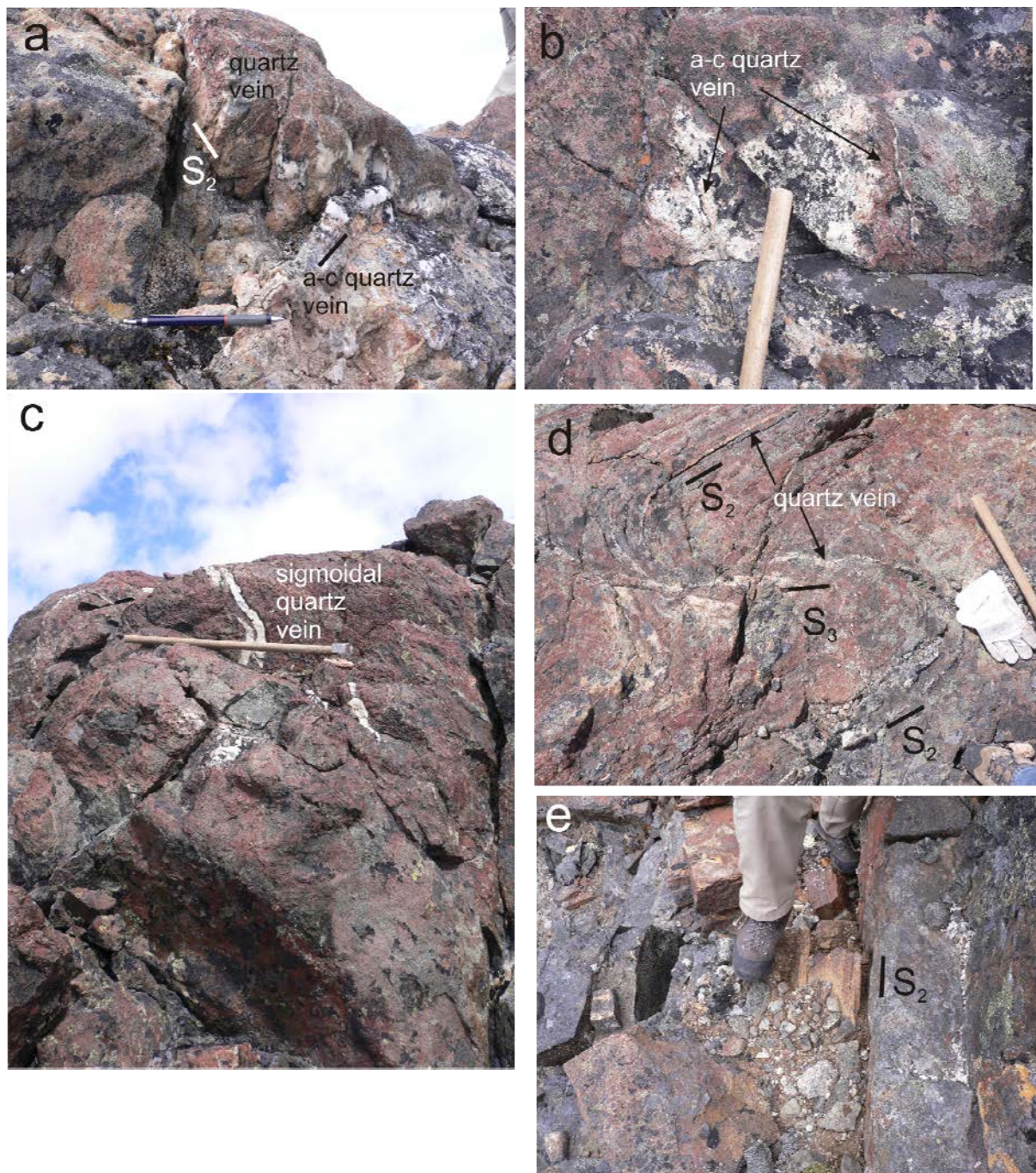


**Figure 24.** Photographs of quartz veins and rusty alteration halos. (a) Intersection zone of two quartz veins (i)  $S_2$  parallel and (ii) in a-c orientation of  $F_3$  folds, showing intense hydrothermal alteration of the host rock. (b) Typical cm-scale quartz veins with ca. 20 cm spacing in a-c orientation of  $F_3$  folds in hydrothermally altered (rusty) host rock. (c) Sigmoidal, en echelon quartz veins indicating dextral sense of shearing on the southwestern limb of the  $F_3$  fold due to flexural slip. (d)  $S_2$  and  $S_3$  parallel quartz veins in a cm-scale  $D_3$  shear zone, showing sinistral strike-slip displacement of about 1 m indicated by transposition of  $S_2$  and the offset of  $S_2$ -parallel quartz veins (cf.; Fig. xb). (e) About 40 cm wide  $S_2$ -parallel hydrothermal alteration zone in mafic granulite with 106 ppb Au.

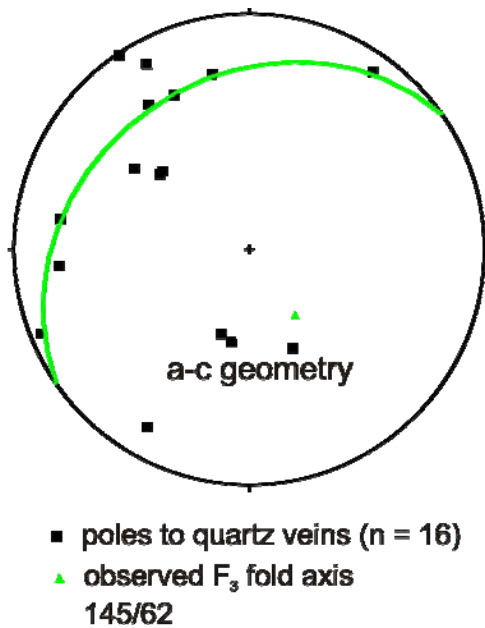


**Figure 25.** Pole figure of quartz veins showing great circle geometry typical for  $F_3$  folds (equal area, lower hemisphere projection). This is interpreted as quartz veins developed parallel to the  $S_2$  foliation during  $F_3$  folding by reactivation of the  $S_2$  foliation by  $D_3$  flexural slip. Note, quartz veins in the a-c orientation to the  $F_3$  fold, furthermore, indicate formation of veins and hydrothermal alteration during formation of the  $F_3$  folds.

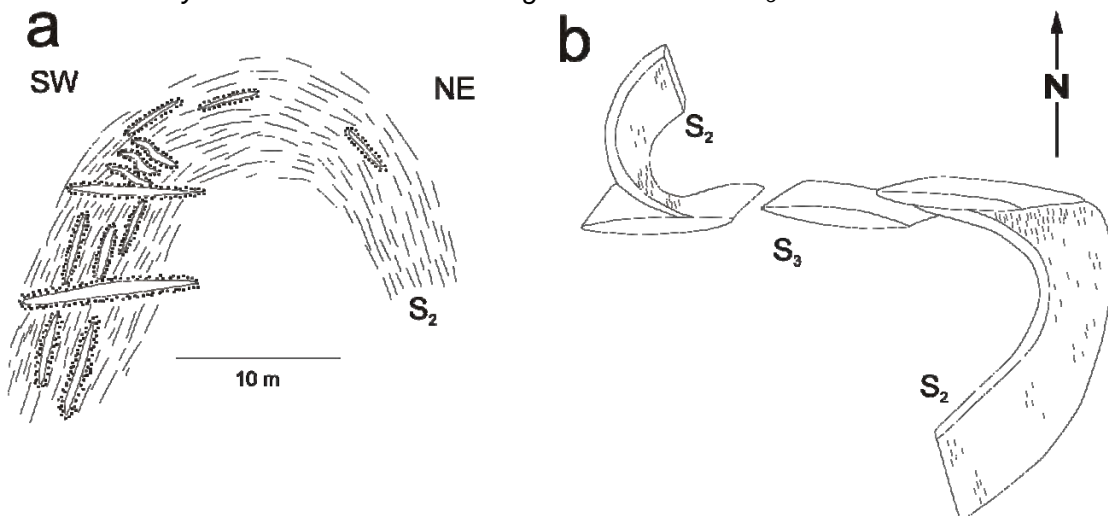


**Figure 26.** Sketches illustrating the structural control of quartz veins and alteration halos: (a) in the various orientations in the  $F_3$  fold (i)  $S_2$ -foliation parallel, (ii) in a-c orientation and (iii) en-echelon sigmoidal; and (b) in a cm-scale  $D_3$  sinistral strike-slip shear zone (cf., Fig. 24d).

The lithological profile (Fig. 27a – station 73; cf.; Fig. 23a) shows the contact of gneiss and meta-pyroxenite. This contact is well marked by the rusty colour and weathered appearance of the meta-ultramafic rocks, which contrasts with the gneiss. Several horizons of the meta-ultramafic rocks are magnetite-rich and contain Opx, Cpx, Ol and Hbl. These rocks (e.g.; 508349) are highly elevated in Ni (2240 ppm), Cr (691 ppm) and Co (114 ppm), have low Si and are Mg-rich. However, Pt, Pd and Au are not elevated.



## Hydrothermal mineralisation and alteration (Buksefjorden)

Only mineralised localities and associated hydrothermal alteration zones in the Buksefjord area studied by Team 4 (Bo Møller Stensgaard and Annika Dziggel) will be addressed in this section of the report.

### Camp 1 area: Qarajat kuat, north of Buksefjorden

The area is dominated by amphibolite, paragneiss, schist, anorthosite and pegmatite. Only few localities with hydrothermal alteration and mineralisation were found (Fig. 3c). Iron sulphide-bearing schist is observed at two localities (08BMS032 and 08BMS034). The mineralised package appears to be silicified and Bt-rich. At locality 08BMS032, the mineralisation is hosted in rusty, gray to whitish Qtz-Pl-Bt-Ms, fine- to medium-grained schist (paragneiss; Fig. 28a), whereas at locality 08BMS034 the mineralisation occurs within dark grey, fine-grained, homogeneous amphibolite (Fig. 28b). The strike of both mineralised structures is E–W. The mineralisation is either controlled by a shear zone and/or by the anisotropy at the contact between the different lithologies.

A pervasive alteration zone is observed at locality 08BMS035 (Fig. 28c). The wall rocks are amphibolite, meta-hornblenditic/ultramafic rock (Fig. 28d), paragneiss and coarse-grained gneiss with Qtz+Plg+Cpx+Opx+Grt+leucosome dykes. The entire zone appears to be silicified and contains, in places, high amounts of biotite. The zone is 20–30 m wide and exposed for 150–200 m. Besides a probably late, 220° trending and cross cutting milky-white, 1 m wide quartz vein, all other rocks have a moderate to strong rusty appearance. A probably early boudinaged and reddish 1–1.5 m wide quartz vein is also observed (Fig. 28d). The rock package is sheared and folded. It appears that the rust zone occurs within the fold closure/core. The entire gossan zone is topped towards the north by a large, 5–10 m wide pegmatite body. A topographic lineament appears to be running parallel to the strike of the pegmatite. The lineament possibly represents a shear zone developed at the steep limb of the observed fold. Disseminated Py, Ccp, Po and possible also Mag occur in various amounts within the different rocks. Hem- and malachite-staining on surfaces is also observed (Fig. 28e).

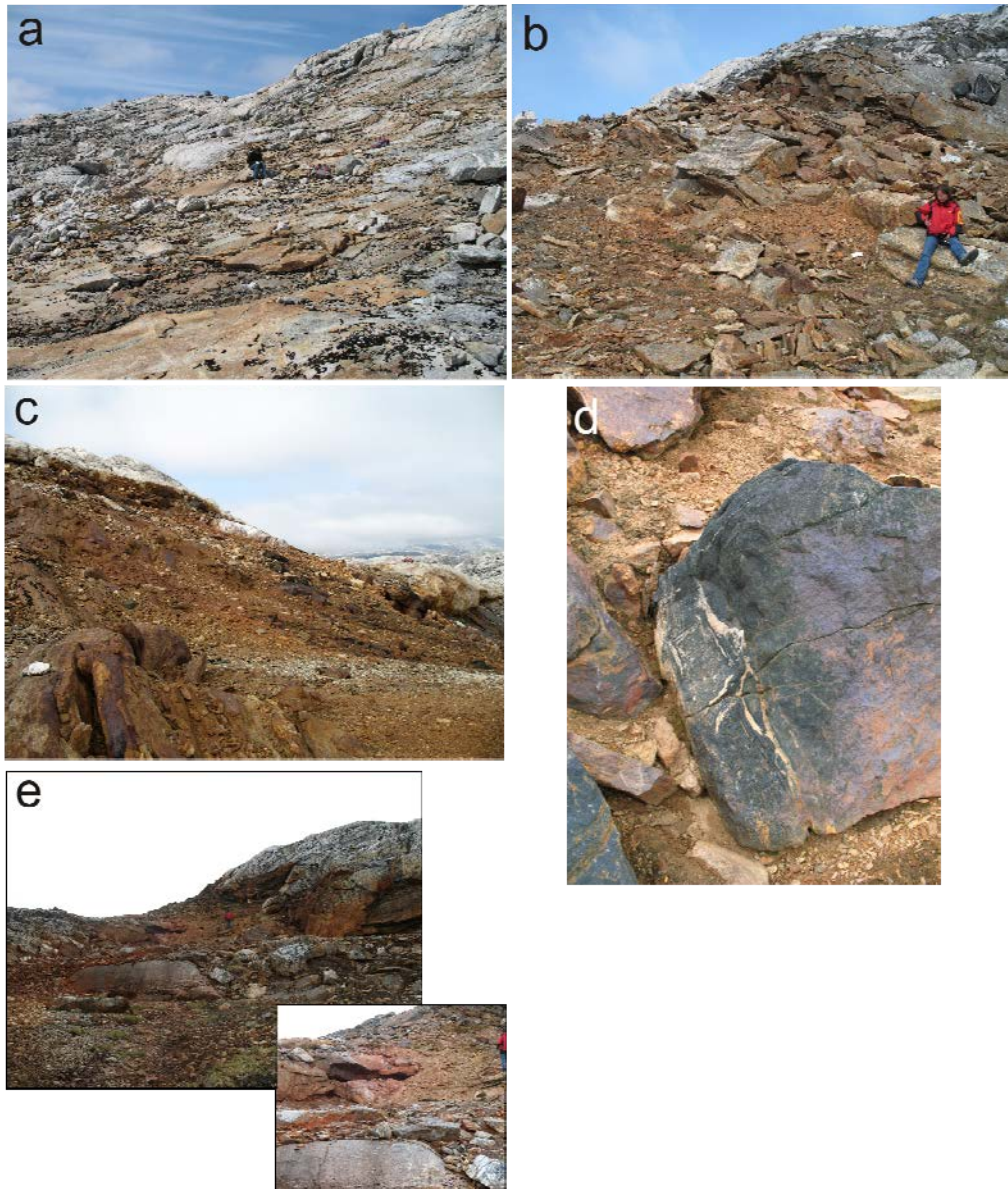
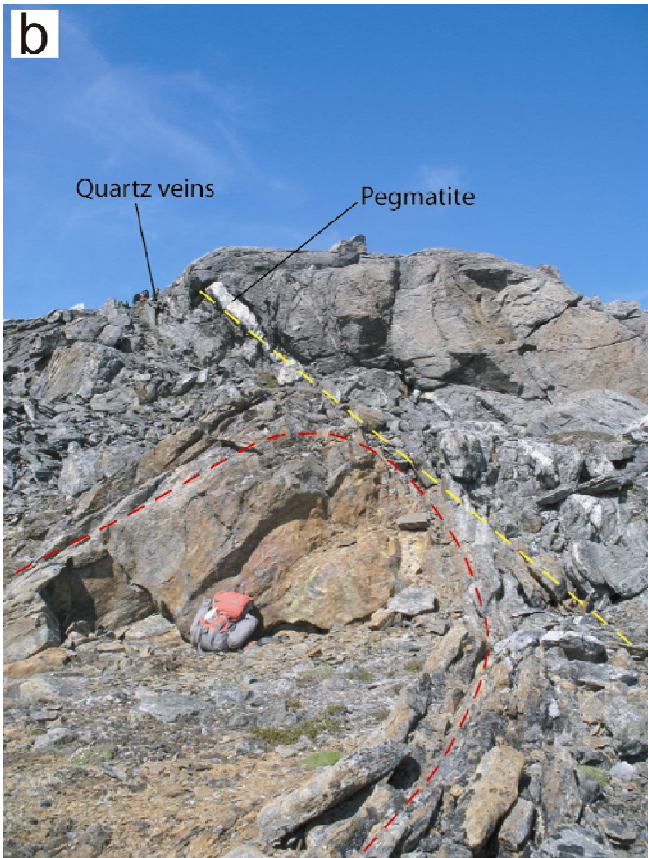


**Figure 28.** (a) Moderate rusty Qtz-Pl-Bt-Ms, fine- to medium-grained schist at locality 08BMS032. (b) Rusty, dark grey fine-grained homogeneous amphibolite at locality 08BMS034. (c) The gossan zone at locality 08BMS035. In the foreground, sulphide-mineralised paragneiss occurs. In the central part of the photo, milky-white late quartz vein can be observed. The zone is “topped” by pegmatite. Notice the red and grey rucksacks for scale in the right side of the photo on top of the pegmatite body. (d) Sulphide-bearing hornblenditic rock with small quartz, feldspar aplite dykes from the gossan zone at locality 08BMS035. (e) Hem-stained, red-coloured, quartz-rich pegmatite beneath the pegmatite body that caps the gossan zone. The pegmatite is intruded into paragneiss. The photo is taken towards the east; smaller inset photo is a close-up of the hematite stained pegmatite.

## **Camp 2 area: south of Qaaqatsiaq, central Tasiusarsuaq terrane**

The area is located within an area dominated by amphibolite, meta-leucogabbroic rocks, granotoid rocks and pegmatites. The supracrustal rocks in the camp 2 area are characterized by a fold interference pattern typical of the Tasiusarsuaq terrane. Several locations with quartz veins and/or hydrothermal alteration were investigated. In general, the mineralization occurs in different structural settings that are closely related to the  $D_3$  structures. The  $D_3$  structures in the Camp 2 area are characterized by open to tight upright folds with axial traces trending NW–SE to W–E. Sinistral strike slip shear zones are commonly developed along the sub-vertical north-eastern limb of these folds, or as conjugate sets of steep shear zones that crosscut the  $S_2$  foliation. The shear zones vary in thickness between several cm and several 10s of m. Mineral assemblages of Hbl, Pl, Qtz, and, locally, Grt, indicate that shearing occurred under amphibolite facies conditions, and thus, postdates the peak of regional granulite facies metamorphism. The shear zones are intruded by foliation-parallel pegmatite dykes. In a NW–SE direction, the pegmatite dykes often display a well-developed proto-mylonitic foliation, indicating that they intruded the shear zones syn-tectonically. Another important feature of these shear zones is the presence of several decimetre wide pseudotachylite veins. The contacts with the wall rocks are often irregular, suggesting that they formed by in situ friction melting of the already solidified pegmatites. The pseudotachylites are commonly recrystallised and well foliated. They are characterised by the presence of large feldspar-crystals that are embedded within the dark grey matrix.

In the camp 2 area, the mineralization occurs (i) as a pervasive hydrothermal overprint in dilational sites at the intersection of the conjugate shear zones; (ii) as bedding-parallel, subhorizontal, highly silicified bodies along the shallowly dipping south-eastern limbs of the  $F_3$  folds; or (iii) in association with foliation-parallel and sigmoidal quartz veins within the NW–SE trending shear zones (Figs. 29 & 30). The ore assemblage in all these settings is similar, and comprises Po, Py, Ccp. The altered wall rocks (both felsic and mafic granulites) contain Qtz, Bt and Ms. The zones are mostly found within fine-grained grey mafic granulites in some cases with gabbroic texture. The zones along the limbs of the folds and the shear zones are generally not more than 1–3 m wide and traceable along strike for 100–200 m. However, larger scale zones have been observed in cliff-walls nearby the investigated area (Fig. 31) but these were not visited during the fieldwork. The zones developed in the hinge zone/line are generally wider (depending on the size of the fold); up to 5–6 m. Quartz veining outside or inside the mineralised zones, parallel to either the shear zone developed along the steep limbs of the fold or along the axial planes of the fold were observed in several localities.



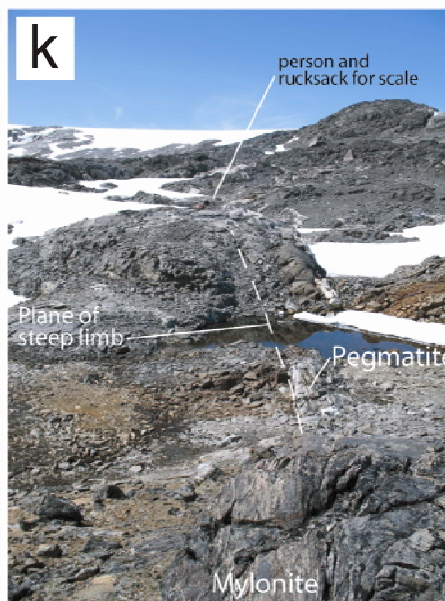
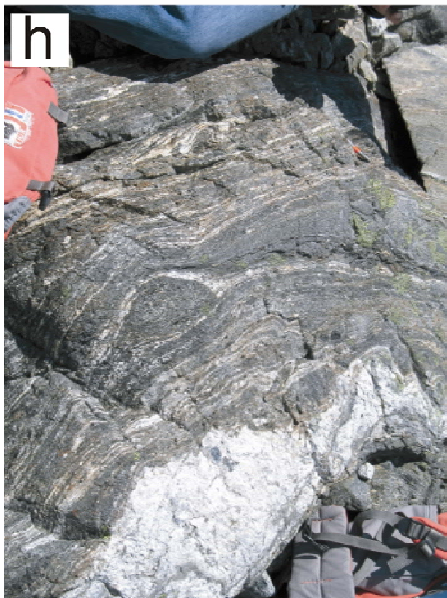
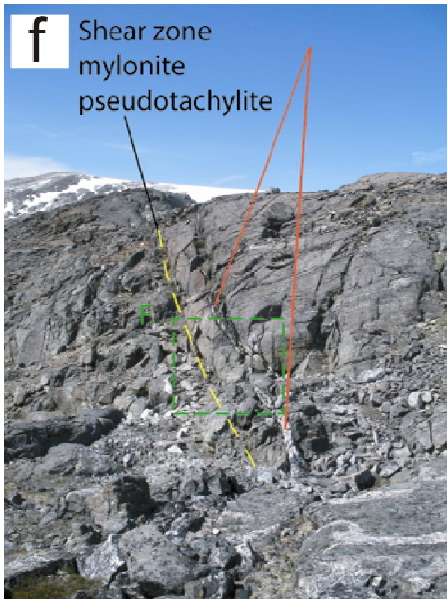


**Figure 29.** (a) Mineralised, ca 1 m wide, rusty alteration zone (beneath the person) parallel to the foliation of the host rock. (b) Iron-sulphide-bearing zone (at the rucksack) developed in the hinge zone of a fold. The axial trace of the fold is indicated by the hatched red line. Pegmatite and quartz vein systems occur at the plane of the steep limb of the fold. This plane also defines a shear zone. (c) and (d) Zone with quartz veinlets approximately 1 m beneath the pegmatite. (e) Greenish and brownish calc-silicate alteration associated with the quartz veins. (f) The shear zone, quartz veins and pegmatite can be followed along strike. 200 m further towards the northwest, the feature develops into a pronounced 2 m wide shear zone with pseudotachylite and leucosome. (g) Close-up of the mylonite zone. (h) and (j) Parts of the mylonite zone have a large content of 0.2–0.5 cm red garnets (red parts of the mylonite bands); often on the rims of more felsic bands in the mylonite. Black bands are glassy in appearance and possibly represent recrystallised pseudotachylite. (j) Close-up of the more massive, blackish bands of the mylonite zone, which contain rounded, deep black minerals. Possibly amphiboles formed during recrystallisation of the pseudotachylite. (k) 200 m further to the northwest; the feature is still present and now with the development of rusty zones below and above the plane of the steep limb in (b).

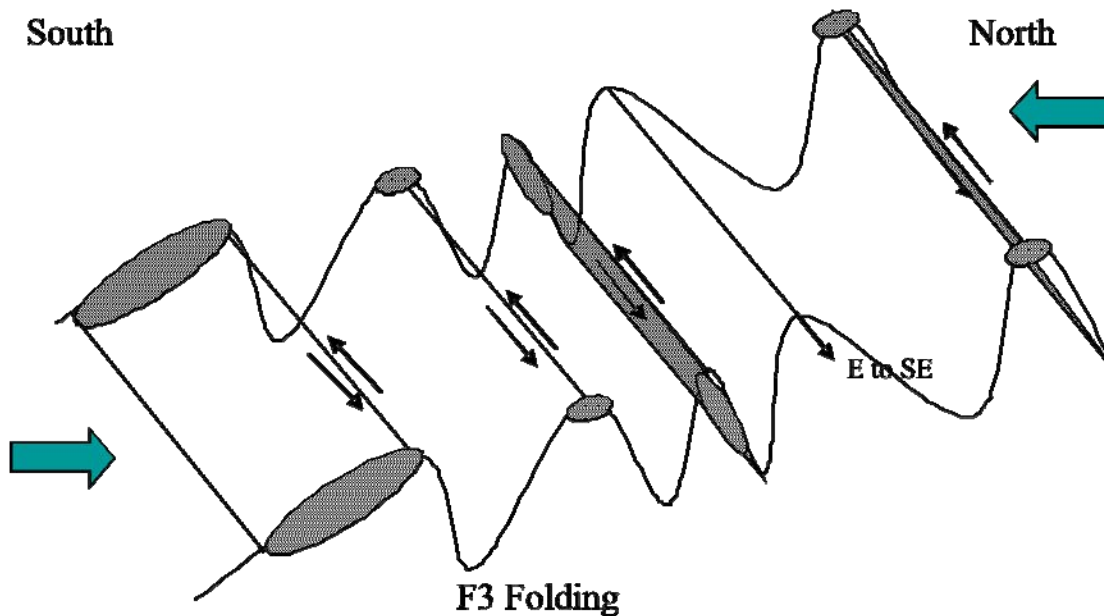


**Figure 30.** Simplified model of  $F_3$  folding and areas with hydrothermal mineralisation (grey shaded area) and shear zones encountered in the area south of Qaaqatsiaq.

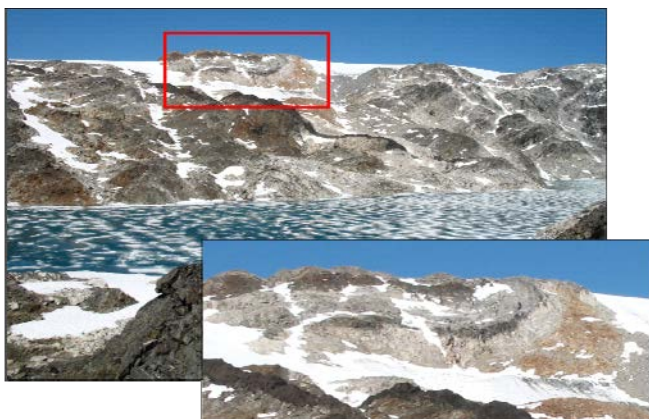


**Figure 31.** *Large-scale recumbent fold in cliff-wall north of the area investigated, south of Qaaqatsiaq. The rusty hydrothermal alteration zone is developed in the hinge zone of the fold. Panorama towards the northwest taken east of camp 2. The photo illustrates the “rusty spots” distributed throughout the landscape created by the cut of the topography and the numerous mineralised zones in the area. The distance along the shoreline furthest away from southwest to northeast is estimated to be around 1.5 km.*

Pseudotachylites with 0.5–5 cm fragments of pegmatite were observed in many of the shear zones parallel to the steep limbs of the folds. The pseudotachylite consists of a very fine-grained, massive, blackish to brownish matrix, recrystallised to amphiboles and mica. The width of the pseudotachylites are generally from 10 to 50 cm, but wider varieties, up to ca. 2–3 m wide, were also found (Fig. 32). This suggests that pegmatites intruded the shear zone pre-, syn- and post-tectonically.

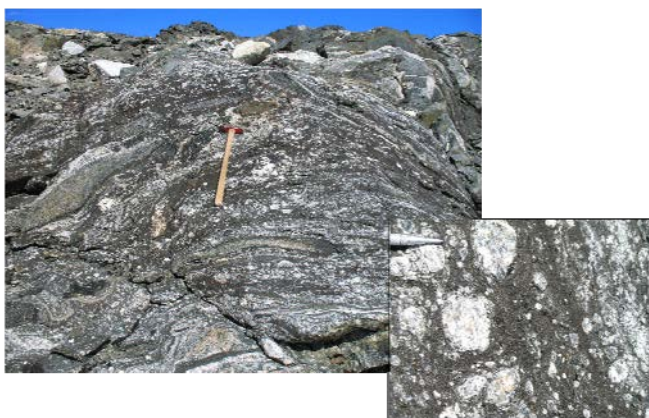


**Figure 32.** *One of the widest recrystallised pseudotachylite zones encountered in the area. White felsic (quartz-feldspar dominated) clast of pegmatite are cut up in a brownish-blackish, fine-grained matrix.*

Another type of mineralisation in the area south of Qaaqatsiaq shows two parallel, ca. 1 m wide, Mag-rich alteration zones parallel to the general foliation in the surrounding intermediate-mafic granulite gneiss (Fig. 33; 08BMS052). The zones are not separated by more than a couple of metres and can be follow ca. 15 m along strike. The central part of the zone is very Mag-rich (~85–90%) and up to 0.7 m wide. This is followed by a green, calc-silicate-bearing part, followed by a garnet- and amphibole-bearing part. The Mag

weathers out in a very distinct skeleton way - removal of most calc-silicate and only the magnetite network is left behind.



**Figure 33.** *The Mag-rich alteration horizon (the blackish rock in the back of the picture) with the calc-silicate(Cpx)+Grt+Pl parts of the horizons in the foreground.*

### **Camp 3 area: north of central Alangordlia, southern Tasiusarsuaq terrane**

The supracrustal rocks in the camp 3 area are dominated by fine- to medium-grained mafic granulites. These are locally intercalated with TTG gneiss, and intruded by younger, but also foliated granitoids. Even though  $D_3$  shear zones and associated pegmatite dykes and pseudotachylites are common, the area appears to be less affected by hydrothermal alteration than the camp 2 area. The  $D_3$  shear zones crosscut the regional  $S_2$  foliation, which dips at moderate angles to the SE. The  $D_3$  shear zones strike NW–SE and NE–SW, and dip at moderate to steep angles to the NE and NW. The mineralization was investigated in one location, where it is situated in a dilational jog at the intersection between two cross cutting, up to 0.5 m wide mylonitic shear zones (Fig. 34). The mineralized zone is strongly silicified and also contains hydrothermal Hbl. The ore mineral assemblage comprises Py and Ccp.

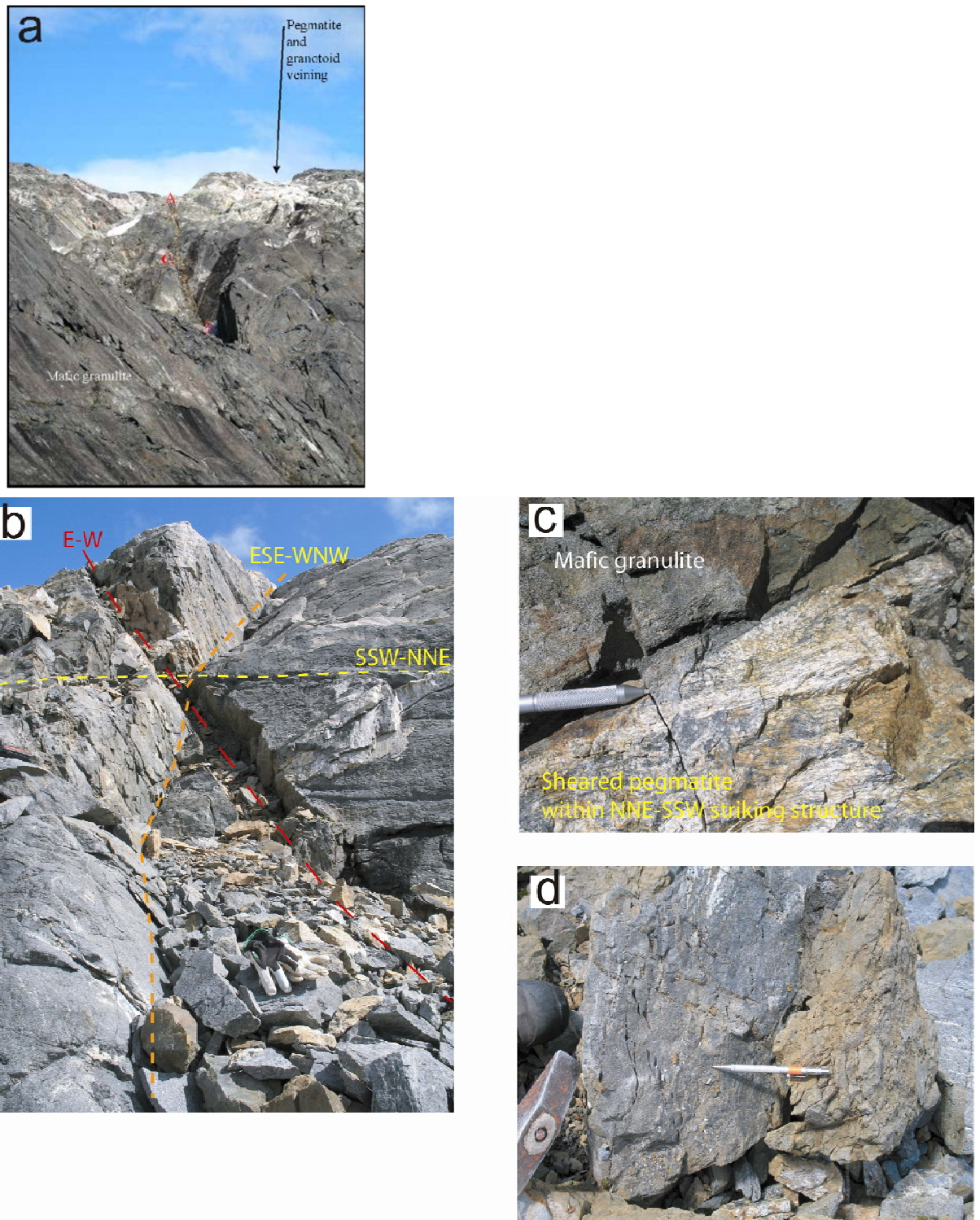


**Figure 34.** (a) The mineralised structure (A-B) in the cliff-wall west of the camp site. Locality 08BMS067 is marked with a C. (b) The different structures at locality 08BMS067. (c) Sheared pegmatite. (d) Grey, silicified, fine-grained mafic granulite. The silicified rock weathers out with a light brownish colour.

## **Camp 4 area: south of the outlet of Buksefjorden, central Tre Brodre terrane**

This area at the estuary mouth of Buksefjorden was visited because of reported elevated gold grades. The TTG gneiss and associated supracrustal rocks are part of the Færingehavn straight belt (McGregor *et al.* 1986), and are characterized by a N–S trending, sub-vertical and often mylonitic foliation. This foliation corresponds to the  $S_3$  foliation in the Færingehavn – Kangerdluarssoruseq profile described above. The peak metamorphic mineral assemblages point to amphibolite facies metamorphism. The mineralization is associated with up to 0.5 m thick quartz-veins oriented along discrete,  $S_3$ -parallel shear zones (Fig. 35). The veins contain abundant enclaves of greenschist facies mafic rocks, which are mainly composed of Act, Ep, Qtz, Pl, and locally Chl. They can be followed along strike for at least 25 m, and are often developed as sheeted quartz veins. The veins are locally very coarse-grained, and contain, in addition to milky-white quartz, up to several cm large crystals of Act, Py, Po, and Ccp. Gold grades are generally below detection limit. The mylonitic wall rocks contain a several cm-wide alteration halo that is composed of an inner Qtz-fuchsite, and an outer Bt alteration. The presence of greenschist facies minerals in these  $S_3$ -parallel shear zones indicates that they postdate  $D_3$  shearing in the Færingehavn straight belt. However, the lineation in the quartz veins and associated alteration zones is parallel to those in the amphibolite facies mylonites, and plunges at moderate degrees to the SW. This may indicate a progressive exhumation during shearing. Shear sense indicators point to an E block up sense of movement with a sinistral strike slip component.

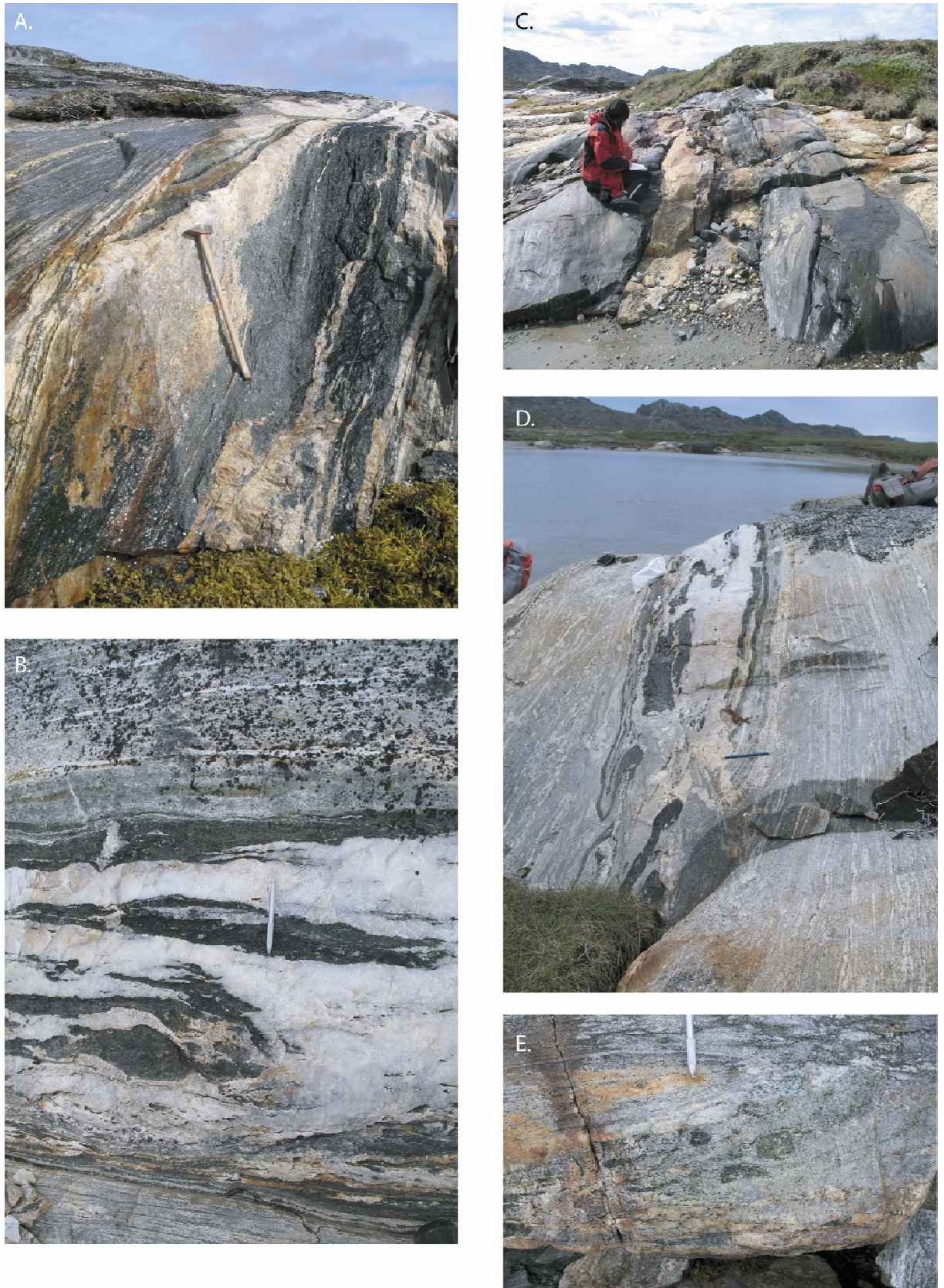


**Figure 35.** A. Quartz vein with mafic amphibolite enclaves. View towards NNW. B. Close-up of the mafic enclaves within the quartz vein, which is intruded into mylonitic tonalitic gneiss. C. Two neighbouring 0.5-1 m wide quartz veins. View towards SSE. D. The mylonitic appearance of the gneiss and the foliation-parallel quartz veins. View towards

SSE. E. Close-up of the fuchsite- and sulphide-bearing milky to transparent quartz vein. Notice the weakly developed foliation within the vein defined by blackish minerals (amphiboles and/or biotite).

## Reco stop: south of Ameralik

This site was revisited because elevated grades up to 200 ppb of gold and 2 wt.% of copper are recorded (Appel *et al.* 2005). However, no comprehensive model for the mineralisation was presented before. The site is characterised by altered gneiss with rusty spots (Fig. 36). The gneiss is white, medium-grained and comprises mainly Qtz and Fsp. Mafic minerals are generally absent due to hydrothermal alteration with only some Bt preserved. Locally, small specks of Py and Ccp are recognised. Stockwork-type, mm-scale quartz-feldspar veinlets cross cut the gneiss (Fig. 36). This hydrothermal stockwork mineralisation is interpreted to be related to the hydrothermal alteration of the host gneiss. The sulphides are oxidised forming hematite, bornite and covellite, which is possibly related to a later hydrothermal meteoric overprint. The petrology of samples taken in 2004 and 2005 show that the gneiss has a hydrothermal alteration assemblage comprising Chl, Ms and Ep and is strongly fractured due to brittle deformation.

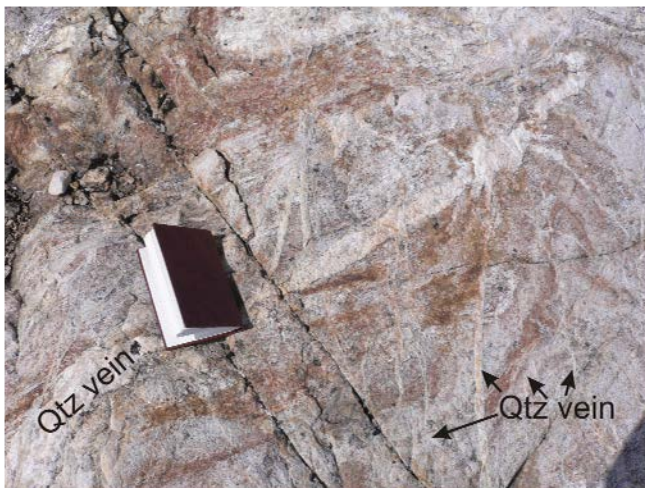


**Figure 36.** Whitish altered gneiss with rusty spots related to sulphide-weathering. The gneiss is cross-cut by quartz veins of various orientations. Note the dominant NW–SE trending set of parallel veins.

Geochemical analysis of the hydrothermal alteration zone (515105, 515107) yields enriched values for Cu, Zn, Ag and to a lesser extent Mo, which is similar to the geochemical signature of the soil sediment sample (530201). Relative high Cu contents of 1050 ppm are found in sample 515107 and Ag contents are 25 ppm in sample 515105.

Nineteen structural readings were taken from the quartz-feldspar veins. The veins show moderate to steep dips and three major strike directions (Fig. 37): (1) NW–SE is the main strike orientation, (2) E–W and (3) N–S are equally represented but clearly subordinate. The hydrothermally mineralised stockwork zone is situated between 2 regional scale, N–S trending faults that display a right lateral step in that area. The brittle deformation and the formation of the quartz-feldspar veins are interpreted to be related to deformation along the faults. This is, furthermore, supported by the widespread Chl-Ep alteration spatially

associated with the faults. The structural position of the stockwork zone represents a dilational jog linking the two faults. The geometry of the faults and the dominant NW–SE strike of quartz-feldspar veins suggest dextral sense of shear along the N–S trending faults in a NW–SE oriented compressional regime. The hydrothermal system is, therefore, interpreted to be controlled by deformation along the faults. Focusing of fluids and stockwork-type veining and mineralisation is controlled by regional anisotropies represented in this case by the dilational jog.

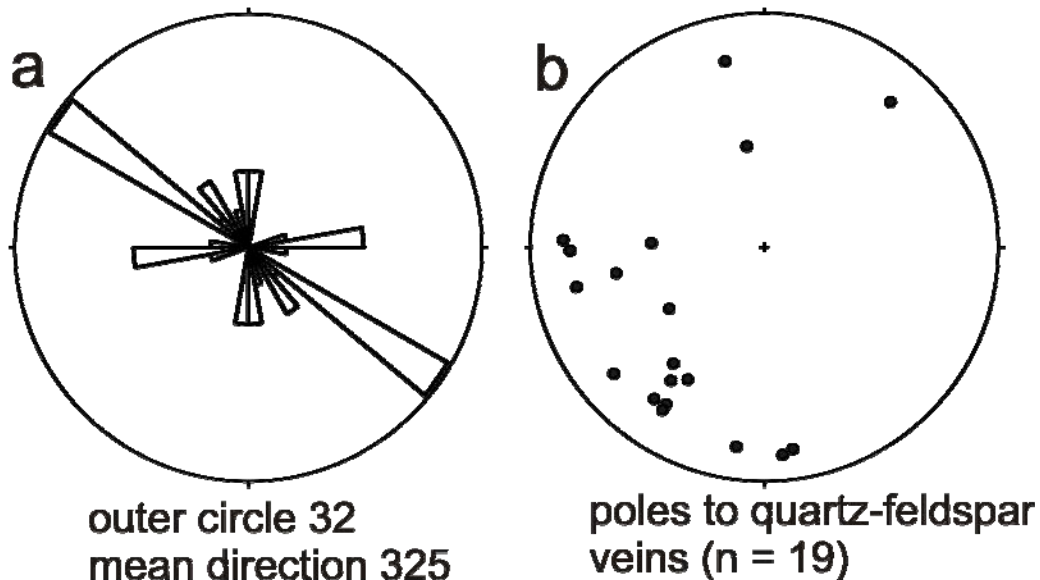


**Figure 37.** Projection of quartz-feldspar veins: (a) in a rose-plot showing the major strike in NW–SE orientation and the subordinate sets in N–S and E–W strike orientation. (b) as poles in an equal area, lower hemisphere projection, showing the geometry of the stockwork zone in 3D.

### Reco stop: south of central Alangordlia

A location in the circular structure of mafic granulite to the south of Alangordlia was studied during a 3 h stop (Fig. 3c). The circular feature is displayed by an about 250 m thick mafic granulite marker horizon in granulite facies TTG gneiss. This circular outcrop pattern is explained by a fold interference pattern of  $F_{2b}$  folds with approximately E–W trending axial traces and  $F_3$  folds with approximately N–S trending axial traces, which yields a type 1 dome and basin interference pattern (Ramsay & Huber 1987). Two rock types are distinguished: (1) a medium-grained mafic granulite comprising Cpx, Opx, Qtz, Grt  $\pm$  Pl and (2) a coarse-to-medium-grained meta-leucogabbro with an Opx, Cpx, Pl and Grt assemblage (Fig. 2c).

Three up to 1 m wide hydrothermal alteration zones occur in an about 200 m wide zone and can be followed over several hundred metres along strike (Fig. 38). The hydrothermal alteration zones form rusty brownish halos surrounding 5–20 cm wide, laminated quartz veins. The proximal hydrothermal alteration comprises Grt, Cpx, Qtz and Py with gradually decreasing Grt and Py away from the quartz vein, representing the distal hydrothermal alteration (Fig. 39). Geochemical analysis of the hydrothermal alteration zone (515184) revealed elevated Fe, Cu, Zn and Mo, but Au below detection limit (< 2 ppb). A quartz vein

sample (515185) also has Au below detection limit (< 1 ppb). Similarly, a soil sample (530214) is enriched in Cu, Zn and Mo, but shows no enrichment in Au.

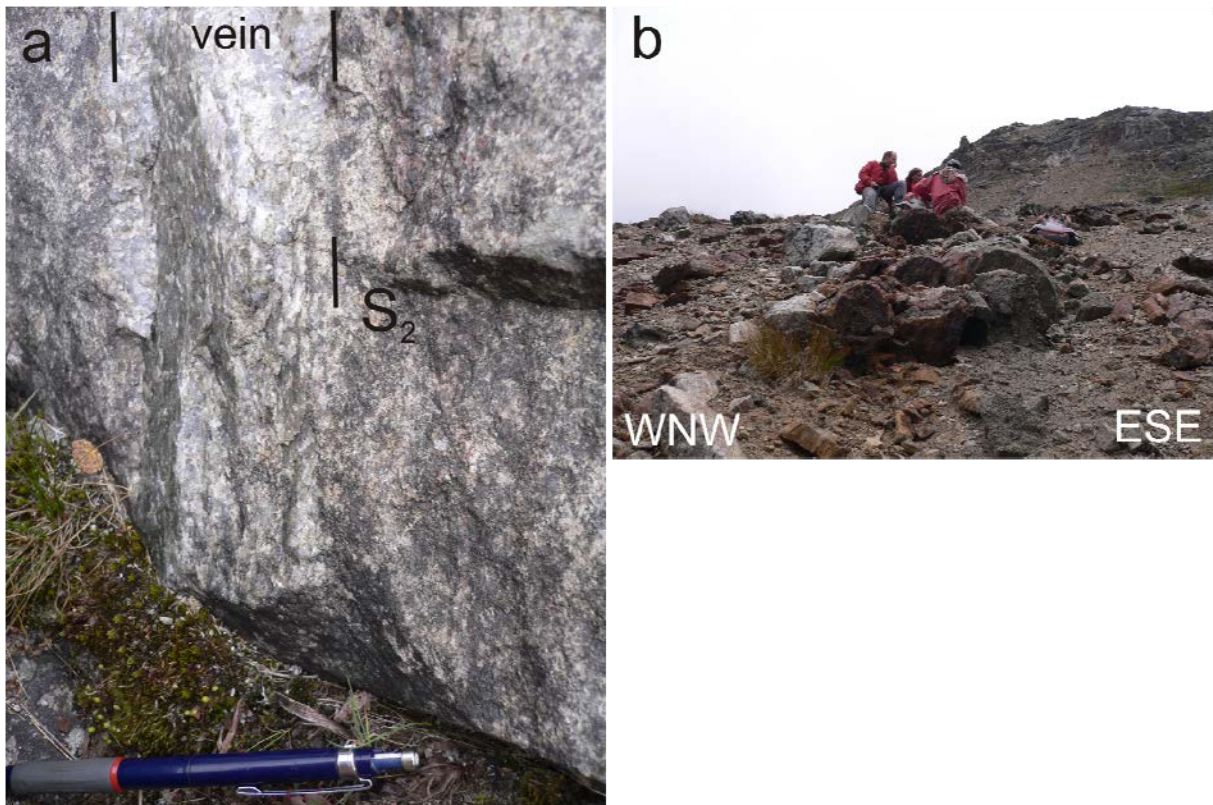
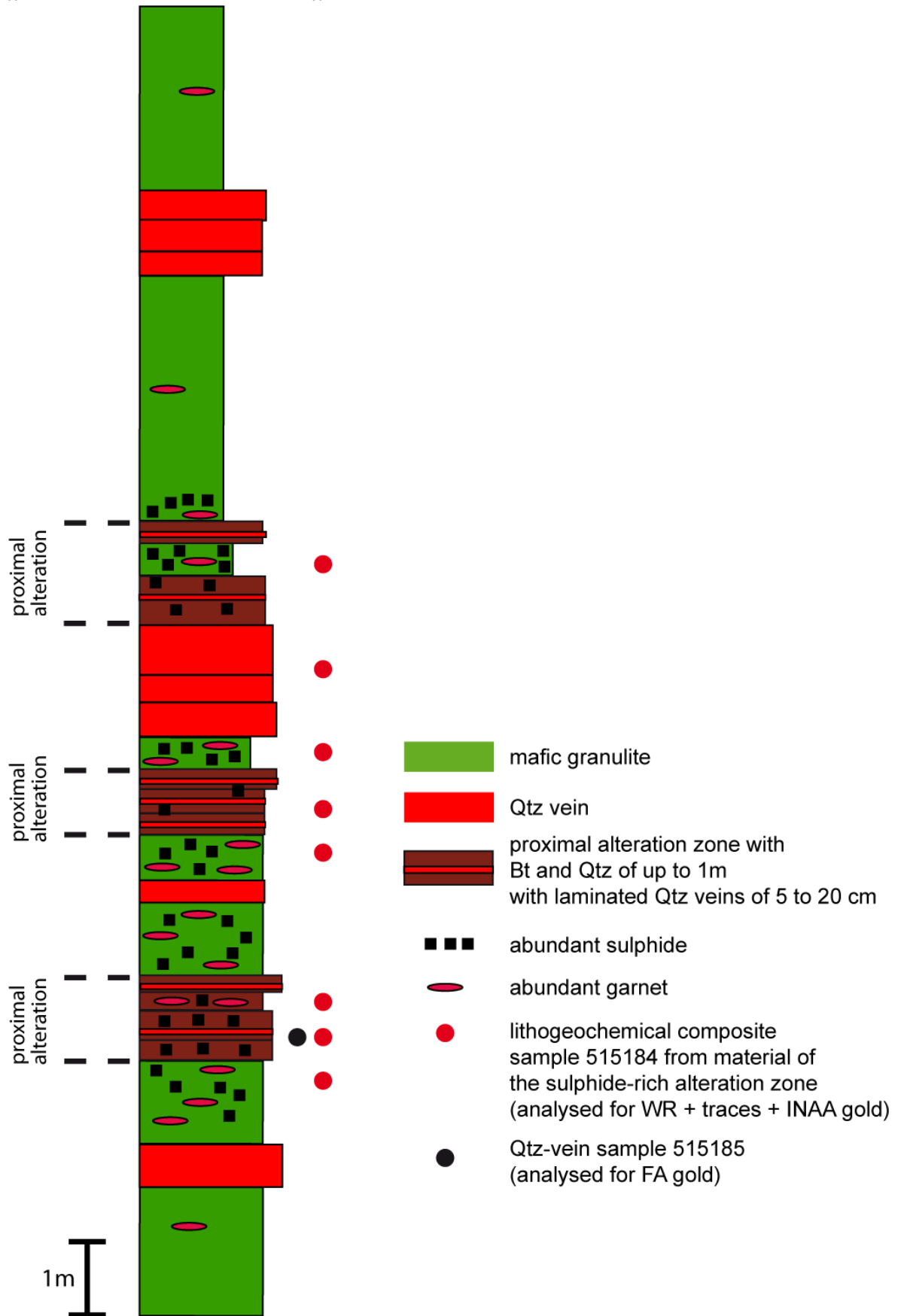


**Figure 38.** (a) Outcrop photograph of a fresh vein in gneissic wall rocks. Note the laminated fabric of the quartz vein. (b) Hydrothermal alteration zone in parasitic  $F_3$  fold. The alteration zone can be followed along strike up to the mountain ridge in the background.

**Figure 39.** Schematic profile across the hydrothermal alteration zone showing the proximal and distal hydrothermal alteration zones and sample locations. Note, that repetition of alteration zones is due to  $F_3$  parasitic folds. However, a correlation of horizons is impossible due to lack of continuous outcrop. Sample locations are given on the right side of the lithological column.

# Lithology: Kang profile-Alangordlia „Station BMS71,,



The quartz veins dip at about 75° to the west parallel to the  $S_2$  foliation in the mafic granulite. Several parasitic  $F_3$  folds with a wavelength of approximately 3 m are observed associated with the hydrothermal mineralisation and alteration (Fig. 38b). The  $F_3$  fold axis plunges at about 15° to the south (194°; Fig. 40). Close to parallel to that is a mineral stretching lineation ( $L_2 - 198/23$ ) defined by cm-scale PI and/or Px rods in the meta-leucogabbro (Figs. 2c & 40).

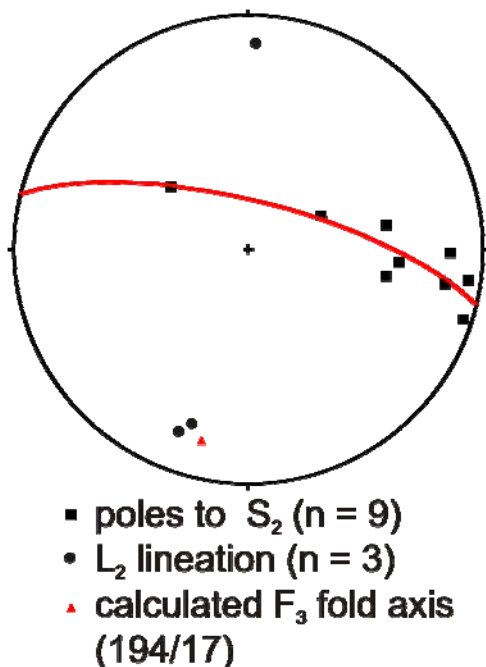


**Figure 40.** Pole figures for  $S_2$  foliations and  $L_2$  lineation (equal area, lower hemisphere projection).  $S_2$  forms a  $F_3$  fold with a  $F_3$  fold axis plunging SSW. The  $L_2$  lineation clusters around the calculated fold axis.

## Narsaq

Narsaq is a small settlement about 20 km south of Nuuk. The geology was studied during a 4 hours stop from Rink and a rubber dinghy. A 100–400 m wide amphibolite band shows a fold interference map pattern with an E–W trending  $F_{2b}$  axial trace and a NNE–SSW trending  $F_3$  axial trace in a tonalitic gneiss basement (Fig. 3c). The gneiss is grey, medium-grained and comprises Qtz, PI, Hbl and Bt (Fig. 41a). Locally, agmatitic fabrics are developed, where the leucosome consists of PI, Kfs, Qtz and Crd and the melanosome consists of Hbl, Bt, PI and minor Qtz with locally Crd porphyroblasts about 5 cm in diameter. The amphibolite is banded with medium-grained, black layers comprising Hbl, PI, Grt and minor Qtz, and 20 cm to 2 m wide, greenish layers rich in Cpx (Fig. 41b). PI forms in many places pseudomorphs after Grt, especially where pegmatites are abundant. Pegmatite dykes are up to 2 m wide and cross cut the regional foliation (Fig. 41a). Four different orientations are distinguished: NNE–SSW dextral, NNW–SSE sinistral, NW–SE and NE–SW trending pegmatites are observed (Fig. 42), which may be interpreted as a progressive conjugate set that formed during E–W compression. The NNE–SSW trending set is parallel to the axial plane of the  $F_3$  folds, which suggests that the pegmatites intruded syn- to late  $D_3$  deformation.

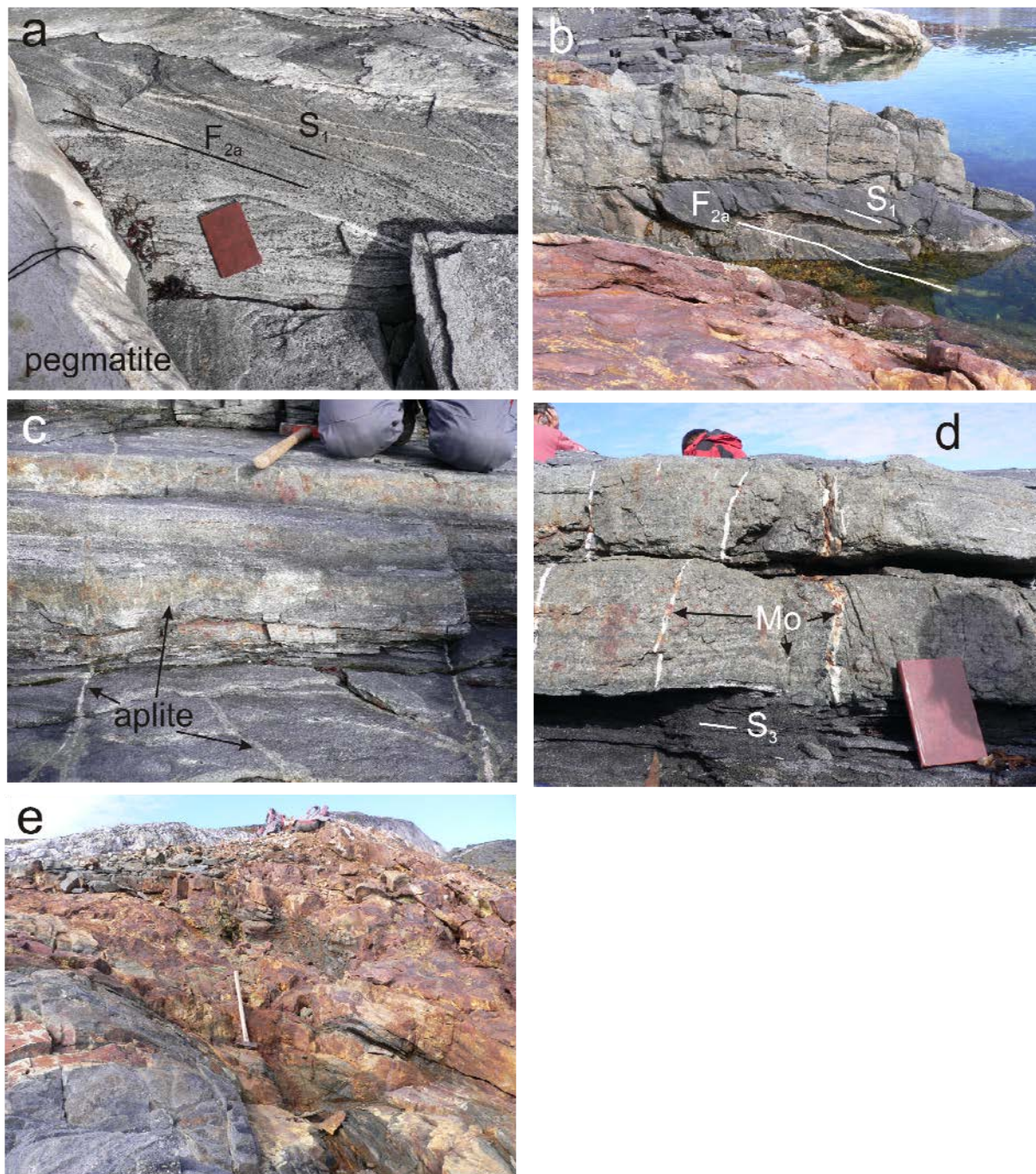


**Figure 41.** (a) Characteristic grey gneiss of the Narsaq area showing cm-scale  $F_{2a}$  folds and a closely-spaced  $S_1$  foliation. The gneiss is intruded by a pegmatite. (b) Isoclinal  $F_{2a}$  fold of amphibolite in gneiss. Note the banded fabric of amphibolite in the background. (c) Aplite dykes cross cutting amphibolite. The rusty spots represent weathered Mo. (d) Enlargement of (c), showing apatite dykes that are restricted to the competent Cpx-rich layers in the amphibolite. (e) Gossan within amphibolite representing the hydrothermal alteration zone.

Locally, cm-scale apatite dykes are developed in the amphibolite comprising Qtz, Pl, Tur and Mo. These dykes are surrounded by a cm-scale, green Cpx alteration halo in the black amphibolite, but are preferably developed in the Cpx-rich layers (Figs. 41c & d). The Cpx-

rich amphibolite (508378) is slightly enriched in Mo (about 15 ppm) and Bi (about 30 ppm). Three different dyke orientations are distinguished: NW–SE, NE–SW and E–W trending sets (Fig. 42), which may be interpreted as a conjugate set with the E–W trending set representing extension veins. The overall geometry of the aplite dykes is consistent with the interpretation that they formed syn- to late  $D_3$  together with the pegmatites, which, however, are barren of Mo. Mo is also observed disseminated in the greenish, Cpx-rich amphibolite layers (Fig. 41d). The spatial association of Mo with aplite dykes, Cpx alteration halos and Cpx-rich layers strongly suggests a genetical relationship between the intrusion of felsic melts, the alteration of amphibolite and Mo mineralisation.

An about 6 m wide hydrothermal alteration zone is developed in the amphibolite in a coastal outcrop about 700 m northwest of the Narsaq settlement (Fig. 41e). The alteration halo envelopes a 10–50 cm wide,  $S_2$  parallel quartz vein (115/36) comprising Ccp, Po and Mag in massive stringers. Locally, large Grt up to 10 cm in diameter are observed. The hydrothermal alteration zone in the amphibolite contains Bt, Grt, Cpx, Hbl, Ep and Qtz. The altered amphibolite (515202, 515206) is enriched in Ca, Sn and Bi. The massive sulphide-magnetite stringers (515204) are elevated in Fe (42 wt.%  $Fe_2O_3$ ), Co, Ni, Cu (ca. 1000 ppm), U, Th and Bi (5 ppm). The hydrothermal mineralisation is situated in an anticlinal structure with a near horizontal  $F_3$  fold axis plunging at  $5^\circ$  to the SSW. The hydrothermal mineralisation is cross cut by a pegmatite, suggesting that the hydrothermal overprint predated pegmatite intrusion syn- to late  $D_3$  deformation. The structural control of the quartz vein and the associated hydrothermal alteration by a  $F_3$  fold, however indicates formation of the quartz vein during  $D_3$  flexural slip folding akin a saddle reef. Therefore, it is likely that the intrusion of felsic melt and the hydrothermal fluid migration are not related to different events but represent successive stages in the structural evolution.

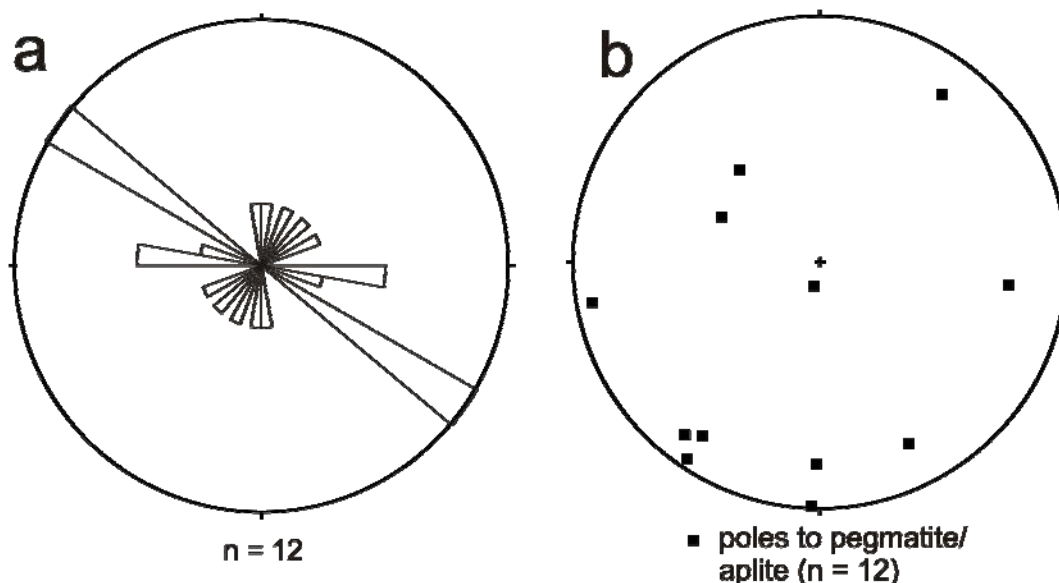


**Figure 42.** (a) Rose diagram indicating the main strike orientation of pegmatite and aplite dykes to be NW–SE. (b) Pole figures of the same data showing the 3D geometry of the dyke-system.

## **Qilangaarsuit**

Field work was carried out on the 15.07 – 22.07.2008 by 4 geologists operating from a camp and the last two days by 3 geologists operating from rubber dinghy. The base of the work forms a field map by Chadwick & Nutman and their descriptions (Chadwick & Nutman 1979; Chadwick & Coe 1983; Chadwick *et al.* 1977).

The geology and the potential for hydrothermal mineralisation were investigated by two detailed geological profiles located in the amphibolites of the Malene supracrustal sequence in the central part of the Qilangaarsuit island (Figs. 43 & 44). The lithology consists of weakly altered amphibolite, Bt-, Sil- and Grt-rich schists, quartz veins and pegmatites.

A hydrothermal alteration zone elevated in gold (up to 672 ppb) is located in an about 8 m wide zone, which contains numerous quartz veins and sulphides in Bt- and Grt-rich schist. This zone is easily identified by its characteristic rust-stained surface (Fig. 45). In detail, several horizons, each about one meter wide, occur in this zone. Each of these horizons consists of a distinct hydrothermal alteration assemblage, comprising Bt, Qtz, Grt, Po, Py, Ccp and, locally, Sil and Tur (Fig. 44). The quartz veins are 10-20 cm wide and locally several parallel veins form a laminated texture. The veins are parallel to the main foliation and can be followed along strike over several hundred meters, whereas, locally, sigmoidal extension veins crosscut the foliation. In places, they are sheared off or boudinaged due to flexural slip folding of the regional syncline structure. Quartz veins lacking hydrothermal alteration halos occur in the structural hanging wall (Fig. 44, profile B). Samples from these veins are only slightly elevated in gold. It appears that quartz veins characterised by a pronounced hydrothermal alteration halo are more favourable to contain gold. At station 08bms110 about 180 m north of profile B (Fig. 43), about one meter wide Bt- and sulphide-rich schist contains several quartz veins with 769 ppb gold.

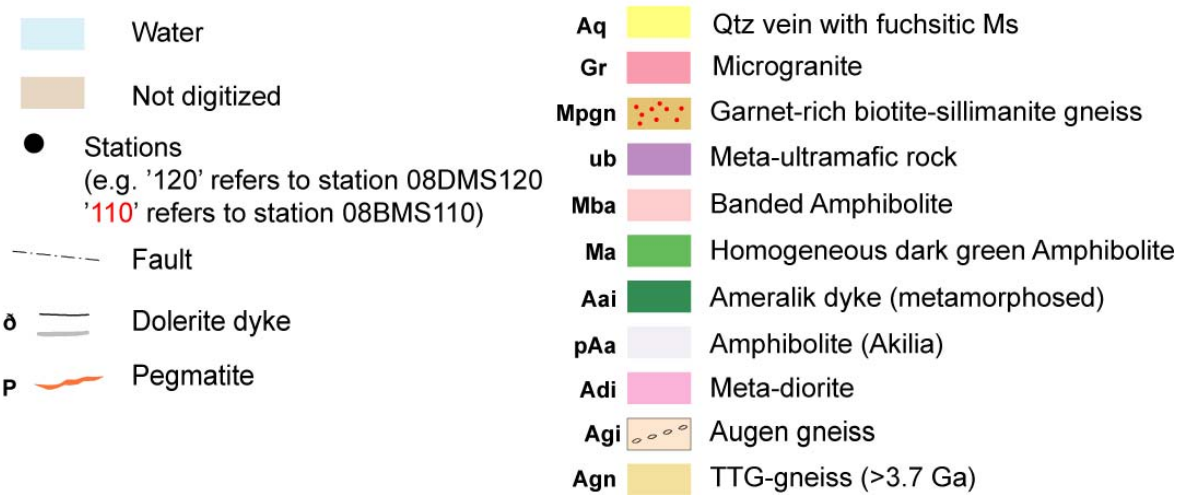
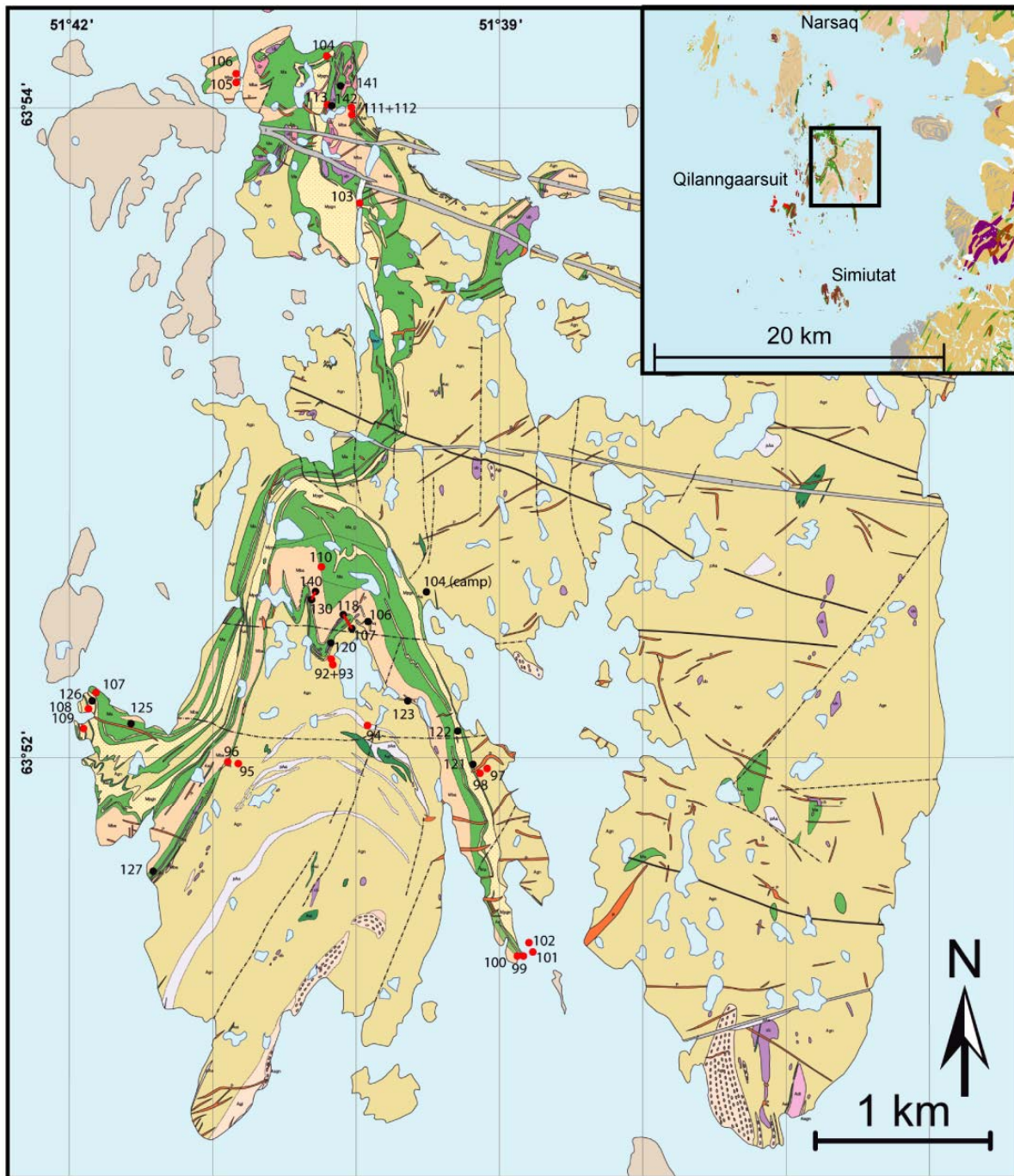


**Figure 43.** Schematic geological map showing the studied locations on Qilanngaarsuit island (redrawn after a field map from Chadwick 1974, GEUS archive). The rocks of the Malene supracrustal assemblage form large-scale  $F_3$  synform-antiform pairs. Two profiles in the central part of the island have been studied in detail and are indicated by red lines. One sample from profile A (station 107 to 118) returned 672 ppb gold.

Quartz veins elevated in gold also occur in an about 10 m wide zone in the northernmost part of Qilanngaarsuit island (station 08bms104; Fig. 43). In detail, this zone consists of marble and paragneiss at the contact with amphibolite. The quartz veins have been chipped over the entire zone and returned 52 ppb gold (sample 515232). The hydrothermal alteration assemblage comprises Cpx, Grt, Cal, Qtz, Po and Ccp. It forms coarse-grained skarn-like rocks with Grt up to 7 cm in diameter. The Grt shows oscillatory zoning on a macroscopic scale. Aplite dykes containing Mo cross cut the quartz veins and alteration zone.

Quartz veins containing green, fuchsitic Ms are widespread. They lack a characteristic alteration halo and are, notably, also barren of gold.

Interestingly, stream sediment samples taken in the northernmost and southernmost part of the greenstone belt on Qilanngaarsuit island (stations 08bms113 and 08bms96; Fig. 43) also yield slightly elevated gold above 25 ppb. Although gold detected in this preliminary investigation is < 1 ppm, it is conceivable that additional work and drilling may identify zones with higher gold than what is known to date.



**Figure 44.** The two profiles from the central part of the Qilangaarsuit island are located about 250 m apart, between stations 08dms107 to 118 and stations 08dms130 to 140, respectively. The Au-zone is located in Bt-rich schist and can be correlated between the two profiles.



**Figure 45.** Photograph from the central part of the Qilangaarsuit island looking south. The Photograph shows the location of profile B. Massive and homogeneous amphibolite (in the centre of the photograph) is flanked by relatively thin hydrothermal alteration zones, which contain narrow quartz veins.

## Simiutat

The small island of Simiutat has a size of about 1.6 x 1 km and is located about 10.5 km south of the Qilangaarsuit island (Fig. 46). The island was visited the 24.06.08 and the 23.07.08. While the first visit was a pre-field work excursion stop with only limited sampling, the second visit was used to study a detailed profile including careful and detailed sampling (Figs. 46 & 47). The main rock types are paragneisses of variable composition and amphibolite. The main foliation ( $S_2$ ) and the lithological units trend approximately NW–SE. The detailed profile was studied perpendicular to the strike of the  $S_2$  foliation in NE-SW direction on the northern tip of the island (Fig. 46). The structural footwall consists of an about 20 m thick paragneiss containing Grt, Qtz, Bt, Tur, Crd, Sil, St and one layer with Po and Ccp (station 154; Fig. 47). A 3 m wide layer of semi-massive to massive sulphide occurs at station 157 and contains mainly Po and Ccp together with black Tur. The massive sulphide samples (508431 and 508444) returned 71%  $Fe_2O_3$ , 1650 ppm Cu, 110 ppm Zn and 7% Pb for sample 508431; and 67 %  $Fe_2O_3$ , 2080 ppm Cu, 130 ppm Zn and 9% Pb for sample 508444. Some rocks contain up to 924 ppm Bi, 26 ppm Mo and 32 Sn. Gold is below detection limit.

The structural hanging wall consists of amphibolite comprising mainly Hbl and Pl. The amphibolite layer immediately above the sulphide layer is Grt-rich, whereas the more distal layers comprise Grt, Ath and Tur. Sulphides, mainly Ccp and Po, are locally present, and at station 160, magnetite was also observed. About 15 m further away from the massive sulphides, amphibolite (Hbl+Pl, station 161) and Bt-rich schist (station 162) occur.

Additional outcrops (stations 165 and 166; Fig. 46) were studied about 200 m towards the east of the profile. The lithology consists of a 1.5 m wide sulphide lens. The wall rocks contain abundant Oam and up to 33 ppm Bi, 70 ppm Mo and 82 ppm Sn.

The spatial association of minerals such as Grt, Oam, Tur and Crd with massive sulphides suggests that the rocks containing these minerals possibly represent metamorphosed primary alteration zones associated with a syngenetic sulphide mineralisation. On the other hand are Grt, Bt, Crd, Sil and St typical minerals of metamorphosed Al-rich sediments. Further petrological and litho-geochemical work is aimed at investigating whether the rocks at Simiutat are altered and to characterise hydrothermal sulphide mineralisation and associated alteration.

Although the semi-massive to massive sulphide lenses are narrow, it is worthwhile to note that these rocks are elevated in not only Cu. It is conceivable that the ore horizon has a down dip potential which could be tested by drilling from surface and detailed geophysical investigations.

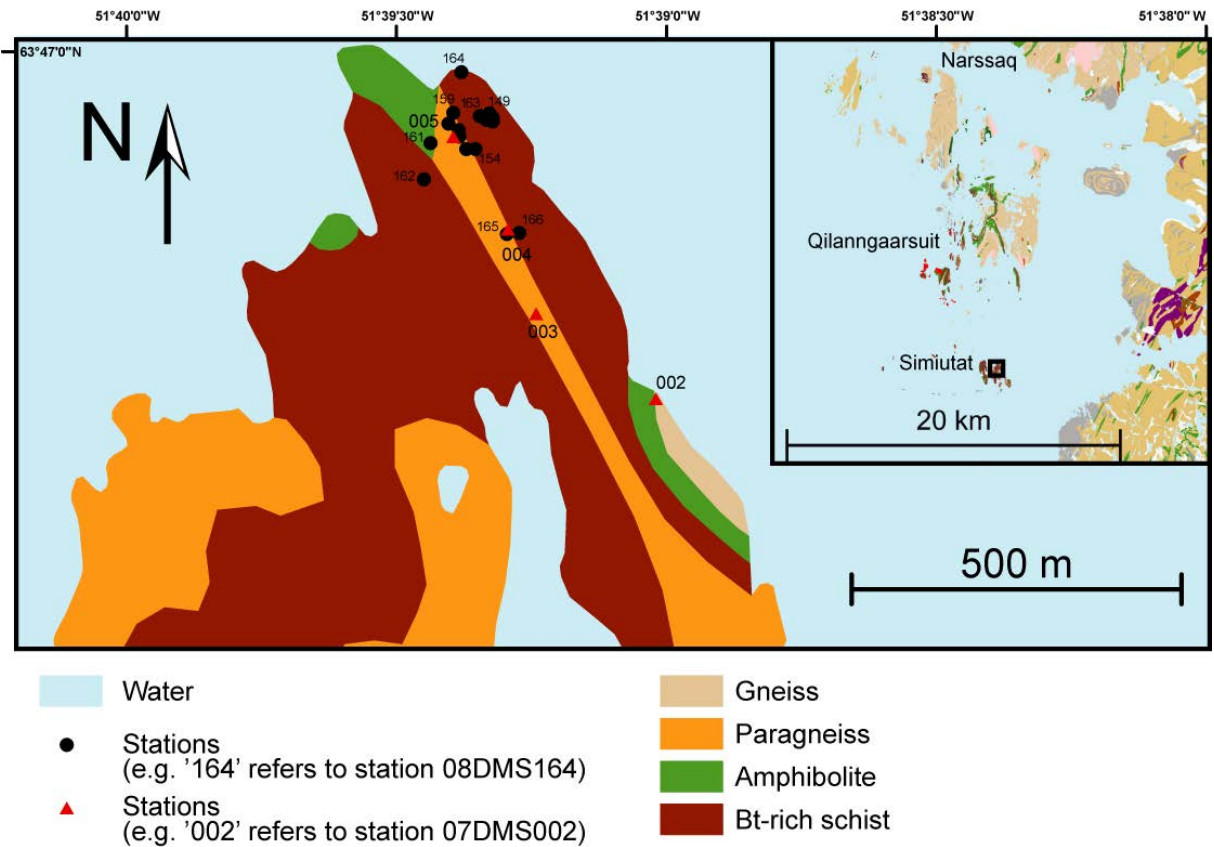


**Figure 46.** Schematic geological map showing the studied locations (stations) on Simiutat island. The Simiutat island consists of a western and eastern island; however only the eastern island has been visited. One profile in the northern part of the eastern island was studied in detail.

## Lithology: Simiutat island

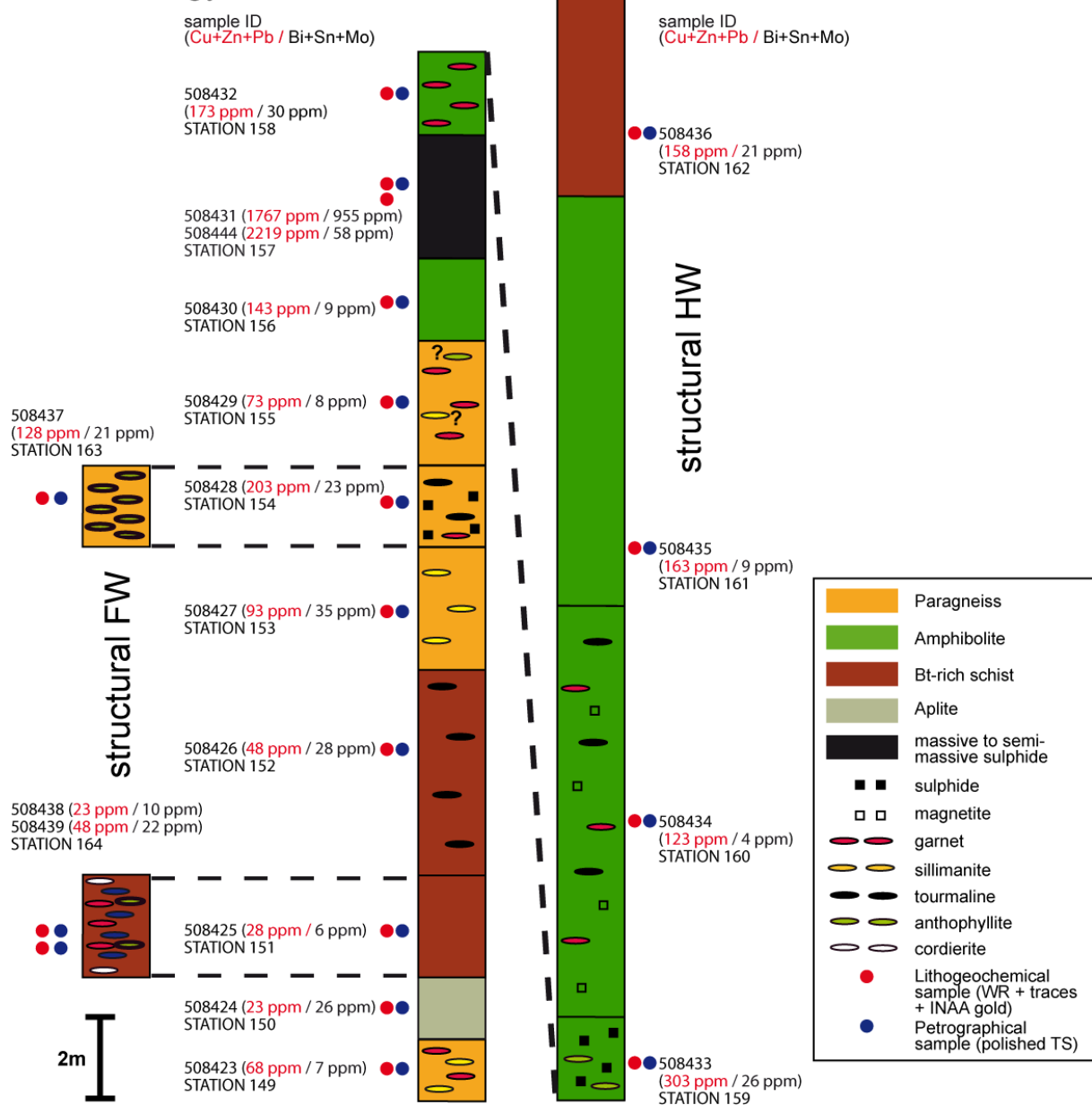


**Figure 47.** Schematic profile from the eastern Simiutat island. The profile is located between stations 08DMS149 and 162. Note, that several layers were followed along strike towards the west of the profile (Station 164 and 163). None of the samples from the profile has returned gold higher than 3 ppb, whereas the base metal contents are anomalous with mostly copper being strongly enriched.

## Summary and discussion

Numerous quartz veins were observed in all terranes. They are 1–20 cm wide and are continuous along strike and down dip over several m to up to 200 m. Besides Qtz they contain minor Po, Py and Ccp. The quartz veins are surrounded by a 5 cm to 1 m wide alteration halo. In gneisses, the hydrothermal alteration comprises Ms, Qtz, Bt, Ccp and Po. In the amphibolite a Bt, Qtz, Act, Po and Ccp alteration formed, locally with Ms and Ep. The mafic granulites contain Bt, Di, Tm, Qtz, Po, Py and Ccp as hydrothermal alteration assemblage. Composite systems of several parallel quartz veins together with alteration zones can be 50–200 m wide and can be followed along strike and down dip 250–1500 m if the outcrop situation allows that.

The quartz veins and associated halos are developed (1) parallel to  $S_3$  in the steep limbs of  $F_3$  folds and  $D_3$  shear zones, (2) occupy m-scale dilational jogs in parasitic  $F_3$  z-folds, (3) parallel to  $S_2$  in recumbent  $F_3$  folds with thicker veins in the steep limb, (4) as extension veins linking stepping  $D_3$  deformation zones in dilational jogs, very similar to the structure described in (2) but cross cutting the  $S_2$  foliation, and (5) as en-echelon sigmoidal veins displaying a dextral sense of rotation on the south-western limb of  $F_3$  synclines. All these structural controls are consistent with the interpretation that the quartz veins and the associated hydrothermal alteration formed synchronous with the  $D_3$  deformation.

On a regional scale, the  $F_3$  folds change systematically from open to tight in cross-section over several km. Very tight folds are sheared off by near vertical, NW–SE trending shear zones. Quartz veins and alteration zones are, in general, more abundant in the tight  $F_3$  folds spatially associated with the  $D_3$  strike-slip shear zones. Such a NNW–SSE trending shear zone, which probably represents a  $D_3$  strike-slip shear zone, was dated at ca. 2630–2610 Ma (Nutman and Friend 2007).

In the Nuuk area further north, the Ivinnguit fault (IVF) represents the northern boundary of the Færingehavn terrane against the Akia terrane. Several gold occurrences are known from the strike extent along the IVF, namely Storø, Qussuk, Bjørneøen and SW Isua. The quartz vein hosted gold mineralisation at Storø formed at about 2630 Ma and is, thus, spatially and genetically linked to terrane collision and deformation along the IVF at 2650–2600 Ma (Nutman *et al.* 2007; van Gool *et al.* 2007). One type of gold mineralisation at Storø occurs in quartz veins and alteration zones comprising Bt, Grt, Qtz, Di, Po and Apy (Eilu *et al.* 2006). The gold mineralisation in Qussuk similarly occurs in quartz veins with distinct alteration halos of Bt, Grt, Qtz and Po (Schlatter unpubl. data). A very similar alteration of Bt, Grt and Qtz associated with quartz veins is observed at SW Isua (Stensgaard 2008). The IVF may, therefore, represent a high permeability zone where hydrothermal fluid flow is concentrated. Structurally controlled gold mineralisation occurs in higher order splays that may have acted as favourable deposit sites.

Although the quartz veins in the study area formed in the same structural environment, are similar in size and mineralogy, and have similar amphibolite facies alteration halos, they have different gold contents. Quartz veins further away from the IVF contain 2–20 ppb gold, whereas closer to this major structure 100–800 ppb are recorded. Stream and soil sediment samples show a similar tendency to higher gold values close to the IVF. Possible explanations for the low concentration of gold in the veins are: (1) the fluids were different and contained no gold; and (2) gold didn't precipitate from the fluid. The most important precipitation mechanisms are phase separation, fluid-rock interaction, and fluid mixing. The hydrothermal quartz veins have the same structural control and very similar wall rocks,

excluding fluid-rock interaction and structurally induced phase separation as a possible explanation for the differences in gold content. The similar hydrothermal alteration systematics associated with mineralized and barren veins indicate that the fluid composition must have been rather similar. Therefore, a different fluid source and modification of the fluid by fluid mixing are regarded as unrealistic processes to explain our observations. Quartz veins formed away from the terrane collision zone by a developing orogenic hydrothermal fluid system. During terrane collision between 2650–2600 Ma, the fluid system concentrated gold. The development of the IVF as a transcrustal structure was a prerequisite for focused fluid migration along that high permeability zone. Orogenic gold mineralization culminated around 2630 Ma (e.g. Storø) in higher order splays from the IVF in favourable deposit sites along the strike extent of the IVF.

## Conclusions and future work

Field work in 2008 has identified several occurrences of hydrothermal quartz veins and associated hydrothermal alteration zones. Quartz veins and hydrothermal alteration are structurally controlled and their location can be predicted based on the mapped structures. However, most of the quartz veins appear not to be of economic interest. In the Buksefjord and Kangiata Nuna areas, most of the veins analysed contain < 30 ppb Au and no other interesting metals. Since the field work area was studied in considerable detail regarding hydrothermal mineralisation, we conclude that the area lacks economically significant mineral occurrences. The only exception to that, are the quartz veins and hydrothermal alteration zones described from Qilangaarsuit west of Buksefjorden, which record up to 800 ppb Au and may, therefore, be interesting for follow-up studies.

In the western part of the study area, several small lenses of massive sulphides were found on Simiutat, Qilangaarsuit and close to Narsaq. These occurrences record anomalous Cu, Zn, Mo and Bi, but they are too small to be of economic interest.

Several scientifically interesting topics that came up during field work will be followed in future work:

- M.Sc. project on hydrothermal quartz veins in Kangiata Nuna (Copenhagen University);
- M.Sc. project on massive sulphides found on Simiutat, Qilangaarsuit and close to Narsaq (Copenhagen University);
- Ph.D. project on hydrothermal alteration and metamorphism on Qilangaarsuit (RWTH Aachen University, application in progress);
- Petrology and structure of the Tasiusarsuaq terrane and its northern boundary (GEUS, RWTH Aachen University).

Since the general approach of this project is regarded as having proven to be rather successful, we will follow a similar approach to organise field work in 2009 covering the area around Sermilik and Grædefjord.

## References

- Appel, P.W.U., Coller, D., Coller, V., Heijlen, W., Moberg, E.D., Polat, A., Raith, J., Schjødt, F., Stendal, H. & Thomassen, B. 2005: Is there a gold province in the Nuuk region? Report from field work carried out in 2004. Danmarks og Grønlands Geologiske Undersøgelse Rapport **2005/27**, 79 pp.
- Bridgwater, D., McGregor, V.R. & Myers, J.S. 1974: A horizontal tectonic regime in the Archaean of Greenland and its implications for early crustal thickening. *Precambrian Research* **1**, 179-197.
- Baadsgaard, H. 1976: Further U-Pb dates on zircons from the early Precambrian rocks of the Godthaabsfjord area, West Greenland. *Earth and Planetary Science Letters* **33**, 261-267.
- Chadwick, B. & Nutman, A.P. 1979: Archaean structural evolution in the northwest of the Buksefjorden Region, southern West Greenland. *Precambrian Research* **9**, 199-226.
- Chadwick, B. & Coe, K. 1983: Buksefjorden 63 V1 Nord Descriptive text Geological map of Greenland 1:100 000 The regional geology of a segment of the Archaean block of southern West Greenland. 70 pp. Copenhagen: Grønlands Geologiske Undersøgelse.
- Chadwick, B., Coe, K., Compton, P.M. & Nutman, A. 1977: Field work on Precambrian rocks in the Buksefjorden region, southern West Greenland. Rapport Grønlands Geologiske Undersøgelse **85**, 60-64.
- Crowley, J.L. 2002: Testing the model of late Archean terrane accretion in southern West Greenland: a comparison of the timing of geological events across the Qarliit nunaat fault, Buksefjorden region. *Precambrian Research* **116**, 57-79.
- Eilu, P., Garofalo, P., Appel, P.W.U. & Heijlen, W. 2006: Alteration patterns in Au-mineralised zones of Storø, Nuuk region - West Greenland. Danmarks og Grønlands Geologiske Undersøgelse Rapport **2006/30**, 73 pp. Copenhagen:
- Escher, J.C. & Pulvertaft, T.C.R. 1995: Geological map of Greenland, 1:2 500 000.pp. Copenhagen: Geological Survey of Greenland.
- Frei, D. & Konnerup-Madsen, J. 2007: Magmatic environment: The Naujat gabbro-anorthosite complex and country rocks - Field report 2006. In: Stendal, H. (ed.): Characterisation of selected geological environments: Mineral resource assessment of the Archaean Craton SW Greenland Contribution no. 1 **2007/20**, 41-58 Copenhagen: Danmarks og Grønlands Geologiske Undersøgelse Rapport.
- Friend, C.R.L. & Nutman, A.P. 1991: Refolded nappes formed during late Archaean terrane assembly, Godthådsfjord, southern West Greenland. *Journal of the Geological Society London* **148**, 507-519.
- Friend, C.R.L. & Nutman, A.P. 2001: U-Pb zircon study of tectonically bounded blocks of 2940-2840 Ma crust with different metamorphic histories, Paamiut region, South-West Greenland: implications for the tectonic assembly of the North Atlantic craton. *Precambrian Research* **105**, 143-164.

- Friend, C.R.L. & Nutman, A.P. 2005: New pieces to the Archaean terrane jigsaw puzzle in the Nuuk region, southern West Greenland: steps in transforming a simple insight into a complex regional tectonothermal model. *Journal of the Geological Society London* **162**, 147 - 162.
- Friend, C.R.L., Nutman, A.P. & McGregor, V.R. 1987: Late-Archaean tectonics in the Færingehavn-Tre Brødre area, south of Buksefjorden, southern West Greenland. *Journal of the Geological Society London* **144**, 369–376.
- Friend, C.R.L., Nutman, A.P. & McGregor, V.R. 1988: Late Archaean terrane accretion in the Godthåb region, southern West Greenland. *Nature* **335**, 535–538.
- Friend, C.R.L., Nutman, A.P., Baadsgaard, H., Kinny, P.D. & McGregor, V.R. 1996: Timing of late Archaean terrane assembly, crustal thickening and granite emplacement in the Nuuk region, southern West Greenland. *Earth and Planetary Science Letters* **142**, 353-365.
- McGregor, V.R. 1973: The early Precambrian gneisses of the Godthåb district, West Greenland. *Philosophical Transactions of the Royal Society London* **A-273**, 343–358.
- McGregor, V.R., Nutman, A.P. & Friend, C.R.L. 1986: The Archean geology of the Godthåbsfjord region, southern West Greenland. In: Ashwal, L.D. (ed.): *Workshop on Early Crustal Genesis: The World's Oldest Rocks* **86-4**, 113–169. Houston: Lunar and Planetary Institute.
- McGregor, V.R., Friend, C.R.L. & Nutman, A.P. 1991: The late Archaean mobile belt through Godthåbsfjord, southern West Greenland: a continent-continent collision zone? *Bulletin of the Geological Society of Denmark* **39**, 179–197.
- Moorbath, S., Taylor, P.N. & Goodwin, R. 1981: Origin of granitic magma by crustal remobilisation: Rb-Sr and Pb/Pb geochronology and isotope geochemistry of the late Archaean Qorqut Granite Complex of southern West Greenland. *Geochimica et Cosmochimica Acta* **45**, 1051-1060.
- Nutman, A.P. & Friend, C.R.L. 2007: Adjacent terranes with ca. 2715 and 2650 Ma high-pressure metamorphic assemblages in the Nuuk region of the North Atlantic Craton, southern West Greenland: Complexities of Neoproterozoic collisional orogeny. *Precambrian Research* **155**, 159-203.
- Nutman, A.P., Christiansen, O. & Friend, C.R.L. 2007: 2635 Ma amphibolite facies gold mineralisation near a terrane boundary (suture?) on Storo, Nuuk region, southern West Greenland. *Precambrian Research* **159**, 19-32.
- Nutman, A.P., Friend, C.R.L., Baadsgaard, H. & McGregor, V.R. 1989: Evolution and assembly of Archean gneiss terranes in the Godthåbsfjord region, southern West Greenland: structural, metamorphic, and isotopic evidence. *Tectonics* **8**, 573–589.
- Nutman, A.P., Friend, C.R.L., Barker, S.L.L. & McGregor, V.R. 2004: Inventory and assessment of Palaeoproterozoic gneiss terrains and detrital zircons in southern West Greenland. *Precambrian Research* **135**, 281-314.
- Næraa, T. & Scherstén, A. 2008: New zircon ages from the Tasiusarsuaq terrane, southern West Greenland. *Geological Survey of Denmark and Greenland Bulletin* **15**, 73-76.

- Pidgeon, R.T. & Kalsbeek, F. 1978: Dating of igneous and metamorphic events in the Fiskenaasset region of southern West Greenland. *Canadian Journal of Earth Sciences* **15**, 2021–2025.
- Ramsay, J.G. & Huber, M.I. 1987: *Folds and fractures. The techniques of modern structural geology* **2**, 700 pp. London: Academic Press Limited.
- Scherstén, A., Stendal, H. & Næraa, T. 2008: Geochemistry of greenstones in the Tasiusarsuaq terrane, southern West Greenland. *Geological Survey of Denmark and Greenland Bulletin* **15**, 69-72.
- Schiøtte, L., Compston, W. & Bridgwater, D. 1989: U-Pb single-zircon age for the Tinissaq gneiss of southern West Greenland: a controversy resolved. *Chemical Geology* **79**, 21–30.
- Stensgaard, B.M. 2008: Gold favourability in the Nuuk region, southern West Greenland: results from fieldwork follow-up on multivariate statistical analysis. **2008/8**, 74 pp. Copenhagen: Danmarks og Grønlands Geologiske Undersøgelse Rapport.
- van Gool, J.A.M., Scherstén, A., Østergaard, C. & Næraa, T. 2007: Geological setting of the Storø gold prospect, Godthåbsfjord region, southern West Greenland; Results of detailed mapping, structural analysis, geochronology and geochemistry. **2007/83**, 158 pp. København: Danmarks og Grønlands Geologiske Undersøgelse Rapport.